

# Clearing the Smoke: Nebular Spectra of 100+ Type Ia Supernovae Exclude Single Degenerate Progenitors

M. A. Tucker<sup>1,★†</sup>, B. J. Shappee<sup>1</sup>, P. J. Vallely<sup>2</sup>, K. Z. Stanek<sup>2,3</sup>, J. Prieto<sup>4,5</sup>, J. Botyanszki<sup>6</sup>, C. S. Kochanek<sup>2,3</sup>, J. P. Anderson<sup>7</sup>, J. Brown<sup>2</sup>, L. Galbany<sup>8</sup>, T. W.-S. Holoien<sup>9</sup>, E. Y. Hsiao<sup>10</sup>, S. Kumar<sup>10</sup>, H. Kuncarayakti<sup>11,12</sup>, N. Morrell<sup>13</sup>, M. M. Phillips<sup>13</sup>, M. D. Stritzinger<sup>14</sup>, and Todd A. Thompson<sup>2,3</sup>

<sup>1</sup> Institute for Astronomy, University of Hawai‘i at Manoa, 2680 Woodlawn Dr., Honolulu, HI 96822

<sup>2</sup> Department of Astronomy, The Ohio State University, 140 West 18th Avenue, Columbus, OH 43210, USA

<sup>3</sup> Center for Cosmology and AstroParticle Physics (CCAPP), The Ohio State University, 191 W. Woodruff Avenue, Columbus, OH 43210, USA

<sup>4</sup> Núcleo de Astronomía de la Facultad de Ingeniería y Ciencias, Universidad Diego Portales, Av. Ejército 441, Santiago, Chile

<sup>5</sup> Millennium Institute of Astrophysics, Santiago, Chile

<sup>6</sup> Physics Department, University of California, Berkeley, CA 94720, USA

<sup>7</sup> European Southern Observatory, Alonso de Cordova 3107 Casilla 19001, Vitacura, Santiago, Chile

<sup>8</sup> Pitt PACC, Department of Physics and Astronomy, University of Pittsburgh, Pittsburgh, PA 15260, USA

<sup>9</sup> Carnegie Observatories, 813 Santa Barbara Street, Pasadena, CA 91101, USA

<sup>10</sup> Department of Physics, Florida State University, 77 Chieftan Way, Tallahassee, FL 32306, USA

<sup>11</sup> Finnish Centre for Astronomy with ESO (FINCA), FI-20014 University of Turku, Finland

<sup>12</sup> Tuorla Observatory, Department of Physics and Astronomy, FI-20014 University of Turku, Finland

<sup>13</sup> Las Campanas Observatory, Carnegie Observatories, Casilla 601, La Serena, Chile

<sup>14</sup> Department of Physics and Astronomy, Aarhus University, Ny Munkegade 120, DK-8000 Aarhus C, Denmark

Accepted XXX. Received YYY; in original form ZZZ

## ABSTRACT

We place statistical constraints on Type Ia supernova (SN Ia) progenitors using 226 nebular phase spectra of 110 SNe Ia. We find no evidence of stripped companion emission in any of the nebular phase spectra. Upper limits are placed on the amount of mass that could go undetected in each spectrum using recent hydrodynamic simulations. With these null detections, we place an observational  $3\sigma$  upper limit on the fraction of SNe Ia that are produced through the classical H-rich non-degenerate companion scenario of < 5.6%. Additionally, we set a tentative upper limit on He star progenitor scenarios of < 6.5%, although further theoretical modelling is required. As part of our analysis, we also derive a Nebular Phase Phillips Relation, which approximates the brightness of a SN Ia in the nebular phase using the peak magnitude and decline rate parameter  $\Delta m_{15}(B)$ .

**Key words:** supernovae – general; galaxies – distances and redshifts

## 1 INTRODUCTION

Type Ia supernovae (SNe Ia) are utilised across many astronomical disciplines, including the extragalactic distance scale, dark energy studies, and Galactic chemical evolution. Despite their prevalence, the origins of SNe Ia are still unclear even after decades of study. The general consensus is that they are explosions of carbon/oxygen (C/O) white dwarfs (Hoyle & Fowler 1960) with fairly homogenous prop-

erties. For example, the magnitude of SNe Ia at peak is well constrained ( $M_{\max} \sim -19$ , e.g.; Folatelli et al. 2010a), and, after correcting for light curve decline and color, they have an intrinsic scatter of  $\sim 0.1$  mag (e.g., Fig. 19, Folatelli et al. 2010a). Many formation mechanisms for SNe Ia have been proposed to reproduce this level of uniformity, which can be grouped into two main categories: the double degenerate (DD) and single degenerate (SD) scenarios (see Maoz et al. 2014; Livio & Mazzali 2018, for reviews on SNe Ia progenitors).

The DD scenario consists of two degenerate stars, usually C/O white dwarfs, which induce a SNe Ia through accre-

\* E-mail: tuckerma@hawaii.edu

† DOE CSGF Fellow

tion, collision, or merger. This can occur due to gravitational wave emission (Tutukov & Yungelson 1979; Iben & Tutukov 1984; Webbink 1984), collision/violent merger due to perturbations by external bodies (Thompson 2011; Katz & Dong 2012; Shappee & Thompson 2013; Pejcha et al. 2013; Antonini et al. 2014), accretion from a low-mass white dwarf onto a smaller, higher-mass white dwarf (Taam 1980; Livne 1990; Pakmor et al. 2012), or a “double detonation” where an accreted helium layer detonates and drives the core to detonate (Woosley & Weaver 1994; Fink et al. 2010; Kromer et al. 2010). Due to the intrinsic faintness of both components in these systems, observational confirmation of DD systems is exceptionally difficult (e.g., Rebassa-Mansergas et al. 2018). Some progress has been made on this front, such as bimodal emission in the nebular phase (Dong et al. 2015a; Valley et al. 2019) and possible hyper-velocity remnants (Shen et al. 2018). However, most of the evidence for DD systems comes from the exclusion of SD progenitors (e.g., Shappee et al. 2017).

The SD scenario involves a WD with a nearby non-degenerate companion (Whelan & Iben 1973; Nomoto 1982; Yoon & Langer 2003), usually undergoing Roche Lobe overflow (RLOF). The WD accumulates material until reaching critical mass and then explodes. This critical mass is typically considered the Chandrasekhar mass ( $M_{ch} \sim 1.4 M_{\odot}$ ), although sub- $M_{ch}$  explosions, including double detonation scenarios, are also possible (e.g., Livne & Arnett 1995). There are several predicted observational signatures of the SD degenerate scenario due to the interaction of the ejecta/explosion and the donor star (Wheeler et al. 1975), including effects on the rising SN Ia light curve (Kasen 2010), soft X-ray emission in the accretion phase (Lanz et al. 2005; Woods et al. 2018), surviving companions with anomalous characteristics (e.g., Canal et al. 2001; Shappee et al. 2013b), and the amount of  $^{56}\text{Ni}$  decay products synthesized in the explosion (e.g., Röpke et al. 2012; Shappee et al. 2017).

One of the most promising signatures of a RLOF companion to an exploding WD are emission lines produced by material stripped/ablated from the non-degenerate companion (e.g., Wheeler et al. 1975; Marietta et al. 2000; Mattila et al. 2005; Pan et al. 2012), observable in nebular-phase spectra once the SN Ia has faded considerably and become optically thin. For example, Boehner et al. (2017) simulated stripping from red giant (RG), main sequence (MS), and sub-giant (SG) stars, finding approximately 0.33, 0.25, and  $0.17 M_{\odot}$ , respectively, of stripped mass. Botyánszki et al. (2018) converted these estimates into expected H $\alpha$  luminosities and found that the emitted H $\alpha$  luminosity does not vary linearly with amount of stripped companion mass, which had been the assumption of previous studies (e.g. Leonard 2007; Shappee et al. 2013a), but instead the relation is closer to exponential. Additionally, the H $\alpha$  emission is powered by the SN Ia and roughly follows the bolometric luminosity.

In this work we compile a comprehensive sample of SNe Ia nebular spectra spanning  $\sim 200 - 500$  days after explosion to search for the expected emission from stripped/ablated material. We find no such emission in any spectrum in our sample, and place new or updated stripped/ablated mass constraints for each SN Ia. The entirety of similar work in the literature totals 25 SNe Ia (Mattila et al. 2005; Leonard 2007; Shappee et al. 2013a; Lundqvist et al. 2013, 2015;

Maguire et al. 2016; Graham et al. 2017; Shappee et al. 2018; Sand et al. 2018a; Holmbo et al. 2018; Dimitriadis et al. 2019; Tucker et al. 2018), a fraction of the sample analyzed in this work. All SNe Ia included in this study are listed in Table B2.

We outline our data sources and reduction techniques, including absolute flux calibration, in §2. In §3, we discuss our methodology in searching for and placing limits on material stripped from a RLOF companion. Our upper limits on stripped material are provided in §4, and our findings are discussed in the context of SNe Ia formation in §5. Included in §5 are discussions about peculiar SNe Ia and their role in our study, plus the curious case of ASASSN-18tb which exhibits broad H $\alpha$  emission in its semi-nebular spectrum (Kollmeier et al. 2019).

## 2 DATA SOURCES AND REDUCTION

Our sample of 226 spectra of 110 SNe Ia comes from the 38 instruments on 27 telescopes listed in Table 1. All spectroscopically peculiar SNe Ia are included except for those exhibiting signatures of circumstellar material (SNe Ia-CSM). These SNe Ia exhibit H $\alpha$  emission, but the velocity and magnitude of the emission is inconsistent with material stripped from a nearby companion. Instead, these SN Ia appear to have exploded in a dense circumstellar environment (e.g., SN 2002ic, Wang et al. 2004). We impose the following criteria when selecting SNe Ia nebular spectra:

- Obtained between 200 and 500 days after explosion to maintain consistency with the models of Botyánszki et al. (2018), assuming a typical rise time of  $t_{rise} \approx 19$  days (Firth et al. 2015).
- Cover  $\pm 1000$  km s $^{-1}$  of at least one H or He line in Table 2.
- Have at least one method of absolute flux calibration, outlined in §2.3.

The complete list of new and archival spectra is provided in Table B3. Additionally, we include new and archival photometry to supplement our spectral data and analysis. Early phase photometry ( $\lesssim 50$  d after maximum light) is used in deriving the photometric properties of each SN Ia using the photometric fitting code SNooPy (Burns et al. 2011), including time of maximum ( $t_{max}$ ), the decline rate parameter  $\Delta m_{15}$ , extinction along line of sight, and the distance modulus. Late- and nebular-phase photometry are used for flux calibrating the nebular spectra and deriving a Nebular Phase Phillips Relation (NPPR). The NPPR approximates the nebular magnitude of a SN Ia given its peak magnitude and decline rate, calibrated to an extensive sample of new and archival SNe Ia photometry. A complete description of the NPPR, its derivation and usage is provided in Appendix A.

### 2.1 New Spectra and Photometry

We present 14 new nebular-phase spectra of 13 SNe Ia, of which 10 have no prior published nebular spectra. These spectra were acquired in our ongoing study of SNe Ia progenitors, taken with MagE on Baade, MUSE on the VLT,

**Table 1.** All telescopes and instruments utilised in this work. If a reference could not be found for a given instrument, the corresponding instrument website is provided in the table notes.

Telescope	Abbrev. <sup>a</sup>	Instrument	Abbrev. <sup>a</sup>	Ref.	$N_{\text{spec}}$
Australian National University 2.3m	ANU2.3m	Wide-Field Spectrograph	WiFeS	<a href="#">Dopita et al. (2007, 2010)</a>	7
Calar Alto 2.2m	CA2.2m	Calar Alto Faint Object Spectrograph	CAFOS	...	<sup>b</sup> 1
Calar Alto 3.5m	CA3.5m	Multi-Object Spectrograph at Calar Alto	MOSCA	...	<sup>c</sup> 2
Danish 1.54m	D1.54m	Danish Faint Object Spectrograph and Camera	DFOSC	<a href="#">Andersen et al. (1995)</a>	1
du Pont Telescope	duPont	Wide Field Reimaging CCD Camera Boller and Chivens Spectrograph	WFCCD BC	...	<sup>d</sup> 4
ESO 1.5m	ESO1.5m	Boller and Chivens Spectrograph	BC	...	<sup>e</sup> 1
ESO 3.6m	ESO3.6m	ESO Faint Object Spectrograph and Camera	EFOSC1/2	<a href="#">Buzzoni et al. (1984)</a>	11
Himalayan Chandra Telescope	HCT	Himalayan Faint Object Spectrograph	HFOSC	...	<sup>g</sup> 2
Hubble Space Telescope	HST	Faint Object Spectrograph	FOS	...	<sup>h</sup> 1
Isaac Newton Telescope	INT	Faint Object Spectrograph (1st Gen.)	FOS1	<a href="#">Breare et al. (1987)</a>	2
Gemini North/South	GN/S	Gemini Multi-Object Spectrograph	GMOS	<a href="#">Hook et al. (2004)</a>	12
Gran Telescopio Canarias	GTC	Optical System for Imaging and low-Intermediate-Resolution Integrated Spectroscopy	OSIRIS	<a href="#">Cepa (2010)</a>	1
Keck I	KeckI	Low Resolution Imaging Spectrograph	LRIS	<a href="#">Oke et al. (1995)</a>	27
Keck II	KeckII	DEep Imaging Multi-Object Spectrograph	DEIMOS	<a href="#">Faber et al. (2003)</a>	9
Large Binocular Telescope	LBT	Echelette Imager and Spectrograph	ESI	<a href="#">Sheinis et al. (2002)</a>	3
Magellan Baade Telescope	Baade	Multi-Object Double Spectrograph Inamori-Magellan Areal Camera and Spectrograph	MODS IMACS	<a href="#">Pogge et al. (2010)</a> <a href="#">Dressler et al. (2011)</a>	10
Magellan Clay Telescope	Clay	Magellan Echelle Spectrograph	MagE	<a href="#">Marshall et al. (2008)</a>	2
Multiple Mirror Telescope	MMT	Low Dispersion Survey Spectrograph	LDSS	...	<sup>i</sup> 5
New Technology Telescope	NTT	Blue Channel Spectrograph	BCS	<a href="#">Angel et al. (1979)</a>	6
		ESO Multi-Mode Instrument	EMMI	<a href="#">D'Odorico (1990)</a>	1
Palomar 200-inch	P200	SOFI	...	<a href="#">Moorwood et al. (1998)</a>	1
Shane 3m Telescope	Shane3m	Double Spectrograph	DBSP	<a href="#">Oke &amp; Gunn (1982)</a>	4
Southern African Large Telescope	SALT	Kast Spectrograph	KAST	<a href="#">Silverman et al. (2013)</a>	11
Subaru	Sub	Robert Stobie Spectrograph	RSS	<a href="#">Buckley et al. (2006)</a>	3
		OH-Airglow Suppressor/Cooled Infrared Spectrograph and Camera for OHS	CISCO	<a href="#">Motohara et al. (2002)</a>	3
		Faint Object Spectrograph and Camera	FOCAS	<a href="#">Kashikawa et al. (2002)</a>	2
Tillinghast 1.5m	Till	FAst Spectrograph for the Tillinghast telescope	FAST	<a href="#">Fabricant et al. (1998)</a>	7
Telescopio Nazionale Galileo Very Large Telescope	TNG VLT	Device Optimized for LOw RESolution FOcal Reducer and low dispersion Spectrograph	DOLORES FORS1/2	<a href="#">Molinari et al. (1999)</a> <a href="#">Appenzeller et al. (1998)</a>	2 43
		Multi-Unit Spectroscopic Explorer	MUSE	<a href="#">Bacon et al. (2010)</a>	8
		XSHOOTER	XSH	<a href="#">Vernet et al. (2011)</a>	16
William Herschel Telescope	WHT	Intermediate dispersion Spectrograph and Imaging System	ISIS	<a href="#">Jorden (1990)</a>	5
		ACAM	...	<a href="#">Benn et al. (2008)</a>	1
		Faint Object Spectrograph (2nd Gen.)	FOS2	<a href="#">Breare et al. (1987)</a>	6
Unknown <sup>j</sup>	...	Unknown	...	...	1
Total	27		38		226

<sup>a</sup> Abbreviations used in Table B3.

<sup>b</sup> [http://w3.caha.es/CAHA/Instruments/CAFOS/cafos\\_overview.html](http://w3.caha.es/CAHA/Instruments/CAFOS/cafos_overview.html)

<sup>c</sup> <http://www.caha.es/CAHA/Instruments/MOSCA/index.html>

<sup>d</sup> <http://www.lco.cl/telescopes-information/lco/telescopes-information/irenee-du-pont/instruments/website/wfccd/wfccd-manuals>

<sup>e</sup> <http://www.lco.cl/telescopes-information/irenee-du-pont/instruments/website/boller-chivens-spectrograph-manuals/user-manual/the-boller-and-chivens-spectrograph>

<sup>f</sup> <http://www.ls.eso.org/lailla/Telescopes/2p2/E1p5M/BC/BC.html>

<sup>g</sup> <https://www.iap.res.in/iao/hfosc.html>

<sup>h</sup> [http://stecf-poa.stsci.edu/poa/FDS/fos\\_doc\\_access.html](http://stecf-poa.stsci.edu/poa/FDS/fos_doc_access.html)

<sup>i</sup> <http://www.lco.cl/telescopes-information/magellan/instruments/ldss-3>

<sup>j</sup> Data not found for the spectrum of SN1981B. See Appendix B2 for details.

and WFCCD on duPont (see Table 1 for telescope and instrument designations). For the new spectra presented here, each spectrum was reduced using telescope and instrument-specific pipelines, if available, otherwise typical IRAF tasks were used. The spectra acquired with MagE/Baade were reduced with a pipeline provided by the Carnegie Observatories<sup>1</sup> (Kelson et al. 2000; Kelson 2003), with the exception of standard star calibrations and stitching together each echelle spectrum, which was done with custom Python routines. For newly presented MUSE data acquired as part of the AMUSING survey (Galbany et al. 2016), spectra were extracted in a 1'' circular aperture at the SN Ia location using the PyMUSE package (Pessa et al. 2018), and corrected for host galaxy contributions using a background annulus extending from 2'' to 3''.

For absolute flux calibrations, we also include nebular photometry for any SNe Ia in our sample. This includes new observations and reprocessed archival images for which we could not find a published magnitude. New photometry includes *V*-band images taken with FORS2, *r*-band images from MODS1, and *BVRI* images from WFCCD. Archival imaging includes *UBVRI* imaging from FORS1/2 and *BVRgri* imaging from EFOSC2 (Table B5). All images are bias subtracted and flat-field corrected before performing aperture photometry with the IRAF *apphot* task. For targets with  $\delta \geq -30^\circ$ , photometry from the Pan-STARRS Stack Object catalog<sup>2</sup> (Chambers et al. 2016; Flewelling et al. 2016) was used in calibrating the images, otherwise *Gaia* DR2 photometry (Gaia Collaboration et al. 2016, 2018; Riello et al. 2018) was used. When transforming reported magnitudes to other photometric systems, Tonry et al. (2012) and Evans et al. (2018) were used for Pan-STARRS and *Gaia*, respectively. The only exceptions to this procedure are the *B*-band FORS2/VLT images, which are calibrated using the reported photometric zeropoints<sup>3</sup>.

## 2.2 Archival Spectra and Photometry

The primary sources of our archival spectra and photometry are the Berkeley SuperNova Ia Program<sup>4</sup> (BSNIP, Silverman et al. 2012, 2013), the Center for Astrophysics ( CfA) Supernova Data Archive<sup>5</sup> (Riess et al. 1999; Jha et al. 2006; Matheson et al. 2008; Blondin et al. 2012), the Carnegie Supernova Project<sup>6</sup> (CSP, Hamuy et al. 2006; Folatelli et al. 2010a; Contreras et al. 2010; Stritzinger et al. 2011; Folatelli et al. 2013; Krisciunas et al. 2017; Phillips et al. 2019), the 100IAs project (Dong et al. 2018a), the ANU WiFeS SuperNovA Program (AWSNAP; Childress et al. 2016), and the All-Sky Automated Survey for SuperNovae (ASAS-SN, Shappee et al. 2014a; Holien et al. 2017a,b,c, 2019, Valley et al., Chen et al., in prep). The majority of the publicly available data were retrieved using the Open Supernova

<sup>1</sup> <http://code.obs.carnegiescience.edu/mage-pipeline>

<sup>2</sup> <http://archive.stsci.edu/panstarrs/stackobject/search.php>

<sup>3</sup> <https://www.eso.org/observing/dfo/quality/FORS2 qc/zeropoints/zeropoints.html>

<sup>4</sup> <http://heracles.astro.berkeley.edu/snadb/>

<sup>5</sup> <https://www.cfa.harvard.edu/supernova/SNarchive.html>

<sup>6</sup> <http://csp.obs.carnegiescience.edu/>

Catalog (OSC, Guillochon et al. 2017) and the Weizmann Interactive Supernova data REPOSITORY (WISEREP, Yaron & Gal-Yam 2012). All data provided by these sources are already reduced with the exception of precise spectral flux calibration, which we outline in §2.3. Additionally, we supplement these sources with archival data obtained from telescope databases, including the Keck Observatory Archive<sup>7</sup> (KOA), the ESO Science Archive Facility<sup>8</sup> (ESO SAF), the Isaac Newton Group Archive<sup>9</sup> and the Gemini Observatory Archive<sup>10</sup> (GOA). Information on all the spectra in this study is presented in Table B3.

Data reduction and calibration was performed as uniformly as possible across all sources of spectra. Data retrieved from public archives were already reduced, with the exception of absolute flux calibration. The reduction of data retrieved from telescope archives was generally less complete. All spectra retrieved from the ESO SAF were already reduced (excluding flux corrections) with the exception of FORS1/2 data. For any ESO SAF data reduction, both spectroscopy and photometry, we used the ESO SAF `esorex` data reduction pipeline (Freudling et al. 2013).

Spectra obtained from the KOA and GOA were not reduced prior to retrieval and had to be manually reduced. Recent LRIS spectra were reduced using Lpipe<sup>11</sup>, while older LRIS and DEIMOS data were reduced using the LowRedux/XIDL pipeline<sup>12</sup>. Gemini North/South GMOS spectra were reduced with the GMOS Data Reduction Cookbook<sup>13</sup>.

We manually reduced any unreduced spectra for which no pipeline exists using standard IRAF<sup>14</sup> procedures. Images were flat-fielded and bias-subtracted using archival calibration images taken near the epoch of observation, and wavelength calibrated with arc lamp exposures. Spectrophotometric standard star observations were used to correct for telescope/instrumental artefacts, atmospheric effects, and to place each spectrum on a reliable relative flux scale.

## 2.3 Accurate Flux Calibration

For our analysis in §3, the spectra must be on a reliable absolute flux scale. While calibrating spectra with spectrophotometric standard stars places these spectra on a dependable relative flux scale, slit losses, atmospheric conditions, and other effects can cause the resulting spectra to deviate from an absolute flux scale. To scale a spectrum to the absolute scale, we employed Eq. 7 from Fukugita et al. (1996) to calculate synthetic photometry from the spectra. The spectra are then scaled so that the synthetic photometry matches the observed photometry. There were several different sources of photometry used to calibrate the spectra. In order of preference and reliability, with accuracy estimates in given parentheses:

<sup>7</sup> <https://koa.ipac.caltech.edu/>

<sup>8</sup> <http://archive.eso.org/cms.html>

<sup>9</sup> <http://casu.ast.cam.ac.uk/casuadc/ingarch/query>

<sup>10</sup> <https://archive.gemini.edu/>

<sup>11</sup> <http://www.astro.caltech.edu/~dperley/programs/lpipe.html>

<sup>12</sup> <http://www.ucolick.org/~xavier/LowRedux/>

<sup>13</sup> <http://ast.noao.edu/sites/default/files/GMOS-Cookbook/>

<sup>14</sup> <http://iraf.noao.edu/>

(i) For spectra with acquisition images taken at the time of observation, we scale the entire spectrum to match these photometric observations, usually in the  $V$  or  $r$  filters ( $\sim 5 - 10\%$ ).

(ii) If acquisition images are unavailable, we next tried to use photometry within  $\pm 5$  d of the spectral observations. Photometry in all available filters within this temporal limit were used in the flux calibration ( $\sim 10 - 15\%$ ).

(iii) If no photometric data was available within  $\pm 5$  d, we searched for photometry within  $\pm 50$  d. If at least 3 photometric data points fell within this time span, we linearly interpolated to estimate the magnitude at the time of the spectral observation ( $\sim 15 - 20\%$ ).

(iv) If none of these were available, the nebular  $BVR$  magnitude was estimated with the NPPR and used to calibrate the spectrum (see Appendix A,  $\sim 20\%$ ).

We required  $> 90\%$  of the filter's transmission curve be covered by the observed spectrum for viable calibrations. If only a single filter was available, the entire spectrum was scaled to match the observation. If two filters were available for flux calibration, a simple linear fit was applied to the scale factors. If  $> 3$  filters were available, we use spline fits with fixed endpoints to ensure a robust flux correction across the entire spectrum. After placing the spectrum on an absolute flux scale, we correct for host galaxy and Milky Way reddening using the  $E(B-V)_{\text{host}}$  derived from the light curve fits. We implement a Fitzpatrick (1999) extinction law and a Schlegel et al. (1998) Milky Way dust map for our reddening corrections. We assume  $R_V = 3.1$  unless stated otherwise (see Appendix B).

### 3 SEARCHING FOR EMISSION FROM A STRIPPED COMPANION

Prior to the work of Botyánszki et al. (2018), the majority of unbound mass limits in the literature utilised the work of Mattila et al. (2005) and Leonard (2007) to compute stripped mass limits from comparing observed spectra to expected  $H\alpha$  luminosities. Several subsequent studies have adopted these methodologies in their work (e.g., Maguire et al. 2016; Graham et al. 2017) with notable success in ruling out hydrogen-rich companions. Yet the models of Mattila et al. (2005) had several shortcomings in observational implementation. In particular, Leonard (2007) assumed a linear scaling between the amount of unbound companion mass and the corresponding  $H\alpha$  luminosity.

Botyánszki et al. (2018), using the MS38 model (a main sequence star undergoing RLOF) from Boehner et al. (2017), instead found the emitted  $H\alpha$  luminosity scales exponentially with the amount of stripped mass. Additionally, Botyánszki et al. (2018) computed a simplified helium-star model, where all the stripped mass from the MS38 model is replaced with helium instead of Solar abundance material. This is not a true helium star model, as helium star companions are expected to have lower amounts of stripped mass than their hydrogen-rich counterparts and a modestly different velocity distribution (e.g. Pan et al. 2012), but it provides a starting point for calculating limits on the amount of unbound helium in a SN Ia spectrum.

While the models of Botyánszki et al. (2018) clarify the

**Table 2.** Line luminosities for both the hydrogen-rich (H-rich) model and the helium-rich (He-rich) model corresponding to the MS38 and helium models from Botyánszki et al. (2018). Helium lines are given letter designations to ease identification in Table B4. FWHM refers to the expected FWHM of a line profile broadened by  $\sim 10^3 \text{ km s}^{-1}$ .

Line	$\lambda$	$L_{200}[10^{38} \text{ erg/s}]$	FWHM [Å]
<b>H-rich Model</b>			
$H\gamma$	4341Å	0.271	14.5
$H\beta$	4831Å	4.38	16.1
$\text{HeI-a}$	5875Å	4.27	19.6
$H\alpha$	6563Å	68.0	21.9
$\text{HeI-b}$	6678Å	2.24	22.3
$\text{HeI-c}$	1.08μm	10.5	36.0
$\text{Pa}\beta$	1.281μm	14.6	42.7
$\text{Pa}\alpha$	1.875μm	14.6	62.5
$\text{HeI-d}$	2.06μm	8.48	68.7
<b>He-rich Model</b>			
$\text{HeI-a}$	5875Å	8.26	19.6
$\text{HeI-b}$	6678Å	6.90	22.3
$\text{HeI-c}$	1.08μm	18.2	36.0
$\text{HeI-d}$	2.06μm	12.9	68.7

mass-luminosity scaling issue and expand to helium emission, they share two other shortcomings with the models of Mattila et al. (2005): the requirement of using  $H\alpha$  to constrain the amount of unbound mass, and only calculating the expected  $H\alpha$  luminosity at a single epoch (200 days post-explosion for Botyánszki et al. 2018 and 350 days post-maximum for Mattila et al. 2005). In the following subsections we discuss our stripped mass limits given these limitations.

#### 3.1 Expanding on these Models

For SNe Ia with star-forming host galaxies, the region around  $H\alpha$  can be contaminated by narrow host galaxy  $H\alpha$  and NII emission lines which complicates setting limits on  $H\alpha$  emission. However, the unbound material has emission lines besides  $H\alpha$ , including  $H\beta$ ,  $H\gamma$ , and the Paschen series. Assuming roughly Solar metallicity, the stripped material will also exhibit prominent HeI lines in the optical and NIR (Botyánszki et al. 2018). We provide the luminosities for each of these lines in Table 2 at  $(t - t_0) = 200$  days for the hydrogen-rich (H-rich) model using the same MS38 model as Botyánszki et al. (2018). Additionally, we supply similar data for the simplified helium star model from Botyánszki et al. (2018), which we refer to as the He-rich model.

Botyánszki et al. (2018) estimated the line luminosity at 200 days as a function of the amount of stripped mass ( $M_{st}$ ). Table 2 provides the expected luminosity  $L_{200}(M_{st})$  of various lines for  $M_{st} = 0.25 M_\odot$ . The dependence on the amount of stripped mass is well approximated by  $\log_{10} L_{200}(M) \simeq \log_{10} L_{200}(0.25M_\odot) + 0.17M - 0.2M^2$ , where  $M = \log_{10}(M_{st}/M_\odot)$ . Botyánszki et al. (2018) do not provide the time dependence of the line emission specifically, but note that the  $H\alpha$  emission is proportional to the FeIII emission over the  $200 < (t - t_0) < 500$  day period they consider. Utilising the synthetic spectra models from Botyánszki

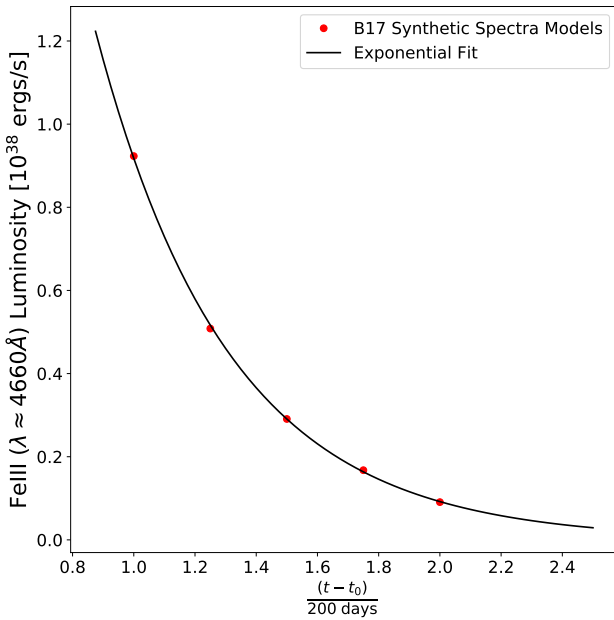


**Figure 1.** Peak luminosity of the FeIII line (red points) versus  $t_0$  from the time-dependent SN Ia spectral models of [Botyánszki & Kasen \(2017\)](#) and the exponential fit (black line).

& [Kasen \(2017\)](#), we find the FeIII emission is well fit by an exponential (Fig. 1), which leads to an estimate for the line luminosity of

$$\log_{10} L(M, t) = \log_{10} L_{200}(M_\odot) + 0.17M - 0.20M^2 - \left( \frac{t - t_0}{200 \text{ days}} \right) \quad (1)$$

provided  $M_{st} < 2M_\odot$ . This should hold well for the Balmer lines, and is at least a better approximation for the Paschen and HeI lines than assuming their luminosities are temporally constant.

### 3.2 Placing Statistical Limits on Stripped Mass

Once each spectrum is flux calibrated and corrected for the reddening, we place statistical limits on the presence of emission lines listed in Table 2, roughly following the methods of [Leonard \(2007\)](#). Each spectrum is rebinned to the approximate spectral resolution, and the spectral continuum is fit with a 2<sup>nd</sup>-order Savitsky-Golay polynomial ([Press et al. 1992](#)), excluding pixels within  $2 \times \text{FWHM}$  of line centers to prevent biasing our continuum fit, as done in previous studies (e.g., [Maguire et al. 2016](#)). However, since we are inspecting a multitude of lines for emission signatures, we apply our continuum model in velocity space instead of wavelength space to incorporate this modification.

No single continuum width adequately fits the continuum for all SNe Ia in our sample, especially considering the spectroscopic and temporal diversity. We tailored the continuum fit width for each spectrum based on the observed SN Ia expansion velocity, measured from the prominent emission lines in the spectrum. Since most of the major emission lines in nebular SNe Ia are blended to some extent (e.g., [Mazzali et al. 2015](#), Fig. 5), we compute the weighted average from

the fitted line profiles assuming a Gaussian emission profile + linear continuum. The lines considered for deriving the expansion velocity are the major FeII, FeIII, and CoIII lines indicated by the vertical dashed lines in Fig. 2. If the SNR of the spectrum is too low for the widths of at least 2 lines to be measured confidently, we assume a typical width of  $3000 \text{ km s}^{-1}$ . For velocities lower than this value, we risk biasing our continuum fit to include possible weak emission, and implement  $3000 \text{ km s}^{-1}$  as a strict lower bound. Additionally, since SNe Iax are known to have narrow line profiles in the nebular phase compared to typical SNe Ia ([Foley et al. 2016](#)), we adopt this lower bound for SNe-Iax as well. Because these velocities are simply a proxy for the width of the continuum fit, this method neglects the intricacies of SNe Ia emission profiles, especially since spectroscopically bi-modal SNe Ia are not uncommon ([Dong et al. 2015a](#); [Valley et al. 2019](#)). However, these complications are unimportant for our analysis, and we consider these simple velocity approximations adequate.

When applying the continuum fit to each spectrum, we minimize biasing our continuum by using  $3\sigma$  clipping to exclude narrow host galaxy lines, telluric absorption, or instrumental artefacts. After fitting the continuum model to the data, we subtract off this continuum and inspect the residuals for emission line signatures from unbound companion material. For each line in Table 2, we compute  $10\sigma$  bounds on the integrated line flux in each region similar to Eq. 4 from [Leonard & Filippenko \(2001\)](#). However, for flux calibrated spectra,

$$F(10\sigma) \equiv EW(10\sigma) \times C_\lambda = 10C_\lambda \Delta I \sqrt{W_{\text{line}} \Delta X} \quad (2)$$

where  $F(10\sigma)$  is the  $10\sigma$  upper limit on the integrated flux,  $EW(10\sigma)$  is the corresponding upper limit on the equivalent width,  $C_\lambda$  is the continuum flux at wavelength  $\lambda$ , and  $\Delta I$  is the RMS scatter around a normalised continuum. Eq. 2 can be re-written as

$$F(10\sigma) = 10 \Delta f_\lambda \mathcal{F}^{-1} \sqrt{W_{\text{line}} \Delta X} \quad (3)$$

where  $\Delta f_\lambda$  is the  $1\sigma$  RMS scatter of the spectrum around the continuum in flux units ( $\text{erg s}^{-1} \text{cm}^{-2} \text{\AA}^{-1}$ ) and  $\mathcal{F}^{-1}$  is the correction term for masked pixels (see §3.3). Our  $10\sigma$  statistical limit may seem overly conservative but it does correspond to a line profile that would be visibly obvious (e.g., Fig. 3). Additionally, other studies have run injection-recovery tests to determine the true detection threshold for  $\sim 1000 \text{ km s}^{-1}$  emission lines in SNe Ia nebula spectra and a purely statistical  $F(3\sigma)$  is difficult to recover (e.g., [Sand et al. 2018a](#)).

$F(10\sigma)$  is then converted into a luminosity via the distance moduli. Distance moduli computed from the SN Ia light curves are used except where more reliable methods are available, such as Cepheid or Tip of the Red Giant Branch (TRGB) distances. Eq. 3 is inverted to numerically calculate a limit on  $M_{st}$ , which we consider a conservative upper bound on the amount of mass removed from a non-degenerate companion undergoing RLOF. This is done for each H/He line, retaining the best mass limit for both the H-rich and He-rich models. Note that the strictest mass limit for each model can come from different spectra, as each spec-

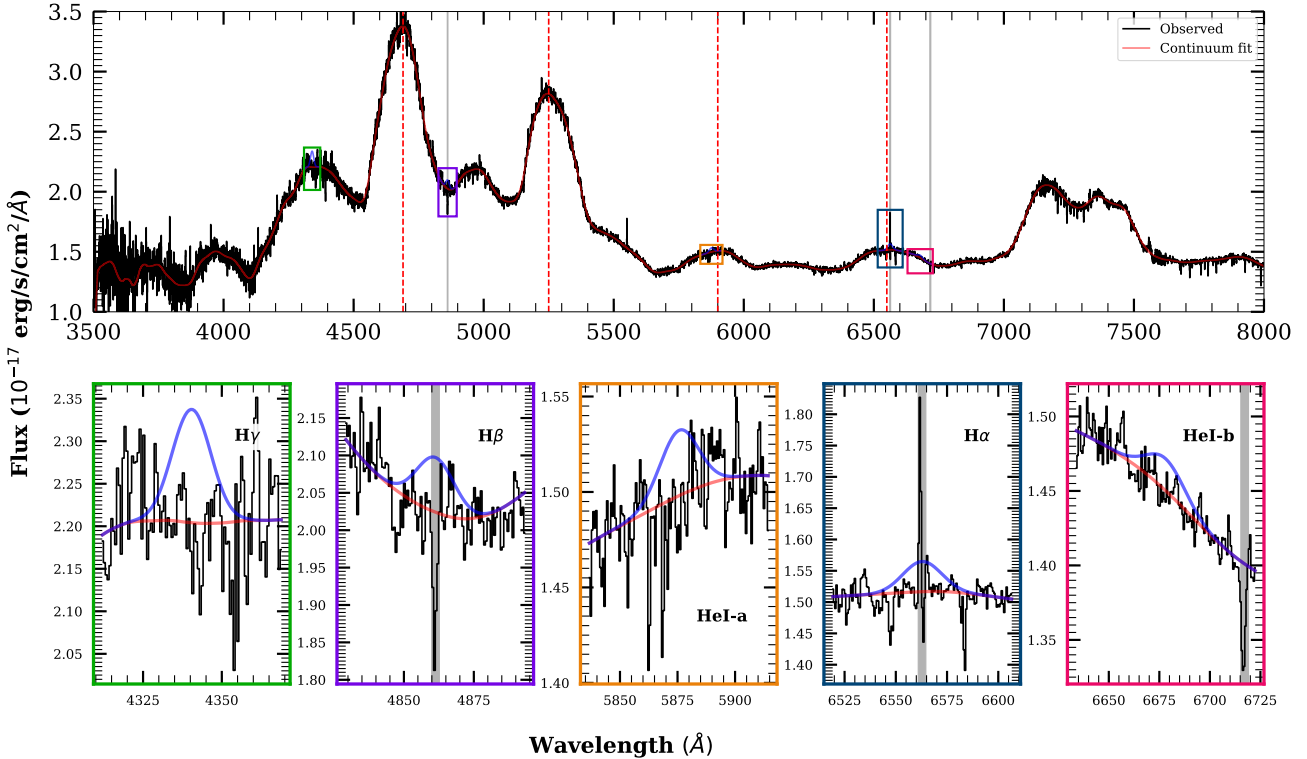


**Figure 2.** Nebular phase spectrum (black), continuum fit (red), and derived  $10\sigma$  flux limits (blue) for the Baade/MagE +295 d spectrum of SN 2015F. The bottom panels show the regions near each possible emission line from Table 2 and correspond to the coloured boxes in the top panel. Gray shaded areas indicate masked spectral regions due to host galaxy contamination or instrumental effects, and vertical dashed lines indicate SNe Ia emission lines used to estimate the smoothing width for each spectrum (see §3). Similar spectral cutouts for all SNe Ia are included as supplementary figures (see Appendix B).

trum will have varying amounts of contamination from host galaxy and telluric lines.

### 3.3 Mitigating Host Galaxy Emission and Other Contaminants

Due to the comprehensive nature of our sample, some spectra have poor quality, significant host-galaxy emission and/or other contaminants. Pixels affected by host galaxy emission, telluric absorption, or instrumental artefacts are masked in the ensuing flux limit calculation, ensuring only informative pixels are used in placing our flux upper limit. Masking these pixels also reduces the effective number of pixels used in the non-detection limit calculation and weakens our statistical limit. In Eq. 3 we include the masked pixel correction term  $\mathcal{F}^{-1}$  from Tucker et al. (2018) to correct our limit to a more robust estimate. Concisely, the correction term  $\mathcal{F}$  is the fraction of unmasked line flux to total line flux ( $\mathcal{F} \in [0, 1]$ ). Thus, masked pixels decrease  $\mathcal{F}$  and increase  $F(10\sigma)$ , but the effect is weighted by the location of the masked pixels relative to the line centre. For example, the masked narrow host galaxy H $\alpha$  and H $\beta$  in the bottom panels of Fig. 2 have larger effects on  $\mathcal{F}$  than the masked [SII] line at 6713 Å since [SII] is on the outskirts of the HeI-a line profile. Masking is only implemented when the derived  $F(10\sigma)$  is not representative of the true flux limit due to contaminated pixels, we leave weak or minor contamination

unmasked as it only solidifies our conservative flux limit and does not introduce extra steps in our analysis.

Another difficulty occurs when the expected emission line is blended with the edge of a steep SN spectral feature. This is especially problematic for 91bg-like and Iax SNe which have intrinsically narrow emission line profiles. If the continuum near H/He varies by more than the amplitude of our flux limit over its FWHM, we increase our flux limit to match the continuum level variation. This results in an unambiguous line profile that would be definitively detected and prevents questionable limits from being included in our statistical analysis.

Some spectra in our study have resolutions of order  $\sim 500 \text{ km s}^{-1}$ , which approaches the lower end of the expected stripped mass velocity distribution (e.g., Boehner et al. 2017). If broad, unresolved H emission was present in a spectrum, we confirm the host galaxy source with other typical galaxy emission lines such as [OII] (3727 Å), [OIII] (4959, 5007 Å), [NII] (6548, 6583 Å), and [SII] (6713, 6731 Å). Any unresolved H $\alpha$  emission with velocity widths  $\gtrsim 300 \text{ km s}^{-1}$  had at least one other unresolved galaxy emission line in the spectrum, indicating the observed H emission was not from stripped material. Additionally, the recent discovery of broad H $\alpha$  emission in ASASSN-18tb (Kollmeier et al. 2019) affirms our treatment of galaxy emission lines, as none of the galaxy emission lines discussed previously were present in the discovery spectrum (see §5).

## 4 RESULTS

We find no evidence of emission from stripped/ablated companion material in any of our nebular phase spectra. Fig. 2 provides an example Baade/MagE spectrum of SN 2015F at +295 days after maximum light, including the observed spectrum, the continuum fit, and the  $10\sigma$  flux limits for each line. We provide a random selection of H $\alpha$  flux limit cutouts in Fig. 3 and the spectral cutouts for all H and He lines are provided as supplementary material.

The distribution of stripped mass limits are shown for the H-rich and the He-rich cases in Figs. 4 and 5, respectively, with colour-shaded regions indicating the expected amounts of stripped mass from various studies in the literature. Fig. 6 shows the H-rich results using the methods and models of Mattila et al. (2005) and Leonard (2007) for comparison with previous estimates. Table B4 gives the phases, flux limits, and derived H-rich and He-rich mass limits for each SN Ia in our study.

We include the range of mass estimates from an H-rich RLOF companion in Figs. 4 and 6 as shaded regions for main-sequence (MS, blue), sub-giant (SG, green), and red giant (RG, red) companions taken from Marietta et al. (2000), Pan et al. (2012), and Boehner et al. (2017). We take  $0.15 M_{\odot}$  as the minimum amount of mass stripped from a companion in the SD scenario, SNe Ia with  $M_{st,H} < 0.15 M_{\odot}$  are considered unlikely to have an H-rich SD progenitor system.

For the He-rich SD channel, only Pan et al. (2012) and Liu et al. (2013a) have published models. We include their expected values for mass stripped from a RLOF helium-star companion in Fig. 5 as the magenta shaded area (Liu et al. 2012) and the cyan line (Pan et al. 2012). However, there are several caveats when considering the He-rich model. The expected line luminosities given in Table 2 are for  $0.25 M_{\odot}$  of stripped He-rich material, more mass than expected for a true He-donor star. We compare our mass limits to the dedicated He-rich models from Pan et al. (2012), Liu et al. (2013a) and take a limit of  $M_{st,He} < 0.023 M_{\odot}$  as our upper limit for He-rich SD systems.

If we assume SNe Ia with  $M_{st,H} < 0.15 M_{\odot}$  and  $M_{st,He} < 0.023 M_{\odot}$  exclude H-rich and He-rich SD progenitor systems, respectively, we can constrain the observed fraction of SD systems. Based on the non-detections in our sample, we can place observed upper limits on the fraction of SD SNe Ia. For a binomial distribution with  $N$  trials and no successes, the upper limit  $f$  at a confidence level  $P$  can be expressed as

$$f < 1 - (1 - P)^{(N+1)^{-1}} \quad (4)$$

with the results for our sample provided in Table 3.  $f_{1\sigma}$  and  $f_{3\sigma}$  correspond to the  $1\sigma$  and  $3\sigma$  fractional upper limits on SD SNe Ia. For our null detections of unbound mass emission, we place statistical constraints on the fraction of SNe Ia that can form through the classical SD scenario for H-rich and He-rich companions. We do not consider SNe Ia with inadequate limits on  $M_{st}$  “successes”, as the spectra do not show any evidence of the expected emission signatures, so these objects are simply omitted from our statistical analysis.

## 5 DISCUSSION

With our updated modelling and comprehensive sample, we place strict constraints on the fraction SNe Ia that can form through the classical SD scenario. At most,  $\sim 6\%$  of SNe Ia can stem from the H-rich formation channel, placing the majority of the production of SNe Ia on the DD channel, unless a modification on the SD scenario can prevent nearly all SNe Ia from exhibiting these expected H and He emission signatures such as the spin-up/spin-down scenario (Di Stefano et al. 2011). Considering the simplest case of only spectroscopically normal SNe Ia, we place a  $1\sigma$  ( $3\sigma$ ) upper limit on SD progenitors of  $< 1.3\%$  ( $< 6.6\%$ ). The full statistical results are provided in Table 3, and we use the *Normal+91T+91bg+SC* sample as the most representative sample from our survey. Unfortunately, our sample prevents an analysis of under- versus over-luminous SNe Ia, as we are biased towards brighter SNe Ia (Fig. 7). This highlights the importance of volume-limited surveys such as 100IAs (Dong et al. 2015a). Still, these stringent constraints on the observed rate of SD SNe Ia provide strong evidence for the DD channel producing the majority of SNe Ia.

Some SNe Ia spectroscopic sub-classes, such as 91T- and 91bg-like, are thought to stem from the same basic mechanism as normal SNe Ia. Because these SNe Ia are thought to be on the edges of typical SN Ia formation, we compare the derived stripped mass limits to the same expected stripped mass values as normal SNe Ia. Our sample has 8 91bg-like and 5 91T-like SNe Ia, for which we place  $1\sigma$  ( $3\sigma$ ) upper limits on H-rich SD progenitors at  $< 12.0\%$  ( $< 48.2\%$ ) and  $< 17.4\%$  ( $< 62.7\%$ ), respectively.

For SNe Iax and “Super Chandrasekhar” (SC) SNe Ia, it is worth discussing their characteristics and applicability. The Iax sub-type (Foley et al. 2013) is thought to stem from an entirely different formation mechanism and appear to never enter a nebular phase but instead have photospheric properties (Foley et al. 2016). Our study includes 4 such systems: SNe 2002cx, 2005hk, 2008A, and 2012Z. Liu et al. (2013b) investigated the expected values of unbound mass for these systems if in a SD system, finding significantly lower values of  $M_{st,H} \approx 0.013 - 0.016 M_{\odot}$  compared to the typical  $\sim 0.1 - 0.5 M_{\odot}$  range. All Iax SNe Ia in our sample have  $M_{st,H} < 0.013 M_{\odot}$ , so the statistics are unchanged if the more stringent mass limit is employed. However, even if material is unbound from non-degenerate donor stars in these SNe Ia, it is still unclear if this material would be visible at late times. For these reasons, our main statistical analysis excludes these objects.

Our sample also includes 4 “Super Chandrasekhar” (SC) SNe Ia explosions (SNe 2006gz, 2007if, 2009dc, and SNF 20080723-012), where the inferred ejecta mass,  $M_{ej}$ , is higher than the Chandrasekhar mass of  $\approx 1.4 M_{\odot}$  (e.g., Howell et al. 2006; Scalzo et al. 2019). The main SD channel formation theory of SC SNe Ia involves a WD above the Chandrasekhar mass spinning rapidly enough to sustain itself from collapse and explosion. The high angular momentum was gained during accretion from a non-degenerate companion onto the WD, which then slows over time and eventually explodes. In some scenarios, the spin-down of the WD is longer than the lifetime of its companion, leading to a SD SN Ia with no stripped mass emission. This mechanism has also been used to explain regular, non-SC SNe Ia (e.g.

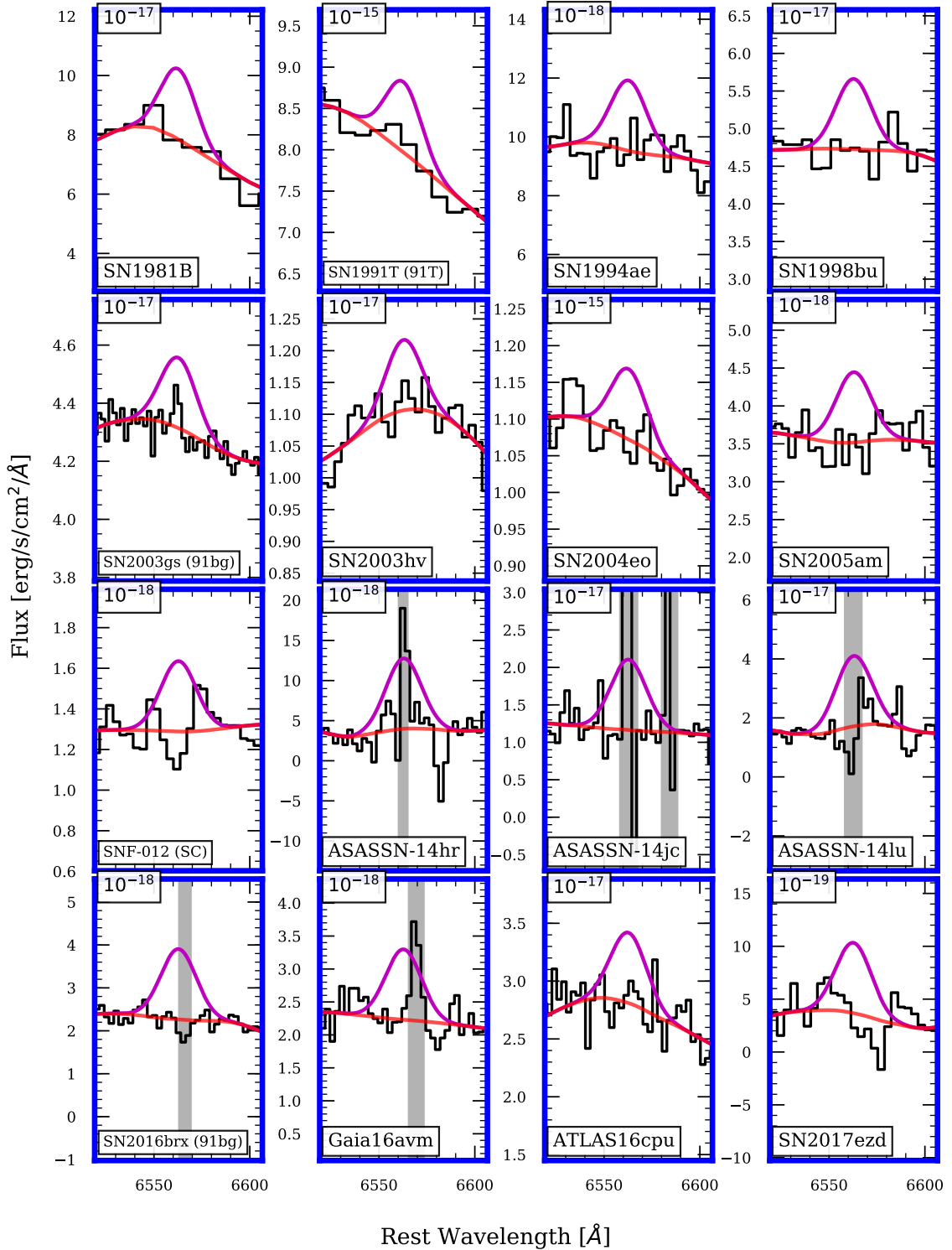


**Figure 3.** Randomly selected cutouts around H $\alpha$  for a portion of the SNe Ia in this work, including the observed spectrum (black), the continuum fit (red), and the empirical  $10\sigma$  line limit (purple). The scale for each spectrum is denoted in the top-left of each panel. Light grey areas mark masked regions (see text) and completely grey boxes signify SNe Ia with no spectra covering the wavelength range. Thick blue axes indicate this spectrum was used for the best  $M_{st}$  limit provided in Table B4. Cutouts for all SNe Ia and all H/He lines are provided as supplementary material (see Appendix B).

**Table 3.** Statistics for each sample considered in our study (see §4).  $N$  is the number of SNe Ia with  $M_{st} < M_{cut}$  and  $f_{n\sigma}$  is the  $n\sigma$  fractional upper limit on their occurrence.  $N_{tot}$  refers to the total number of SNe Ia in that sample.

Sample	$N_{tot}$	H-rich ( $M_{st,H} < 0.15 M_{\odot}$ )			He-rich ( $M_{st,He} < 0.023 M_{\odot}$ )		
		$N$	$f_{1\sigma}$	$f_{3\sigma}$	$N$	$f_{1\sigma}$	$f_{3\sigma}$
<i>Normal</i>	89	85	< 1.3%	< 6.6%	72	< 1.6%	< 7.8%
<i>91T-like</i>	5	5	< 17.4%	< 62.7%	4	< 20.5%	< 69.4%
<i>91bg-like</i>	8	8	< 12.0%	< 48.2%	7	< 13.4%	< 52.3%
<i>SC</i>	4	4	< 20.5%	< 69.4%	4	< 20.5%	< 69.4%
<i>Iax</i>	4	4	< 20.5%	< 69.4%	4	< 20.5%	< 69.4%
<i>Normal+91T</i>	94	90	< 1.3%	< 6.3%	76	< 1.5%	< 7.4%
<i>Normal+91bg</i>	97	93	< 1.2%	< 6.1%	79	< 1.4%	< 7.1%
<i>Normal+91T+91bg</i>	102	98	< 1.2%	< 5.8%	83	< 1.4%	< 6.8%
<i>Normal+91T+91bg+SC</i>	106	102	< 1.1%	< 5.6%	87	< 1.3%	< 6.5%
<i>All</i>	110	106	< 1.1%	< 5.4%	91	< 1.2%	< 6.2%

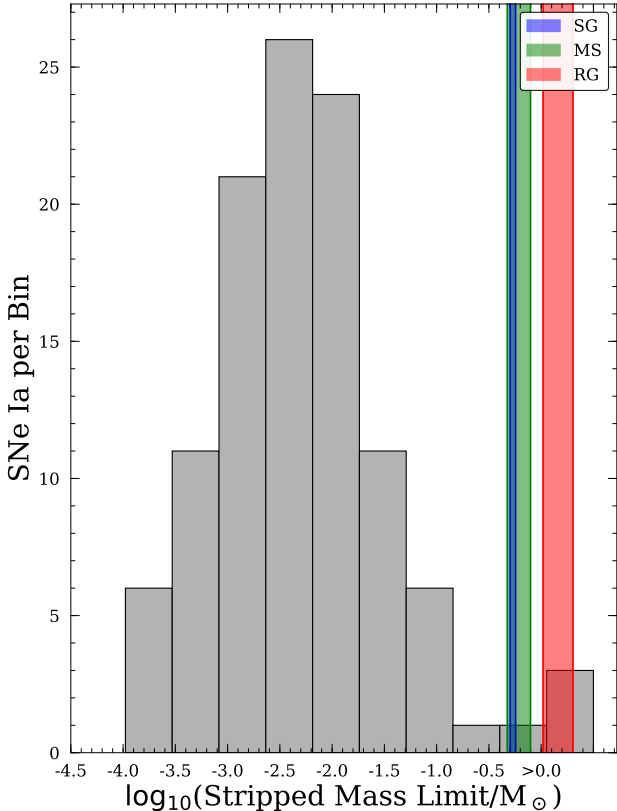


**Figure 4.** Distribution of mass limits on stripped H-rich material for all SNe Ia in our sample. Colour-shaded areas indicate expected amounts of unbound mass for sub-giant (SG, blue), main sequence (MS, green), and red giant (RG, red) companions, taken from Marietta et al. (2000), Pan et al. (2012), and Boehmer et al. (2017).

the spin-up/spin-down scenario, Di Stefano et al. 2011). However, conclusive evidence that the WD *always* outlives the donor star has not been presented, so we include these SNe Ia in our preferred sample.

For completeness and comparison to the literature, we also derive mass limits using the prior models of Marietta et al. (2000) and Mattila et al. (2005) which are shown in Fig. 6. Considering the same preferred *Normal+91T+91bg+SC*

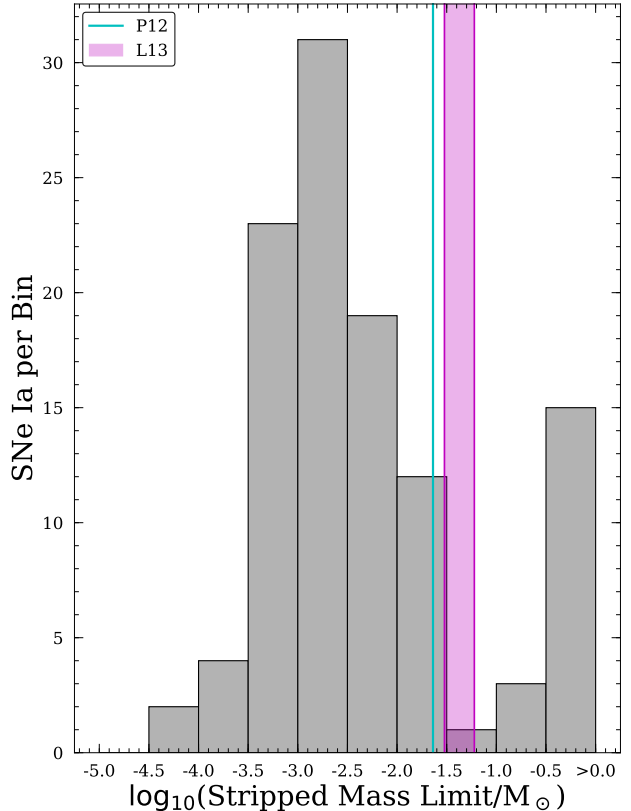


**Figure 5.** Similar to Fig. 4, except for the He-rich model. The magenta shaded region corresponds to stripped mass estimates from Liu et al. (2013a) and the cyan line marks the estimate from Pan et al. (2012).

sample, we still rule out H-rich non-degenerate companions ( $M_{st,H} < 0.15 M_{\odot}$ ) for 60 SNe Ia, corresponding to a  $1\sigma$  ( $3\sigma$ ) fractional upper limit of  $< 1.9\%$  ( $< 9.2\%$ ). This result differs slightly from the upper limit provided in Table 3 due to the assumed linear (instead of exponential) scaling between stripped mass and emitted luminosity (e.g., Leonard 2007). Regardless, the majority of SNe Ia cannot stem from the SD scenario unless there is a systematic flaw or unincorporated physical process shrouding or suppressing the expected emission.

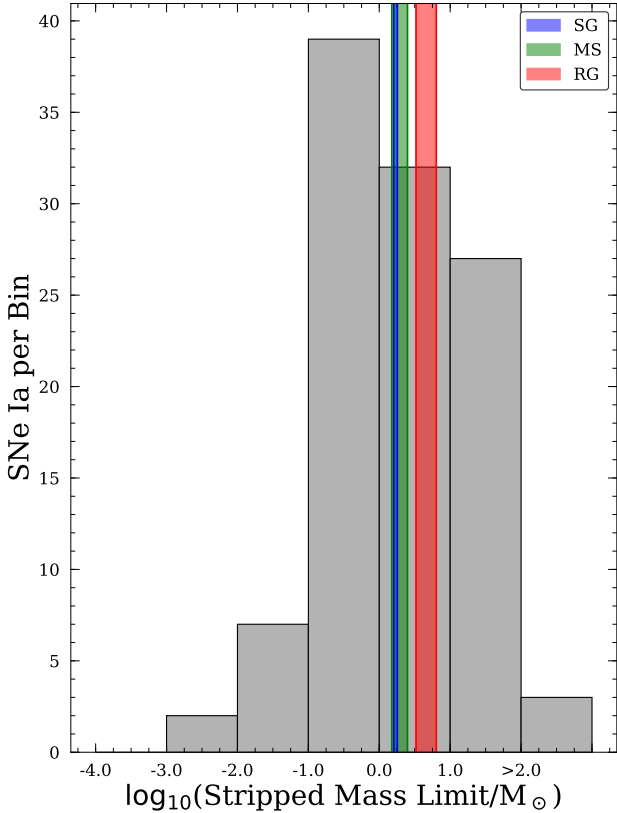


**Figure 6.** Similar to Fig. 4, except using the models of Mattila et al. (2005). The assumed linear scaling between luminosity and stripped mass leads to higher derived  $M_{st}$ .

In addition to the observational limitations discussed in §3, the companion-interaction models are developed for normal SNe Ia. The amount of mass stripped from a RLOF companion for over- and under-luminous SNe Ia may differ from the results of Boehner et al. (2017), although the magnitude of these effects is currently unexplored. Specific stripped mass models exist for Iax SNe (Liu et al. 2013b), but do not exist for the other sub-types included in this paper. Furthermore, quantifying these effects is beyond the scope of this work.

There are other studies which place quantitative or qualitative limits on the fraction of SD progenitor systems using a range of wavelengths and techniques (e.g., Gilfanov & Bogdán 2010; Hayden et al. 2010; Bianco et al. 2011; Brown et al. 2012; Chomiuk et al. 2016, this work). Most of these studies focus on WD+RG systems, as these are the easiest to observationally detect. Each study individually does not definitively rule out SD SNe Ia progenitors, however, when considered as a whole it is clear that most SNe Ia cannot form through the classical SD scenario. Thus, the DD scenario must account for the majority of normal SNe Ia. However, detecting and characterising double WD binaries is exceptionally difficult (e.g., Rebassa-Mansergas et al. 2018). Even accounting for observational difficulties, it is still unclear if the current formulation of the DD channel, including extensions, can provide  $\gtrsim 95\%$  of observed SNe Ia.

At present, there is one exception to the lack of nebular H $\alpha$  emission, ASASSN-18tb (Kollmeier et al. 2019).

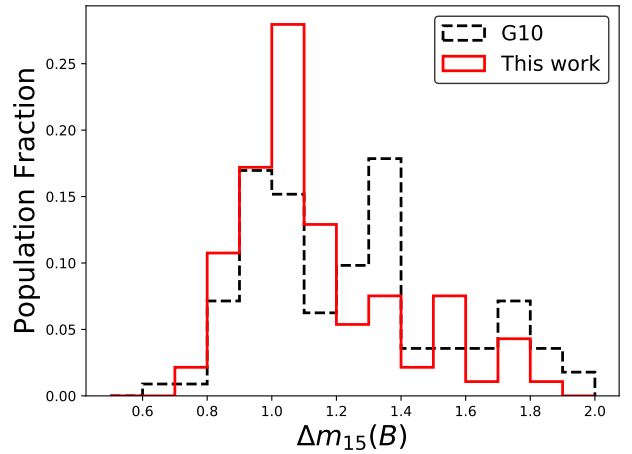


**Figure 7.** Distribution of  $\Delta m_{15}(B)$  in this sample compared to the photometric sample from Ganeshalingam et al. (2010). As expected, the nebular sample is biased towards brighter and broader SNe Ia.

The origin of the emission is unclear, as the observed flux is lower than typical SNe Ia-CSM but the inferred stripped mass value of  $\sim 10^{-3} M_\odot$  is inconsistent with the SD model. However, these models have limitations (see §3) and the current simulations do not investigate the effects of subluminous explosions, which likely produce lower amounts of stripped mass. Late-onset SNe Ia-CSM have also been discovered (Dilday et al. 2012; Graham et al. 2019) and the velocity width of H $\alpha$  emission increases with time in these systems, indicating this could also be similar to CSM objects although a SD progenitor system is definitely possible. Regardless, the true origin of the H $\alpha$  observed in ASASSN-18tb is unknown and the early spectrum ( $\sim +140$  d) lies outside the temporal bounds of our study ( $200$  d  $\leq (t - t_0) \leq 500$  d). Thus, we cannot include this object in our statistical analysis, although if this unique object is not a member of the SNe Ia-CSM class this discovery highlights the inherent rarity of such SNe Ia.

In summary, we find no evidence of emission from stripped/ablated companion material in any of nebular phase spectra. With this null result, we calculate the upper limit on the fraction of SNe Ia that can form through the SD channel for both H-rich and He-rich companions. At  $3\sigma$  confidence, we find H-rich companions are restricted to  $< 5.6\%$  and He-rich companions restricted to  $< 6.5\%$ . These results provide strict constraints on the SD channel of SNe Ia formation, requiring  $\gtrsim 95\%$  of SNe Ia to stem from the DD channel.

*Facilities:* duPont, Magellan, Very Large Telescope  
*Software:* Python2.7, astropy (The Astropy Collaboration et al. 2018), astroquery (Ginsburg et al. 2019) numpy, scipy, PyMUSE (Pessa et al. 2018), SpectRes (Carnall 2017), extinction<sup>15</sup>, SExtractor (Bertin & Arnouts 1996), Montage<sup>16</sup>, Lpipe, IDL8.6, LowRedux, IRAF, SNooPy (Burns et al. 2011)

<sup>15</sup> <https://github.com/kbarbary/extinction>

<sup>16</sup> <http://montage.ipac.caltech.edu/>

## ACKNOWLEDGEMENTS

We thank K. Maguire, K. Graham, K. Motohara, K. Maeda, S. Taubenberger, T. Diamond, G. Dimitriadis, C. Ashall, and D. Sand for supplying nebular spectra. We thank A. Laity for assisting with the KOA data search and retrieval. Additionally, we thank C. Auge, G. Anand, A. Payne, and O. Graur for useful conversations about the project. We thank P. Chen from providing several SNe Ia light curves prior to publication.

M.A.T. acknowledges support from the United States Department of Energy through the Computational Sciences Graduate Fellowship (DOE CSGF). M.D.S. is supported in part by a generous grant (13261) from VILLUM FONDEN and a project grant from the Independent Research Fund Denmark. Support for J.L.P. is provided in part by FONDECYT through the grant 1191038 and by the Ministry of Economy, Development, and TourismâŽs Millennium Science Initiative through grant IC120009, awarded to The Millennium Institute of Astrophysics, MAS.

This work is Based on (in part) observations collected at the European Organisation for Astronomical Research in the Southern Hemisphere under ESO programmes 0100.D-0191(A), 0101.D-0173(A), 0102.D-0287(A), and 096.D-0296(A). This paper includes data gathered with the 6.5 meter Magellan Telescopes located at Las Campanas Observatory, Chile. The CSP has been supported by the National Science Foundation under grants AST0306969, AST0607438, AST1008343, AST1613426, and AST1613472.

This paper made use of the modIDL spectral data reduction reduction pipeline developed in part with funds provided by NSF Grant AST-1108693.

This research made use of Montage. It is funded by the National Science Foundation under Grant Number ACI-1440620, and was previously funded by the National Aeronautics and Space Administration's Earth Science Technology Office, Computation Technologies Project, under Cooperative Agreement Number NCC5-626 between NASA and the California Institute of Technology.

This work has made use of data from the European Space Agency (ESA) mission *Gaia* (<https://www.cosmos.esa.int/gaia>), processed by the *Gaia* Data Processing and Analysis Consortium (DPAC, <https://www.cosmos.esa.int/web/gaia/dpac/consortium>). Funding for the DPAC has been provided by national institutions, in particular the institutions participating in the *Gaia* Multilateral Agreement.

The Pan-STARRS1 Surveys (PS1) and the PS1 public science archive have been made possible through contributions by the Institute for Astronomy, the University of Hawaii, the Pan-STARRS Project Office, the Max-Planck Society and its participating institutes, the Max Planck Institute for Astronomy, Heidelberg and the Max Planck Institute for Extraterrestrial Physics, Garching, The Johns Hopkins University, Durham University, the University of Edinburgh, the Queen's University Belfast, the Harvard-Smithsonian Center for Astrophysics, the Las Cumbres Observatory Global Telescope Network Incorporated, the National Central University of Taiwan, the Space Telescope Science Institute, the National Aeronautics and Space Administration under Grant No. NNX08AR22G issued through the Planetary Science Division of the NASA Science Mis-

sion Directorate, the National Science Foundation Grant No. AST-1238877, the University of Maryland, Eotvos Lorand University (ELTE), the Los Alamos National Laboratory, and the Gordon and Betty Moore Foundation.

Based on observations obtained at the Gemini Observatory acquired through the Gemini Observatory Archive and processed with the Gemini PyRAF package, which is operated by the Association of Universities for Research in Astronomy, Inc., under a cooperative agreement with the NSF on behalf of the Gemini partnership: the National Science Foundation (United States), the National Research Council (Canada), CONICYT (Chile), Ministerio de Ciencia, Tecnología e Innovación Productiva (Argentina), and Ministério da Ciência, Tecnologia e Inovação (Brazil).

This paper makes use of data obtained from the Isaac Newton Group of Telescopes Archive which is maintained as part of the CASU Astronomical Data Centre at the Institute of Astronomy, Cambridge.

The LBT is an international collaboration among institutions in the United States, Italy and Germany. LBT Corporation partners are: The University of Arizona on behalf of the Arizona Board of Regents; Istituto Nazionale di Astrofisica, Italy; LBT Beteiligungsgesellschaft, Germany, representing the Max-Planck Society, The Leibniz Institute for Astrophysics Potsdam, and Heidelberg University; The Ohio State University, and The Research Corporation, on behalf of The University of Notre Dame, University of Minnesota and University of Virginia.

## REFERENCES

- Abazajian K., et al., 2005, *AJ*, **129**, 1755
- Abolfathi B., et al., 2018, *The Astrophysical Journal Supplement Series*, **235**, 42
- Adelman-McCarthy J. K., et al., 2008, *The Astrophysical Journal Supplement Series*, **175**, 297
- Akerlof C., et al., 2007, *Central Bureau Electronic Telegrams*, **1059**, 2
- Aksenov E. P., 1981, *International Astronomical Union Circular*, **3580**, 1
- Altavilla G., et al., 2004, *MNRAS*, **349**, 1344
- Amanullah R., et al., 2014, *ApJ*, **788**, L21
- Andersen J., et al., 1995, *The Messenger*, **79**, 12
- Angel J. R. P., et al., 1979, in *The MMT and the Future of Ground-Based Astronomy, Proceedings of a Symposium held to mark the dedication of the Multiple Mirror Telescope at the Mount Hopkins Observatory, Arizona on May 9, 1979*. Edited by Trevor C. Weekes. SAO Special Report #385, 1979., p.87. p. 87
- Antognini J. M., et al., 2014, *MNRAS*, **439**, 1079
- Anupama G. C., et al., 2005, *A&A*, **429**, 667
- Appenzeller I., et al., 1998, *The Messenger*, **94**, 1
- Arbour R., et al., 1999, *International Astronomical Union Circular*, **7156**, 1
- Arbour R., et al., 2004, *International Astronomical Union Circular*, **8406**, 1
- Arcavi I., et al., 2014, *The Astronomer's Telegram*, **6661**, 1
- Ardeberg A., et al., 1973, *A&A*, **28**, 295
- Argyle R. W., et al., 1994, *International Astronomical Union Circular*, **5976**, 3
- Armstrong M., et al., 1999, *International Astronomical Union Circular*, **7108**, 1
- Ayani K., et al., 1998, *International Astronomical Union Circular*, **6878**, 2

- Ayani K., et al., 1998, International Astronomical Union Circular, [6905](#), 1
- Bacon R., et al., 2010, in Proceedings of the SPIE, Volume 7735, id. 773508 (2010).., doi:[10.1117/12.856027](#)
- Barbon R., et al., 1972, International Astronomical Union Circular, [2411](#), 1
- Barbon R., et al., 1982, A&A, [116](#), 35
- Barbon R., et al., 1990, A&A, [237](#), 79
- Benetti S., et al., 1995, International Astronomical Union Circular, [6135](#), 1
- Benetti S., et al., 2004, MNRAS, [348](#), 261
- Benetti S., et al., 2017, The Astronomer's Telegram, [11036](#), 1
- Benn C., et al., 2008, in Ground-based and Airborne Instrumentation for Astronomy II. Edited by McLean, Ian S.; Casali, Mark M. Proceedings of the SPIE, Volume 7014, article id. 70146X, 12 pp. (2008).., doi:[10.1117/12.788694](#)
- Bertin E., et al., 1996, *Astronomy and Astrophysics Supplement Series*, [117](#), 393
- Beutler B., et al., 2003, International Astronomical Union Circular, [8197](#), 1
- Bianco F. B., et al., 2011, ApJ, [741](#), 20
- Blanco V. M., et al., 1980, International Astronomical Union Circular, [3556](#), 2
- Blanco V. M., et al., 1986, International Astronomical Union Circular, [4224](#), 1
- Blondin S., et al., 2008, Central Bureau Electronic Telegrams, [1198](#), 1
- Blondin S., et al., 2012, AJ, [143](#)
- Boehner P., et al., 2017, MNRAS, [465](#), 2060
- Botyánszki J., et al., 2017, ApJ, [845](#)
- Botyánszki J., et al., 2018, ApJ, [852](#)
- Branch D., et al., 1983, ApJ, [270](#), 123
- Branch D., et al., 1993, AJ, [106](#), 2383
- Breare J. M., et al., 1987, MNRAS, [227](#), 909
- Brimacombe J., et al., 2011, Central Bureau Electronic Telegrams, [2928](#), 1
- Brimacombe J., et al., 2014a, The Astronomer's Telegram, [6737](#), 1
- Brimacombe J., et al., 2014b, The Astronomer's Telegram, [6803](#), 1
- Brimacombe J., et al., 2015, The Astronomer's Telegram, [6950](#), 1
- Brimacombe J., et al., 2016, The Astronomer's Telegram, [8979](#), 1
- Brimacombe J., et al., 2017, The Astronomer's Telegram, [10108](#), 1
- Brimacombe J., et al., 2018, The Astronomer's Telegram, [11521](#), 1
- Brown P. J., et al., 2012, ApJ, [749](#)
- Brown P. J., et al., 2014, Ap&SS, [354](#), 89
- Brown P. J., et al., 2015, ApJ, [805](#), 74
- Brown J. S., et al., 2016, The Astronomer's Telegram, [9666](#), 1
- Brown J. S., et al., 2018, The Astronomer's Telegram, [11253](#), 1
- Buckley D. A. H., et al., 2006, in Society of Photo-Optical Instrumentation Engineers (SPIE) Conference Series. p. 62690A, doi:[10.1117/12.673838](#)
- Bues I., et al., 1986, International Astronomical Union Circular, [4215](#), 2
- Bureau M., et al., 1996, ApJ, [463](#), 60
- Burns C. R., et al., 2011, AJ, [141](#)
- Burns C. R., et al., 2014, ApJ, [789](#), 32
- Busko I., et al., 1981, International Astronomical Union Circular, [3589](#), 2
- Buta R. J., et al., 1983, *Publications of the Astronomical Society of the Pacific*, [95](#), 72
- Buzzoni B., et al., 1984, The Messenger, [38](#), 9
- Cacella P., et al., 2002, International Astronomical Union Circular, [7847](#), 1
- Canal R., et al., 2001, ApJ, [550](#), L53
- Candia P., et al., 2003, *Publications of the Astronomical Society of the Pacific*, [115](#), 277
- Cappellari M., et al., 2011, MNRAS, [413](#), 813
- Cappellaro E., et al., 2001, ApJ, [549](#), L215
- Carnall A. C., 2017, preprint, p. arXiv:[1705.05165](#) (arXiv:1705.05165)
- Casper C., et al., 2013, Central Bureau Electronic Telegrams, [3588](#), 1
- Catinella B., et al., 2005, AJ, [130](#), 1037
- Cenko S. B., et al., 2011, The Astronomer's Telegram, [3583](#), 1
- Cenko S. B., et al., 2012, Central Bureau Electronic Telegrams, [3014](#), 1
- Cepa J., 2010, *Astrophysics and Space Science Proceedings*, [14](#), 15
- Challis P., et al., 2009, Central Bureau Electronic Telegrams, [2025](#), 1
- Chambers K. C., et al., 2016, preprint, p. arXiv:[1612.05560](#) (arXiv:1612.05560)
- Childress M. J., et al., 2015, MNRAS, [454](#), 3816
- Childress M. J., et al., 2016, *Publications of the Astronomical Society of Australia*, [33](#), e055
- Chomiuk L., et al., 2016, ApJ, [821](#), 119
- Chornock R., et al., 2000, International Astronomical Union Circular, [7463](#), 1
- Christensen L., et al., 2003, A&A, [401](#), 479
- Colless M., et al., 2003, arXiv e-prints, pp astro-ph/0306581
- Collobert M., et al., 2006, MNRAS, [370](#), 1213
- Contreras C., et al., 2010, AJ, [139](#), 519
- Corsini E. M., et al., 2003, ApJ, [599](#), L29
- Cortini G., et al., 2014, Central Bureau Electronic Telegrams, [3911](#), 1
- Cousins A. W. J., 1972, Information Bulletin on Variable Stars, [700](#), 1
- Cox L., et al., 2010, Central Bureau Electronic Telegrams, [2612](#), 1
- Cox L., et al., 2011, Central Bureau Electronic Telegrams, [2676](#), 1
- Cragg T., et al., 1981, International Astronomical Union Circular, [3583](#), 1
- Cristiani S., et al., 1992, A&A, [259](#), 63
- Cumming R. J., et al., 1994, International Astronomical Union Circular, [5951](#), 1
- D'Odorico S., 1990, The Messenger, [61](#), 51
- D'Onofrio M., et al., 1995, A&A, [296](#), 319
- Delgado A., et al., 2016, Transient Name Server Discovery Report, [2016-485](#), 1
- Di Stefano R., et al., 2011, ApJ, [738](#), L1
- Dilday B., et al., 2012, Science, [337](#), 942
- Dimitriadis G., et al., 2014, The Astronomer's Telegram, [6749](#), 1
- Dimitriadis G., et al., 2019, ApJ, [870](#), L14
- Dong S., et al., 2015a, MNRAS, [454](#), L61
- Dong S., et al., 2015b, The Astronomer's Telegram, [7447](#), 1
- Dong S., et al., 2018a, MNRAS, [479](#), L70
- Dong S., et al., 2018b, The Astronomer's Telegram, [11346](#), 1
- Dopita M., et al., 2007, Ap&SS, [310](#), 255
- Dopita M., et al., 2010, Ap&SS, [327](#), 245
- Downes D., et al., 1993, ApJ, [414](#), L13
- Drake A. J., et al., 2011a, Central Bureau Electronic Telegrams, [2636](#), 1
- Drake A. J., et al., 2011b, Central Bureau Electronic Telegrams, [2703](#), 1
- Drescher C., et al., 2012, Central Bureau Electronic Telegrams, [3346](#), 1
- Dressler A., et al., 2003, International Astronomical Union Circular, [8198](#), 2
- Dressler A., et al., 2011, *Publications of the Astronomical Society of the Pacific*, [123](#), 288
- Elias J. H., et al., 1983, ApJ, [268](#), 718

- Elias-Rosa N., et al., 2005, International Astronomical Union Circular, [8479](#), 3
- Elias-Rosa N., et al., 2006, *MNRAS*, [369](#), 1880
- Epinat B., et al., 2008, *MNRAS*, [388](#), 500
- Evans R., et al., 1986, International Astronomical Union Circular, [4208](#), 1
- Evans R., et al., 2003, International Astronomical Union Circular, [8171](#), 1
- Evans D. W., et al., 2018, preprint, p. [arXiv:1804.09368](#) ([arXiv:1804.09368](#))
- Everson R. W., et al., 2017, The Astronomer's Telegram, [10518](#), 1
- Faber S. M., et al., 2003, in Instrument Design and Performance for Optical/Infrared Ground-based Telescopes. Edited by Iye, Masanori; Moorwood, Alan F. M. Proceedings of the SPIE, Volume 4841, pp. 1657–1669 (2003).. pp 1657–1669, doi:[10.1117/12.460346](#)
- Fabricant D., et al., 1998, *Publications of the Astronomical Society of the Pacific*, [110](#), 79
- Falco E. E., et al., 1999, *Publications of the Astronomical Society of the Pacific*, [111](#), 438
- Feast M. W., et al., 1986, International Astronomical Union Circular, [4210](#), 1
- Filippenko A. V., et al., 1999, International Astronomical Union Circular, [7108](#), 2
- Filippenko A. V., et al., 2007, Central Bureau Electronic Telegrams, [1101](#), 1
- Fink M., et al., 2010, *A&A*, [514](#), A53
- Firth R. E., et al., 2015, *MNRAS*, [446](#), 3895
- Fitzpatrick E. L., 1999, *Publications of the Astronomical Society of the Pacific*, [111](#), 63
- Flewelling H. A., et al., 2016, preprint, p. [arXiv:1612.05243](#) ([arXiv:1612.05243](#))
- Folatelli G., et al., 2010a, *AJ*, [139](#), 120
- Folatelli G., et al., 2010b, Central Bureau Electronic Telegrams, [2390](#), 1
- Folatelli G., et al., 2013, *ApJ*, [773](#)
- Foley R. J., et al., 2013, *ApJ*, [767](#), 57
- Foley R. J., et al., 2014, *MNRAS*, [443](#), 2887
- Foley R. J., et al., 2015, *ApJ*, [798](#), L37
- Foley R. J., et al., 2016, *MNRAS*, [461](#), 433
- Foley R. J., et al., 2018, *MNRAS*, [475](#), 193
- Ford C. H., et al., 1993, *AJ*, [106](#), 1101
- Fossey S. J., et al., 2014, Central Bureau Electronic Telegrams, [3792](#), 1
- Freudling W., et al., 2013, *A&A*, [559](#), A96
- Friedman A. S., et al., 2015, *The Astrophysical Journal Supplement Series*, [220](#)
- Frieman J., et al., 2006, International Astronomical Union Circular, [8754](#), 1
- Frohmaier C., et al., 2015, The Astronomer's Telegram, [7452](#), 1
- Frye R., et al., 1972, International Astronomical Union Circular, [2398](#), 1
- Fukugita M., et al., 1996, *AJ*, [111](#), 1748
- Gagliano R., et al., 2016, Transient Name Server Discovery Report, [2016-761](#), 1
- Gagliano R., et al., 2017, Transient Name Server Discovery Report, [2017-961](#), 1
- Gaia Collaboration et al., 2016, *A&A*, [595](#), A1
- Gaia Collaboration et al., 2018, preprint, p. [arXiv:1804.09365](#) ([arXiv:1804.09365](#))
- Galbany L., et al., 2014, *A&A*, [572](#), A38
- Galbany L., et al., 2016, *MNRAS*, [457](#), 525
- Gall C., et al., 2018, *A&A*, [611](#), A58
- Ganeshalingam M., et al., 2010, *The Astrophysical Journal Supplement Series*, [190](#), 418
- Gao J., et al., 2015, *ApJ*, [807](#), L26
- Garnavich P. M., et al., 2004, *ApJ*, [613](#), 1120
- Garradd G. J., et al., 1996, International Astronomical Union Circular, [6380](#), 1
- Gaskell C. M., et al., 1989, International Astronomical Union Circular, [4761](#), 2
- Gerardy C., et al., 1999, International Astronomical Union Circular, [7158](#), 2
- Gilfanov M., et al., 2010, *Nature*, [463](#), 924
- Gilmore A. C., 1991, International Astronomical Union Circular, [5309](#), 3
- Ginsburg A., et al., 2019, arXiv e-prints, p. [arXiv:1901.04520](#)
- Giovanelli R., et al., 1997, *AJ*, [113](#), 22
- Gomez G., et al., 1996, *AJ*, [112](#), 2094
- Gonzalez S., et al., 2004, International Astronomical Union Circular, [8409](#), 2
- Goobar A., et al., 2014, *ApJ*, [784](#)
- Graham D. A., et al., 1978, *A&A*, [70](#), L69
- Graham A. W., et al., 1998, *Astronomy and Astrophysics Supplement Series*, [133](#), 325
- Graham M. L., et al., 2017, *MNRAS*, [472](#), 3437
- Graham M. L., et al., 2019, *ApJ*, [871](#), 62
- Grogan N. A., et al., 1998, *The Astrophysical Journal Supplement Series*, [119](#), 277
- Guillochon J., et al., 2017, *ApJ*, [835](#)
- Guthrie B. N. G., et al., 1996, *A&A*, [310](#), 353
- Gutiérrez C. P., et al., 2016, *A&A*, [590](#), A5
- Halevi G., et al., 2016, The Astronomer's Telegram, [9309](#), 1
- Hamuy M., et al., 1991, *AJ*, [102](#), 208
- Hamuy M., et al., 1996, *AJ*, [112](#), 2408
- Hamuy M., et al., 2006, *Publications of the Astronomical Society of the Pacific*, [118](#), 2
- Harutyunyan A., et al., 2009, Central Bureau Electronic Telegrams, [1768](#), 1
- Hayden B. T., et al., 2010, *ApJ*, [722](#), 1691
- Heraudeau P., et al., 1994, International Astronomical Union Circular, [5952](#), 3
- Herbig G. H., et al., 1972, International Astronomical Union Circular, [2407](#), 1
- Hernandez M., et al., 2000, *MNRAS*, [319](#), 223
- Hicken M., et al., 2007, *ApJ*, [669](#), L17
- Hicken M., et al., 2009, *ApJ*, [700](#), 331
- Hicken M., et al., 2012, *The Astrophysical Journal Supplement Series*, [200](#)
- Ho W. C. G., et al., 2001, *Publications of the Astronomical Society of the Pacific*, [113](#), 1349
- Höflich P., et al., 2004, *ApJ*, [617](#), 1258
- Holberg J., et al., 1991, International Astronomical Union Circular, [5270](#), 3
- Holmbo S., et al., 2018, arXiv e-prints, p. [arXiv:1809.01359](#)
- Holoien T. W. S., et al., 2014, The Astronomer's Telegram, [6637](#), 1
- Holoien T. W. S., et al., 2017a, *MNRAS*, [464](#), 2672
- Holoien T. W. S., et al., 2017b, *MNRAS*, [467](#), 1098
- Holoien T. W. S., et al., 2017c, *MNRAS*, [471](#), 4966
- Holoien T. W. S., et al., 2019, *MNRAS*, p. 93
- Holtzman J. A., et al., 2008, *AJ*, [136](#), 2306
- Hook I. M., et al., 2004, *Publications of the Astronomical Society of the Pacific*, [116](#), 425
- Hosseinzadeh G., et al., 2017a, The Astronomer's Telegram, [10164](#), 1
- Hosseinzadeh G., et al., 2017b, The Astronomer's Telegram, [10639](#), 1
- Howell D. A., et al., 2006, *Nature*, [443](#), 308
- Howerton S., et al., 2011, Central Bureau Electronic Telegrams, [2658](#), 1
- Howerton S., et al., 2013, Central Bureau Electronic Telegrams, [3533](#), 1
- Hoyle F., et al., 1960, *ApJ*, [132](#), 565

- Huchra J. P., et al., 1999, *The Astrophysical Journal Supplement Series*, **121**, 287
- Hurst G. M., et al., 1998, International Astronomical Union Circular, **6875**, 1
- Hutchings D., et al., 2002, International Astronomical Union Circular, **7918**, 1
- Iben I., et al., 1984, *The Astrophysical Journal Supplement Series*, **54**, 335
- Iijima T., et al., 1994, International Astronomical Union Circular, **6108**, 1
- Inserra C., et al., 2013, *ApJ*, **770**
- Itagaki K., et al., 2014, Central Bureau Electronic Telegrams, **3792**, 2
- Jha S., et al., 1999, *The Astrophysical Journal Supplement Series*, **125**, 73
- Jha S., et al., 2006, *AJ*, **131**, 527
- Jha S. W., et al., 2017, The Astronomer's Telegram, **10261**, 1
- Jones D. H., et al., 2006, *MNRAS*, **369**, 25
- Jones D. H., et al., 2009, *MNRAS*, **399**, 683
- Jones S., et al., 2017, The Astronomer's Telegram, **11092**, 1
- Jorden P. R., 1990, in Proc. SPIE Vol. 1235, p. 790–798, Instrumentation in Astronomy VII, David L. Crawford; Ed.. pp 790–798, doi:10.1117/12.19163
- Kand rashoff M., et al., 2012, Central Bureau Electronic Telegrams, **3111**, 1
- Karamehmetoglu E., et al., 2015, The Astronomer's Telegram, **7476**, 1
- Kasen D., 2010, *ApJ*, **708**, 1025
- Kashikawa N., et al., 2002, *Publications of the Astronomical Society of Japan*, **54**, 819
- Katz B., et al., 2012, preprint, p. arXiv:1211.4584 (arXiv:1211.4584)
- Kawakita H., et al., 2002, International Astronomical Union Circular, **7848**, 2
- Kelson D. D., 2003, *Publications of the Astronomical Society of the Pacific*, **115**, 688
- Kelson D. D., et al., 2000, *ApJ*, **531**, 159
- Kent B. R., et al., 2008, *AJ*, **136**, 713
- Khan R., et al., 2011, *ApJ*, **726**, 106
- Kim H., et al., 2013, Central Bureau Electronic Telegrams, **3743**, 1
- Kirshner R. P., et al., 1975, *ApJ*, **200**, 574
- Kirshner R., et al., 1991, International Astronomical Union Circular, **5403**, 2
- Kirshner R. P., et al., 1993, *ApJ*, **415**, 589
- Kiyota S., et al., 2014a, The Astronomer's Telegram, **6594**, 1
- Kiyota S., et al., 2014b, The Astronomer's Telegram, **6683**, 1
- Kiyota S., et al., 2014c, The Astronomer's Telegram, **6802**, 1
- Kiyota S., et al., 2014d, The Astronomer's Telegram, **6809**, 1
- Kleiser I., et al., 2009, Central Bureau Electronic Telegrams, **1918**, 1
- Klotz A., et al., 2012, Central Bureau Electronic Telegrams, **3277**, 2
- Kollmeier J. A., et al., 2019, arXiv e-prints, p. arXiv:1902.02251
- Koribalski B. S., et al., 2004, *AJ*, **128**, 16
- Kosai H., et al., 1991, International Astronomical Union Circular, **5400**, 1
- Kotak R., et al., 2003a, International Astronomical Union Circular, **8099**, 1
- Kotak R., et al., 2003b, International Astronomical Union Circular, **8122**, 3
- Kotak R., et al., 2005, *A&A*, **436**, 1021
- Kowal C. T., 1972, International Astronomical Union Circular, **2405**, 1
- Kowalski M., et al., 2008, *ApJ*, **686**
- Krisciunas K., et al., 2000, *ApJ*, **539**, 658
- Krisciunas K., et al., 2003, *AJ*, **125**, 166
- Krisciunas K., et al., 2004, *AJ*, **128**, 3034
- Krisciunas K., et al., 2007, *AJ*, **133**, 58
- Krisciunas K., et al., 2009, *AJ*, **138**, 1584
- Krisciunas K., et al., 2017, *AJ*, **154**, 211
- Kromer M., et al., 2010, *ApJ*, **719**, 1067
- Krumm N., et al., 1980, *AJ*, **85**, 1312
- Lair J. C., et al., 2006, *AJ*, **132**, 2024
- Lanz T., et al., 2005, *ApJ*, **619**, 517
- Lauberts A., et al., 1989, The surface photometry catalogue of the ESO-Uppsala galaxies
- Lavery R. J., 1989, International Astronomical Union Circular, **4743**, 2
- Leadbeater R., 2016, Transient Name Server Classification Report, **2016-793**, 1
- Leadbeater R., 2018, Transient Name Server Classification Report, **2018-159**, 1
- Lee T. A., et al., 1972, *ApJ*, **177**, L59
- Leibengut B., et al., 1993, *AJ*, **105**, 301
- Leloudas G., et al., 2009, *A&A*, **505**, 265
- Leonard D. C., 2007, *ApJ*, **670**, 1275
- Leonard D. C., et al., 2001, *Publications of the Astronomical Society of the Pacific*, **113**, 920
- Li W. D., et al., 1999, *AJ*, **117**, 2709
- Li W., et al., 2001, *Publications of the Astronomical Society of the Pacific*, **113**, 1178
- Li W., et al., 2003a, *Publications of the Astronomical Society of the Pacific*, **115**, 453
- Li W., et al., 2003b, International Astronomical Union Circular, **8245**, 1
- Liller W., et al., 1992, International Astronomical Union Circular, **5431**, 3
- Liller W., et al., 1992, International Astronomical Union Circular, **5428**, 1
- Lira P., et al., 1998, *AJ*, **115**, 234
- Liu Z. W., et al., 2012, *A&A*, **548**, A2
- Liu Z.-W., et al., 2013a, *ApJ*, **774**, 37
- Liu Z.-W., et al., 2013b, *ApJ*, **778**, 121
- Livio M., et al., 2018, *Phys. Rep.*, **736**, 1
- Livne E., 1990, *ApJ*, **354**, L53
- Livne E., et al., 1995, *ApJ*, **452**, 62
- Longhetti M., et al., 1998, *Astronomy and Astrophysics Supplement Series*, **130**, 251
- Lundqvist P., et al., 2013, *MNRAS*, **435**, 329
- Lundqvist P., et al., 2015, *A&A*, **577**, A39
- Maeda K., et al., 2009, *ApJ*, **690**, 1745
- Maguire K., et al., 2014, *MNRAS*, **444**, 3258
- Maguire K., et al., 2016, *MNRAS*, **457**, 3254
- Maguire K., et al., 2018, *MNRAS*, **477**, 3567
- Malesani D., et al., 2018, The Astronomer's Telegram, **11516**, 1
- Maoz D., et al., 2014, *Annual Review of Astronomy and Astrophysics*, **52**, 107
- Marietta E., et al., 2000, *The Astrophysical Journal Supplement Series*, **128**, 615
- Marion G. H., et al., 2012, Central Bureau Electronic Telegrams, **3146**, 2
- Marshall J. L., et al., 2008, in Ground-based and Airborne Instrumentation for Astronomy II. Edited by McLean, Ian S.; Casali, Mark M. Proceedings of the SPIE, Volume 7014, article id. 701454, 10 pp. (2008).., doi:10.1117/12.789972
- Martin R., et al., 2004, International Astronomical Union Circular, **8282**, 1
- Martin R., et al., 2005, International Astronomical Union Circular, **8490**, 1
- Matheson T., et al., 2002, International Astronomical Union Circular, **7903**, 2
- Matheson T., et al., 2008, *AJ*, **135**, 1598
- Mathewson D. S., et al., 1992, *The Astrophysical Journal Supplement Series*, **81**, 413
- Mattila S., et al., 2005, *A&A*, **443**, 649

- Mattila S., et al., 2016, The Astronomer's Telegram, [8992](#), 1
- Maury A., et al., 1990, International Astronomical Union Circular, [5039](#), 1
- Maza J., et al., 2010, Central Bureau Electronic Telegrams, [2388](#), 1
- Mazzali P. A., et al., 2015, *MNRAS*, [450](#), 2631
- McCully C., et al., 2014, *Nature*, [512](#), 54
- Menzies J., et al., 1991, International Astronomical Union Circular, [5246](#), 2
- Meyer M. J., et al., 2004, *MNRAS*, [350](#), 1195
- Mikuz H., 1994, International Astronomical Union Circular, [5958](#), 3
- Mikuz H., 1995, International Astronomical Union Circular, [6166](#), 2
- Misra K., et al., 2005, *MNRAS*, [360](#), 662
- Modjaz M., et al., 2005a, Central Bureau Electronic Telegrams, [160](#), 1
- Modjaz M., et al., 2005b, International Astronomical Union Circular, [8491](#), 2
- Molinari E., et al., 1999, in *Looking Deep in the Southern Sky, Proceedings of the ESO/Australia Workshop held at Sydney, Australia, 10-12 December 1997*. Edited by Faffaella Morganti and Warrick J. Couch. Berlin: Springer-Verlag, 1999. p. 157.. p. 157
- Monard L. A. G., et al., 2010, Central Bureau Electronic Telegrams, [2434](#), 1
- Monard L. A. G., et al., 2001, International Astronomical Union Circular, [7720](#), 1
- Monard L. A. G., et al., 2007, Central Bureau Electronic Telegrams, [1100](#), 1
- Monard L. A. G., et al., 2011, Central Bureau Electronic Telegrams, [2635](#), 1
- Monard L. A. G., et al., 2015, Central Bureau Electronic Telegrams, [4081](#), 1
- Moorwood A., et al., 1998, *The Messenger*, [91](#), 9
- Morrell N., et al., 2016, The Astronomer's Telegram, [9170](#), 1
- Morrell N., et al., 2007, Central Bureau Electronic Telegrams, [1131](#), 1
- Morrell N., et al., 2014a, The Astronomer's Telegram, [6508](#), 1
- Morrell N., et al., 2014b, The Astronomer's Telegram, [6765](#), 1
- Morrell N., et al., 2015, The Astronomer's Telegram, [6988](#), 1
- Motohara K., et al., 2002, *Publications of the Astronomical Society of Japan*, [54](#), 315
- Motohara K., et al., 2006, *ApJ*, [652](#), L101
- Munari U., et al., 2013, *New Astron.*, [20](#), 30
- Munch G., et al., 1986, International Astronomical Union Circular, [4183](#), 1
- Nakano S., et al., 2007, Central Bureau Electronic Telegrams, [863](#), 1
- Nakano S., et al., 1995, International Astronomical Union Circular, [6134](#), 1
- Nakano S., et al., 2003, International Astronomical Union Circular, [8097](#), 1
- Nakano S., et al., 2005, International Astronomical Union Circular, [8475](#), 1
- Nakano S., et al., 2008, Central Bureau Electronic Telegrams, [1193](#), 1
- Nakano S., et al., 2011, Central Bureau Electronic Telegrams, [2783](#), 1
- Nakano S., et al., 2012, Central Bureau Electronic Telegrams, [3209](#), 1
- Nakano S., et al., 2015, Central Bureau Electronic Telegrams, [4106](#), 1
- Nicolas J., et al., 2014, The Astronomer's Telegram, [6500](#), 1
- Nishiyama K., et al., 2012, Central Bureau Electronic Telegrams, [3349](#), 1
- Noguchi T., et al., 2011a, Central Bureau Electronic Telegrams, [2940](#), 1
- Noguchi T., et al., 2011b, Central Bureau Electronic Telegrams, [2943](#), 1
- Nomoto K., 1982, *ApJ*, [253](#), 798
- Nucita A. A., et al., 2017, *ApJ*, [850](#), 111
- Nugent P. E., et al., 2011a, *Nature*, [480](#), 344
- Nugent P., et al., 2011b, The Astronomer's Telegram, [3581](#), 1
- Nyholm A., et al., 2017, The Astronomer's Telegram, [10131](#), 1
- Ochner P., et al., 2016, The Astronomer's Telegram, [9018](#), 1
- Ogando R. L. C., et al., 2008, *AJ*, [135](#), 2424
- Oke J. B., et al., 1982, *Publications of the Astronomical Society of the Pacific*, [94](#), 586
- Oke J. B., et al., 1995, *Publications of the Astronomical Society of the Pacific*, [107](#), 375
- Olszewski E. W., 1982, *Information Bulletin on Variable Stars*, [2065](#), 1
- Osmer P. S., et al., 1972, *Nature Physical Science*, [238](#), 21
- Pakmor R., et al., 2012, *ApJ*, [747](#), L10
- Pan K.-C., et al., 2012, *ApJ*, [750](#), 151
- Pan Y. C., et al., 2015, *MNRAS*, [452](#), 4307
- Pan Y. C., et al., 2017, The Astronomer's Telegram, [10225](#), 1
- Parker S., 2016, Transient Name Server Discovery Report, [2016-304](#), 1
- Parker S., 2017, Transient Name Server Discovery Report, [2017-700](#), 1
- Parker S., et al., 2013a, Central Bureau Electronic Telegrams, [3416](#), 1
- Parker P., et al., 2013b, Central Bureau Electronic Telegrams, [3539](#), 1
- Pastorello A., et al., 2007, *MNRAS*, [376](#), 1301
- Paturel G., et al., 2003, *A&A*, [412](#), 57
- Pejcha O., et al., 2013, *MNRAS*, [435](#), 943
- Pessa I., et al., 2018, preprint, p. [arXiv:1803.05005](#) ([arXiv:1803.05005](#))
- Petrushevska T., et al., 2016, The Astronomer's Telegram, [9049](#), 1
- Phillips M. M., et al., 1987, *Publications of the Astronomical Society of the Pacific*, [99](#), 592
- Phillips M. M., et al., 2006, *AJ*, [131](#), 2615
- Phillips M. M., et al., 2007, *Publications of the Astronomical Society of the Pacific*, [119](#), 360
- Phillips M. M., et al., 2013, *ApJ*, [779](#), 38
- Phillips M. M., et al., 2019, *Publications of the Astronomical Society of the Pacific*, [131](#), 014001
- Pignata G., et al., 2004, *MNRAS*, [355](#), 178
- Pignata G., et al., 2008, *MNRAS*, [388](#), 971
- Pignata G., et al., 2009, Central Bureau Electronic Telegrams, [2022](#), 1
- Pignata G., et al., 2010, Central Bureau Electronic Telegrams, [2344](#), 1
- Pisano D. J., et al., 2011, *The Astrophysical Journal Supplement Series*, [197](#), 28
- Pogge R. W., et al., 2010, in *Proceedings of the SPIE*, Volume 7735, id. 77350A (2010).. , doi:[10.1117/12.857215](#)
- Pollas C., et al., 2007, Central Bureau Electronic Telegrams, [1121](#), 1
- Pollas C., et al., 1989, International Astronomical Union Circular, [4742](#), 2
- Ponticello N. J., et al., 2006, International Astronomical Union Circular, [8667](#), 1
- Prentice S., et al., 2017, Transient Name Server Classification Report, [2017-978](#), 1
- Press W. H., et al., 1992, Numerical recipes in FORTRAN. The art of scientific computing
- Prieto J. L., et al., 2011, Central Bureau Electronic Telegrams, [2613](#), 1
- Prieto J. L., et al., 2006, Central Bureau Electronic Telegrams, [651](#), 1

- Prieto J. L., et al., 2010, Central Bureau Electronic Telegrams, [2453](#), 1
- Przybylski A., 1972, International Astronomical Union Circular, [2434](#), 1
- Puckett T., et al., 2009, Central Bureau Electronic Telegrams, [1762](#), 1
- Pugh H., et al., 2005, Central Bureau Electronic Telegrams, [158](#), 1
- Quimby R., et al., 2005, International Astronomical Union Circular, [8625](#), 2
- Quimby R., et al., 2006a, Central Bureau Electronic Telegrams, [393](#), 1
- Quimby R., et al., 2006b, International Astronomical Union Circular, [8723](#), 2
- Rand R. J., 1995, *AJ*, [109](#), 2444
- Rebassa-Mansergas A., et al., 2018, preprint, p. [arXiv:1809.07158](#) ([arXiv:1809.07158](#))
- Rhee M. H., et al., 1996, *Astronomy and Astrophysics Supplement Series*, [115](#), 407
- Richmond M. W., et al., 2012, *Journal of the American Association of Variable Star Observers (JAAVSO)*, [40](#), 872
- Richmond M. W., et al., 1995, *AJ*, [109](#), 2121
- Riello M., et al., 2002, International Astronomical Union Circular, [7919](#), 2
- Riello M., et al., 2018, preprint, p. [arXiv:1804.09367](#) ([arXiv:1804.09367](#))
- Riess A. G., et al., 1999, *AJ*, [117](#), 707
- Riess A. G., et al., 2005, *ApJ*, [627](#), 579
- Romero-Canizales C., et al., 2014, *The Astronomer's Telegram*, [6618](#), 1
- Röpke F. K., et al., 2012, *ApJ*, [750](#), L19
- Rothberg B., et al., 2006, *AJ*, [131](#), 185
- Rudy R. J., et al., 2015, *The Astronomer's Telegram*, [7825](#), 1
- Sahu D. K., et al., 2008, *ApJ*, [680](#), 580
- Sako M., et al., 2014, preprint, ([arXiv:1401.3317](#))
- Salgado F., et al., 2007, Central Bureau Electronic Telegrams, [865](#), 1
- Salvo M. E., et al., 2001, *MNRAS*, [321](#), 254
- Salvo M., et al., 2006, Central Bureau Electronic Telegrams, [557](#), 1
- Sand D. J., et al., 2017, *The Astronomer's Telegram*, [10569](#), 1
- Sand D. J., et al., 2018a, preprint, p. [arXiv:1804.03666](#) ([arXiv:1804.03666](#))
- Sand D., et al., 2018b, *The Astronomer's Telegram*, [11328](#), 1
- Sand D., et al., 2018c, *The Astronomer's Telegram*, [11330](#), 1
- Sand D., et al., 2018d, *The Astronomer's Telegram*, [11371](#), 1
- Scalzo R. A., et al., 2010, *ApJ*, [713](#), 1073
- Scalzo R. A., et al., 2019, *MNRAS*, [483](#), 628
- Schaefer B., 1987, International Astronomical Union Circular, [4421](#), 1
- Schlegel D. J., et al., 1998, *ApJ*, [500](#), 525
- Schmidt B. P., et al., 1994, *ApJ*, [434](#), L19
- Schneider S. E., et al., 1990, *The Astrophysical Journal Supplement Series*, [72](#), 245
- Schneider S. E., et al., 1992, *The Astrophysical Journal Supplement Series*, [81](#), 5
- Schwartz M., et al., 2003, International Astronomical Union Circular, [8121](#), 1
- Serdusek F. J. D., et al., 2005, Central Bureau Electronic Telegrams, [269](#), 1
- Shappee B. J., et al., 2013, *ApJ*, [766](#)
- Shappee B. J., et al., 2013a, *ApJ*, [762](#)
- Shappee B. J., et al., 2013b, *ApJ*, [765](#), 150
- Shappee B. J., et al., 2014a, *ApJ*, [788](#), 48
- Shappee B. J., et al., 2014b, *The Astronomer's Telegram*, [6812](#), 1
- Shappee B. J., et al., 2015, *The Astronomer's Telegram*, [6882](#), 1
- Shappee B. J., et al., 2017, *ApJ*, [841](#), 48
- Shappee B. J., et al., 2018, *ApJ*, [855](#), 6
- Sheinis A. I., et al., 2002, *Publications of the Astronomical Society of the Pacific*, [114](#), 851
- Shen K. J., et al., 2018, preprint, p. [arXiv:1804.11163](#) ([arXiv:1804.11163](#))
- Silverman J. M., et al., 2011, *MNRAS*, [410](#), 585
- Silverman J. M., et al., 2012, *MNRAS*, [425](#), 1789
- Silverman J. M., et al., 2013, *MNRAS*, [430](#), 1030
- Smartt S. J., et al., 2002, International Astronomical Union Circular, [7961](#), 2
- Smartt S. J., et al., 2015a, *A&A*, [579](#)
- Smartt S. J., et al., 2015b, *A&A*, [579](#), A40
- Smith R. J., et al., 2000, *MNRAS*, [313](#), 469
- Smoker J. V., et al., 2000, *A&A*, [361](#), 19
- Sollerman J., et al., 2001, International Astronomical Union Circular, [7723](#), 2
- Sollerman J., et al., 2004, *A&A*, [428](#), 555
- Springob C. M., et al., 2014, *MNRAS*, [445](#), 2677
- Spyromilio J., et al., 2004, *A&A*, [426](#), 547
- Srivastav S., et al., 2016, *MNRAS*, [457](#), 1000
- Stanek K. Z., 2018, *Transient Name Server Discovery Report*, [2018-234](#), 1
- Stanek K. Z., et al., 2014, *The Astronomer's Telegram*, [6830](#), 1
- Stanishev V., et al., 2008, Central Bureau Electronic Telegrams, [1232](#), 1
- Stanishev V., et al., 2007, *A&A*, [469](#), 645
- Stone G., et al., 2018, *The Astronomer's Telegram*, [11343](#), 1
- Strauss M. A., et al., 1992, *The Astrophysical Journal Supplement Series*, [83](#), 29
- Stritzinger M., 2010, Central Bureau Electronic Telegrams, [2346](#), 1
- Stritzinger M., et al., 2006, *A&A*, [460](#), 793
- Stritzinger M., et al., 2010, *AJ*, [140](#), 2036
- Stritzinger M. D., et al., 2011, *AJ*, [142](#)
- Stritzinger M. D., et al., 2015, *A&A*, [573](#), A2
- Strohmayer T., et al., 1996, International Astronomical Union Circular, [6484](#), 1
- Suntzeff N., et al., 1989, International Astronomical Union Circular, [4728](#), 1
- Suntzeff N., et al., 1992, International Astronomical Union Circular, [5432](#), 2
- Suntzeff N. B., et al., 1996, International Astronomical Union Circular, [6381](#), 1
- Suntzeff N. B., et al., 1999, *AJ*, [117](#), 1175
- Suntzeff N., et al., 2004, International Astronomical Union Circular, [8283](#), 1
- Szabó G. M., et al., 2003, *A&A*, [408](#), 915
- Taam R. E., 1980, *ApJ*, [237](#), 142
- Tartaglia L., et al., 2017a, *The Astronomer's Telegram*, [10158](#), 1
- Tartaglia L., et al., 2017b, *The Astronomer's Telegram*, [10260](#), 1
- Tartaglia L., et al., 2017c, *The Astronomer's Telegram*, [10439](#), 1
- Tartaglia L., et al., 2017d, *The Astronomer's Telegram*, [10629](#), 1
- Taubenberger S., et al., 2013a, *MNRAS*, [432](#), 3117
- Taubenberger S., et al., 2013b, *ApJ*, [775](#), L43
- Taubenberger S., et al., 2015, *MNRAS*, [448](#), L48
- Terreran G., et al., 2016, *The Astronomer's Telegram*, [9403](#), 1
- The Astropy Collaboration et al., 2018, preprint, p. [arXiv:1801.02634](#) ([arXiv:1801.02634](#))
- Theureau G., et al., 1998, *Astronomy and Astrophysics Supplement Series*, [130](#), 333
- Theureau G., et al., 2007, *A&A*, [465](#), 71
- Thompson T. A., 2011, *ApJ*, [741](#), 82
- Tinella V., 2016, *Transient Name Server Discovery Report*, [2016-305](#), 1
- Tony J. L., et al., 2012, *ApJ*, [750](#), 99
- Tony J., et al., 2016, *Transient Name Server Discovery Report*, [2016-583](#), 1
- Tony J., et al., 2017a, *Transient Name Server Discovery Report*, [2017-1371](#), 1

- Tonry J., et al., 2017b, Transient Name Server Discovery Report, [2017-1431](#), 1
- Tonry J., et al., 2017c, Transient Name Server Discovery Report, [2017-361](#), 1
- Tonry J., et al., 2017d, Transient Name Server Discovery Report, [2017-860](#), 1
- Toth I., et al., 2000, *A&A*, **361**, 63
- Treffers R. R., et al., 1993, International Astronomical Union Circular, [5870](#), 3
- Treffers R. R., et al., 1994, International Astronomical Union Circular, [5946](#), 2
- Tsvetkov D. Y., 1982, Soviet Astronomy Letters, **8**, 115
- Tsvetkov D. Y., 1986, *Peremennye Zvezdy*, **22**, 279
- Tsvetkov D. Y., et al., 1997, Astronomy Letters, **23**, 26
- Tsvetkov D. Y., et al., 1990, *A&A*, **236**, 133
- Tsvetkov D. Y., et al., 2013, Contributions of the Astronomical Observatory Skalnate Pleso, **43**, 94
- Tsvetkov D. Y., et al., 2014, Contributions of the Astronomical Observatory Skalnate Pleso, **44**, 67
- Tucker M. A., et al., 2018, arXiv e-prints, p. [arXiv:1811.09635](#)
- Tully R. B., et al., 2008, *ApJ*, **676**, 184
- Turatto M., et al., 1990, *AJ*, **100**, 771
- Turatto M., et al., 1996, *MNRAS*, **283**, 1
- Tutukov A. V., et al., 1979, *Acta Astron.*, **29**, 665
- Uddin S., et al., 2017, The Astronomer's Telegram, [10605](#), 1
- Valenti S., et al., 2017, Transient Name Server Classification Report, [2017-613](#), 1
- Valentini G., et al., 2003, *ApJ*, **595**, 779
- Valleye P., et al., 2019, Bimodal SNe Ia in the Nebular Phase
- Vanmunster T., et al., 1994, International Astronomical Union Circular, [6115](#), 3
- Verheijen M. A. W., et al., 2001, *A&A*, **370**, 765
- Vernet J., et al., 2011, *A&A*, **536**
- Vettolani G., et al., 1981, International Astronomical Union Circular, [3584](#), 1
- Villi M., et al., 1998, International Astronomical Union Circular, [6899](#), 1
- Villi M., et al., 2008, Central Bureau Electronic Telegrams, [1228](#), 1
- Vinkó J., et al., 2003, *A&A*, **397**, 115
- Vladimirov V., et al., 2015, The Astronomer's Telegram, [7732](#), 1
- Volkov I. M., 1991, Information Bulletin on Variable Stars, **3581**, 1
- Waagen E., et al., 1991, International Astronomical Union Circular, [5239](#), 1
- Walker A., et al., 1994, International Astronomical Union Circular, [5950](#), 1
- Walker E. S., et al., 2015, *The Astrophysical Journal Supplement Series*, **219**
- Wang L., et al., 2004, *ApJ*, **604**, L53
- Wang X., et al., 2008, *ApJ*, **675**, 626
- Webbink R. F., 1984, *ApJ*, **277**, 355
- Wells L. A., et al., 1994, *AJ*, **108**, 2233
- Weyant A., et al., 2018, *AJ*, **155**
- Wheeler J. C., et al., 1975, *ApJ*, **200**, 145
- Whelan J., et al., 1973, *ApJ*, **186**, 1007
- Wiethoff W., et al., 2017, The Astronomer's Telegram, [10521](#), 1
- Wood-Vasey W. M., et al., 2002a, International Astronomical Union Circular, [7902](#), 3
- Wood-Vasey W. M., et al., 2002b, International Astronomical Union Circular, [7959](#), 1
- Woods D. F., et al., 2006, *AJ*, **132**, 197
- Woods T. E., et al., 2018, *ApJ*, **863**, 120
- Woosley S. E., et al., 1994, *ApJ*, **423**, 371
- Wyrzykowski L., et al., 2015, The Astronomer's Telegram, [8484](#), 1
- Yamanaka M., et al., 2015, *ApJ*, **806**, 191
- Yaron O., et al., 2012, *Publications of the Astronomical Society of the Pacific*, **124**, 668
- Yoon S. C., et al., 2003, *A&A*, **412**, L53
- Yu C., et al., 2000, International Astronomical Union Circular, [7458](#), 1
- Zhai Q., et al., 2016, *AJ*, **151**
- Zhang J., et al., 2014, The Astronomer's Telegram, [6813](#), 1
- Zhang T., et al., 2011, Central Bureau Electronic Telegrams, [2708](#), 3
- Zhang J.-J., et al., 2014, *AJ*, **148**
- Zhang J., et al., 2018, Transient Name Server Classification Report, [2018-293](#), 1
- Zheng W., et al., 2013, The Astronomer's Telegram, [5637](#), 1
- de Vaucouleurs G., et al., 1991, Third Reference Catalogue of Bright Galaxies
- van Driel W., et al., 2001, *A&A*, **378**, 370
- van Dyk S. D., et al., 1994, International Astronomical Union Circular, [6105](#), 1
- van Genderen A. M., 1975, *A&A*, **45**, 429

## APPENDIX A: A NEBULAR PHASE PHILLIP'S RELATION

In most SNe Ia, the peak luminosity and photospheric phase decline rate (e.g.,  $\Delta m_{15}$ ) are correlated with the amount of  $^{56}\text{Ni}$  produced in the explosion (e.g., Stritzinger et al. 2006; Scalzo et al. 2019). Therefore, these same observables should also correlate with the magnitude of SNe Ia as they enter the nebular phase. For SNe Ia with nebular spectra but no usable nebular photometry, this relation provides a method for estimating the nebular magnitude using near-peak photometry.

The photometric sample used in deriving the NPPR excludes Iax, CSM, and SC SNe Ia. Although 91T- and 91bg-like do not strictly follow the relation between luminosity and decline rate of normal SNe Ia, they are powered by the radioactive decay of  $^{56}\text{Ni}$  to stable  $^{56}\text{Fe}$ . As mentioned before,  $\Delta m_{15}$  is indicative of the amount of  $^{56}\text{Ni}$  synthesised in the explosion, and therefore our parameterization described below still accurately models 91T- and 91bg-like SNe Ia. However, SC and Iax SNe Ia have unique ionisation properties, which is further exemplified by their nebular spectra which lack the prominent [FeII/III] and [CoII/III] emission features of their normal, 91T-, and 91bg-like counterparts (e.g., Taubenberger et al. 2013a; Foley et al. 2016). It is possible that the photometric intricacies of 91T- and 91bg-like SNe Ia are washed out by our heterogeneous sample, and more precise results can be attained with distinct samples of SNe Ia spectral types.

Taking all available nebular phase photometry of viable SNe Ia from this work and the literature, we derive an approximate functional form for calculating the apparent magnitude of a SN Ia with a measured  $m_{\max}$  and  $\Delta m_{15}$ . Since SNe Ia have nearly linear decays in magnitude space at nebular epochs, we use the functional form

$$m_{\lambda,\text{neb}}(t_p) = m_{\lambda,\max} + \Delta m_{\lambda}(t_p), \quad (\text{A1})$$

where  $m_{\lambda,\text{neb}}(t_p)$  is the nebular magnitude in filter  $\lambda$  at phase  $t_p = t - t_{\max}$ ,  $m_{\lambda,\max}$  the magnitude at peak in filter  $\lambda$ , and  $\Delta m_{\lambda}$  is the change in brightness between maximum light and  $t_p$  for that filter. By formulating our relation for individual filters, we can neglect extinction from the Milky Way and the host galaxy since the maximum light and nebular magnitude of a SN Ia will be affected equally. Thus, we parameterize  $\Delta m_{\lambda}$  as a function a SN Ia's  $\Delta m_{15}$ ,

$$\Delta m_{\lambda} = A_{\lambda}(\Delta m_{15}) \times (t_p - 250 \text{ d}) + B_{\lambda}(\Delta m_{15}), \quad (\text{A2})$$

where

$$A_{\lambda}(\Delta m_{15}) = a_{\lambda}(\Delta m_{15} - 1.1 \text{ mag}) + b_{\lambda}, \quad (\text{A3})$$

and

$$B_{\lambda}(\Delta m_{15}) = c_{\lambda}(\Delta m_{15} - 1.1 \text{ mag}) + d_{\lambda}. \quad (\text{A4})$$

Here,  $m_{\lambda,\max}$  is the apparent magnitude at maximum light in filter  $\lambda$ ,  $m_{\lambda}(t)$  is the nebular magnitude,  $t_p$  is the phase of the observations,  $\Delta m_{15}$  the decline rate, and measured coefficients  $\{a, b, c, d\}$  which are provided in Table A1.  $t_p$  and  $\Delta m_{15}$  are offset by typical values to reduce their covariance in the fitting process.

The coefficients in Table A1 were computed using all

available nebular photometry between 150–500 d after maximum light. The coefficients were first approximated using a sample of well-studied SNe Ia with  $\geq 5$  measurements in a given filter in the temporal bounds listed above, such as SNe 2011fe, 2012fr, 2013gy, and 2015F, then expanded to include all photometric points. The SNe Ia used in deriving the NPPR have decline rates that span  $\Delta m_{15} \sim 0.8 - 1.8$  mag and are denoted with a  $*$  in Table B6. For publicly available photometry for which there are no reported uncertainties, we assign a nominal uncertainty of 0.1 mag. In fitting the data, we implement non-linear least squares fitting coupled with a bootstrap-resampling technique to derive reasonable estimates for the uncertainties. The residuals of the best-fit solution are shown in the left panel of Fig. A1, and the collapsed distribution is provided in the right panel.

For SNe Ia with a measured peak magnitude and  $\Delta m_{15}$ , we show the nebular *BVR* magnitude can be approximated to  $\sim 20\%$ . These results were derived using a heterogeneous data set and likely can be improved with a consistent photometric system and targeted observations across a reasonable span of  $\Delta m_{15}$ . This technique can also be used in identifying peculiar or strange SNe Ia that deviate from their expected brightness at a given epoch, such as “late-onset” CSM interaction (e.g., Graham et al. 2019). Additionally, we attempted to expand this methodology to other photometric filters (e.g.,  $g$ ,  $r$ ), but there were too few observations to build a quality model.

## APPENDIX B: SUPPLEMENTARY TABLES AND FIGURES

In Table B2, we provide the name of the SN Ia, redshift, and references for discovery and classification. For information on each spectrum, including the date, telescope, instrument, and reference, see Table B3. Flux limits and derived mass limits are given in Table B4. New photometry presented in this work is provided in Table B5 and all photometry references are given in Table B6.

### B1 Data Tables

For SNe Ia with redshifts measured from the supernova lines near maximum light, we tweak the redshift using host galaxy emission lines when necessary. Major host galaxy lines such as H $\alpha$ , H $\beta$ , [NII], and [OIII] are fit with Gaussian line profiles to estimate the line centre and then used to measure the host redshift.

For SNe Ia with insufficient photometry for a reliable light curve fit in SNooPy, we consider two approaches. If there are  $\geq 3$  photometric points near maximum light, we use linear least-squares coupled with bootstrap-resampling to fit a quadratic curve to the data and estimate  $t_{\max}$  and the associated uncertainty. Otherwise, the value for  $t_{\max}$  is taken from the spectroscopic classification reference given in Table B2 and assigned a nominal uncertainty of  $\pm 5$  d.

SNe-Iax do not conform to the standard SNe Ia templates utilised by SNooPy and other SN Ia light curve fitters. Thus, we compute  $\Delta m_{15}$  and  $t_{\max}$  using spline fits in the SNooPy environment. This prevents us from deriving the host reddening  $E(B-V)_{\text{host}}$ , however, the Iax SNe in our sample have negligible reddening (Li et al. 2003a; Phillips et al.

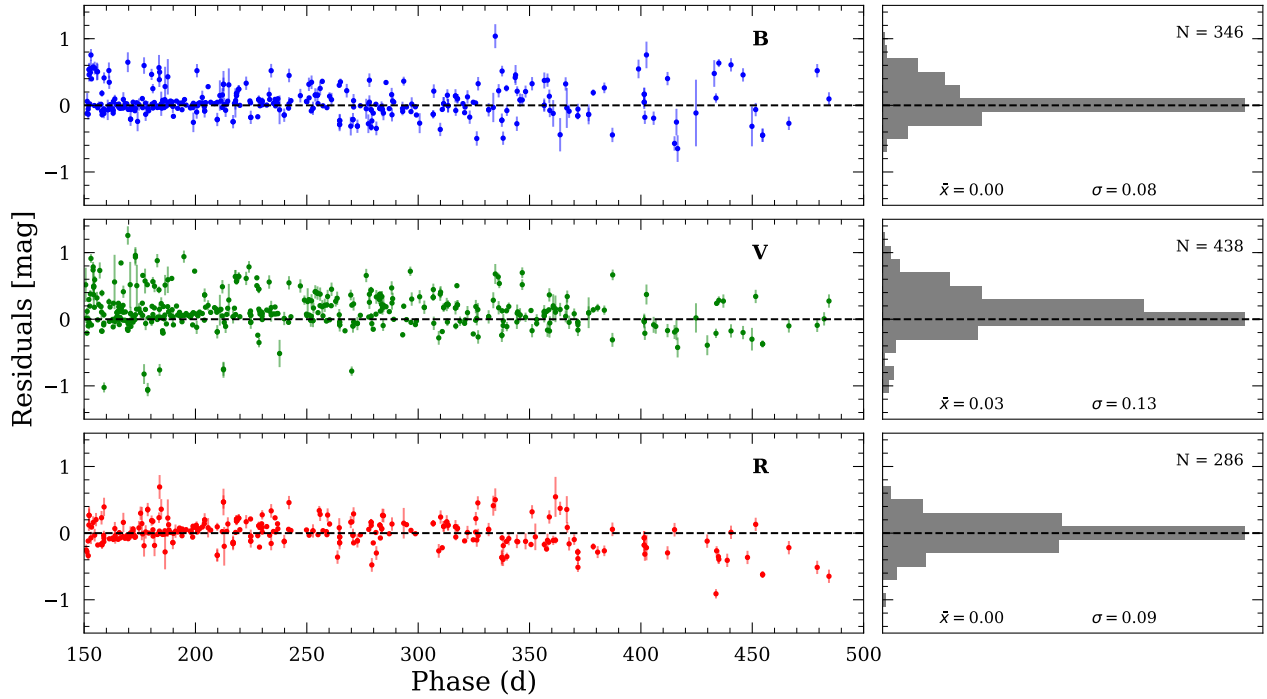


**Figure A1.** *Left:* Residuals of the late-time relation bootstrap fit from Eqs. A2-A4 using the values in Table A1. *Right:* Collapsed residual distribution of the best-fit solution.

**Table A1.** Values of the coefficients for Eqs. A2-A4 and fit statistics.  $N_{tot}$  is the total number of photometric points used in each filter from  $N_{SN}$  SNe Ia.

Filter	$a_\lambda$ [ $10^{-3}$ day $^{-1}$ ]	$b_\lambda$ [ $10^{-2}$ mag day $^{-1}$ ]	$c_\lambda$	$d_\lambda$ [mag]	$N_{SN}$	$N_{tot}$	$\bar{x}$	$\sigma$
B	$-7.66^{+0.53}_{-0.62}$	$1.443^{+0.005}_{-0.005}$	$0.48^{+0.04}_{-0.04}$	$6.168^{+0.003}_{-0.004}$	42	346	0.00	0.08
V	$-13.68^{+0.33}_{-0.37}$	$1.620^{+0.003}_{-0.003}$	$2.58^{+0.02}_{-0.02}$	$6.050^{+0.002}_{-0.002}$	67	438	0.03	0.13
R	$4.22^{+0.41}_{-0.33}$	$1.650^{+0.004}_{-0.003}$	$1.00^{+0.03}_{-0.03}$	$6.776^{+0.002}_{-0.002}$	34	286	0.00	0.09

2007; McCully et al. 2014; Stritzinger et al. 2015; Foley et al. 2015).

The ‘‘Quality’’ column in Table B3 provides a rough estimate of the quality of the spectrum. This is mostly qualitative, and intended to provide readers with an estimate of the spectral quality for each SN Ia in our sample. The rankings are as follows:

*High:* The spectrum clearly shows the major Fe and Co emission lines between  $\sim 4000 - 7000\text{\AA}$ . The spectrum exhibits little to no host contamination or instrumental artefacts.

*Med(ium):* The major Fe lines are visible, while the Co lines are noisy or absent. The spectrum may also suffer from minor to moderate host galaxy contamination and/or instrumental artefacts.

*Low:* The major Fe lines are barely detectable above the spectral noise, and the Co lines mostly below the detection threshold. This category also includes overall medium-quality spectra with significant host galaxy contamination and/or instrumental artefacts.

**Table B1.**  $R_V$  values and references for SNe Ia with  $\geq 3\sigma$  deviations from the assumed  $R_V = 3.1$ .

Name	$R_V$	Ref.
SN2002bo	1.2	Phillips et al. (2013)
SN2004eo	0.8	Burns et al. (2014)
SN2006X	1.5	Wang et al. (2008); Phillips et al. (2013); Burns et al. (2014)
SN2007le	1.6	Phillips et al. (2013); Burns et al. (2014)
SN2014J	1.5	Amanullah et al. (2014); Foley et al. (2014); Gao et al. (2015); Brown et al. (2015)

## B2 Special Cases

We discuss any extenuating circumstances or any other relevant details about specific SNe Ia that differ from the general

methodology described in §2. Examples include alternative flux calibration methods, spectroscopic oddities noticed in our analysis, and spectrum reference discrepancies. SNe Ia with  $R_V$  values known to deviate from the standard  $R_V = 3.1$  are listed in Table B1. For ensemble studies (e.g., Phillips et al. 2013; Burns et al. 2014), we require a  $\geq 3\sigma$  deviation from  $R_V = 3.1$  to include the value in our calculation. When drawing  $R_V$  values from Burns et al. (2014), we implement the F99+uniform prior results.

*SN1981B:* The nebular spectrum on the OSC and WISEREP refer to Branch et al. (1983) as the source of the spectrum, however, we find no mention therein. Therefore, we include this reference in Table B3, with the caveat that we could not verify its source. Additionally, there are no definitive narrow features in the spectrum to confidently determine the spectral resolution. We assume a resolution of 10Å across the entire spectral range.

*SN1998bu:* The two nebular spectra from Cappellaro et al. (2001) do not have any specific mention in that manuscript, however, the reference on WiseRep points to this paper. Thus, we include the reference, but acknowledge we could not verify this paper was the true source for these spectra.

*SN2002bo:* The OSC and WiseRep also report several nebular phase NIR spectra for this SN. However, cross-referencing the reported spectra with the observational parameters given in Bennett et al. (2004), we believe the dates provided for the NIR spectra are off by a year, and these spectra are closer to a few months after maximum light instead of several hundred days after maximum light. We exclude these spectra from our sample.

### B3 Supplementary Figures

We provide cutouts around each spectral line inspected for H/He emission (Table 2) for the spectrum used in calculating the limits provided in Table B4 for each SN Ia as supplementary figures. An example of the format of these figures is provided in Fig. 3. The black line is the observed spectrum, with the continuum fit and flux upper limit in red and purple, respectively. Gray shaded areas indicate masked spectral regions and completely gray boxes indicate that particular SN Ia had no spectra covering that spectral region. When multiple nebular spectra of a SN Ia cover the same expected H/He line, we provide the spectrum corresponding to the best mass limit *for that line*. Therefore, the panel for H $\alpha$  may show a different spectrum than the panel for H $\beta$  for the same SN Ia. This ensures all adequate spectra are presented, even when some spectra do not cover all the optical and NIR lines considered in this study. The border colour of a given panel indicates whether it is used in the final stripped mass determination, the results of which are provided in Table B4. Blue borders indicate the panels used in the H-rich mass limit, red borders indicate He-rich limits, and purple borders indicate He lines used for both H- and He-rich limits.

**Table B2.** All SNe Ia studied in this work.

Disc. Name	IAU Name	Pec?	$z$	Redshift Ref.	Discovery	Classification
...	ASASSN-14hr	N	0.03362	Jones et al. (2009)	Nicolas et al. (2014)	Morrell et al. (2014a)
...	ASASSN-14jc	N	0.01132	Jones et al. (2009)	Kiyota et al. (2014a)	Romero-Canizales et al. (2014)
...	ASASSN-14jg	N	0.01483	Jones et al. (2009)	Holoien et al. (2014)	Arcavi et al. (2014)
...	ASASSN-14jz	N	0.01550	This Work	Kiyota et al. (2014b)	Dimitriadis et al. (2014)
...	ASASSN-14kq	N	0.03360	Jones et al. (2009)	Brimacombe et al. (2014a)	Morrell et al. (2014b)
...	ASASSN-14lt	N	0.03205	Springob et al. (2014)	Kiyota et al. (2014c)	Zhang & Wang (2014)
...	ASASSN-14lu	N	0.02700	Collobert et al. (2006)	Brimacombe et al. (2014b)	Shappee et al. (2014b)
...	ASASSN-14lv	N	0.04919	Jones et al. (2006)	Kiyota et al. (2014d)	Shappee et al. (2015)
...	ASASSN-14me	N	0.01800	Shappee et al. (2015)	Stanek et al. (2014)	Shappee et al. (2015)
...	ASASSN-15be	N	0.02190	Colless et al. (2003)	Brimacombe et al. (2015)	Morrell et al. (2015)
...	ASASSN-15hx	N	0.00810	This Work	Dong et al. (2015b)	Frohmaier et al. (2015)
...	PSN J1149 <sup>a</sup>	N	0.00560	Meyer et al. (2004)	Vladimirov et al. (2015)	Rudy et al. (2015)
...	SN1972E	N	0.00136	Koribalski et al. (2004)	Kowal (1972)	Herbig et al. (1972)
...	SN1981B	N	0.00603	Grogan et al. (1998)	Aksenov (1981)	Vettolani et al. (1981)
...	SN1986G	91bg-like	0.00182	Graham et al. (1978)	Evans et al. (1986)	Feast et al. (1986)
...	SN1990N	N	0.00340	Meyer et al. (2004)	Maury et al. (1990)	Maury et al. (1990)
...	SN1991T	91T-like	0.00579	Strauss et al. (1992)	Waagen et al. (1991)	Waagen et al. (1991)
...	SN1991bg	91bg-like	0.00339	Cappellari et al. (2011)	Kosai et al. (1991)	Kirshner et al. (1991)
...	SN1992A	N	0.00626	D'Onofrio et al. (1995)	Liller et al. (1992)	Liller et al. (1992)
...	SN1993Z	N	0.00450	Epinat et al. (2008)	Treffers et al. (1993)	Treffers et al. (1993)
...	SN1994ae	N	0.00427	Krumm & Salpeter (1980)	van Dyk et al. (1994)	Iijima et al. (1994)
...	SN1995D	N	0.00656	Cappellari et al. (2011)	Nakano et al. (1995)	Benetti et al. (1995)
...	SN1996X	N	0.00694	Ogando et al. (2008)	Garradd et al. (1996)	Suntzeff et al. (1996)
...	SN1998aq	N	0.00370	de Vaucouleurs et al. (1991)	Hurst et al. (1998)	Ayani & Yamaoka (1998)
...	SN1998bu	N	0.00299	de Vaucouleurs et al. (1991)	Villi et al. (1998)	Ayani et al. (1998)
...	SN1999aa	91T-like	0.01444	de Vaucouleurs et al. (1991)	Armstrong & Schwartz (1999)	Filippenko et al. (1999)
...	SN1999by	91bg-like	0.00213	de Vaucouleurs et al. (1991)	Arbour et al. (1999)	Gerardy & Fesen (1999)
...	SN2000cx	91T-like	0.00802	Cappellari et al. (2011)	Yu et al. (2000)	Chornock et al. (2000)
...	SN2001el	N	0.00389	Koribalski et al. (2004)	Monard et al. (2001)	Sollerman et al. (2001)
...	SN2002bo	N	0.00424	Theureau et al. (1998)	Cacella et al. (2002)	Kawakita et al. (2002)
...	SN2002cx	Iax	0.02396	Falco et al. (1999)	Wood-Vasey et al. (2002a)	Matheson et al. (2002)
...	SN2002dj	N	0.00939	Rothberg & Joseph (2006)	Hutchings & Li (2002)	Riello et al. (2002)
...	SN2002er	N	0.00857	de Vaucouleurs et al. (1991)	Wood-Vasey et al. (2002b)	Smartt et al. (2002)
...	SN2003cg	N	0.00413	van Driel et al. (2001)	Nakano et al. (2003)	Kotak et al. (2003a)
...	SN2003du	N	0.00638	Schneider et al. (1992)	Schwartz & Holvorcem (2003)	Kotak et al. (2003b)
...	SN2003gs	91bg-like	0.00477	Smith et al. (2000)	Evans et al. (2003)	Evans et al. (2003)
...	SN2003hv	N	0.00562	Ogando et al. (2008)	Beutler & Li (2003)	Dressler et al. (2003)
...	SN2003kf	N	0.00739	Theureau et al. (1998)	Li et al. (2003b)	Li et al. (2003b)
...	SN2004S	N	0.00936	Theureau et al. (2007)	Martin & Biggs (2004)	Suntzeff et al. (2004)
...	SN2004eo	N	0.01570	Theureau et al. (1998)	Arborea et al. (2004)	Gonzalez et al. (2004)
...	SN2005W	N	0.00889	de Vaucouleurs et al. (1991)	Nakano et al. (2005)	Elias-Rosa et al. (2005)
...	SN2005am	N	0.00790	Theureau et al. (1998)	Martin et al. (2005)	Modjaz et al. (2005b)
...	SN2005cf	N	0.00646	de Vaucouleurs et al. (1991)	Pugh & Li (2005)	Modjaz et al. (2005a)
...	SN2005hk	Iax	0.01299	Abolfathi et al. (2018)	Quimby et al. (2005)	Serdeke et al. (2005)
...	SN2006X	N	0.00524	Rand (1995)	Ponticello et al. (2006)	Quimby et al. (2006a)
...	SN2006dd	N	0.00587	Longhetti et al. (1998)	Quimby et al. (2006b)	Salvo et al. (2006)
...	SN2006gz	SC	0.02800	Falco et al. (1999)	Frieman et al. (2006)	Prieto et al. (2006)
...	SN2007af	N	0.00546	Koribalski et al. (2004)	Nakano & Itagaki (2007)	Salgado et al. (2007)
...	SN2007if	SC	0.07416	Scalzo et al. (2010)	Akerlof et al. (2007)	Akerlof et al. (2007)
...	SN2007le	N	0.00672	Koribalski et al. (2004)	Monard et al. (2007)	Filippenko et al. (2007)
...	SN2007on	N	0.00649	Graham et al. (1998)	Pollas & Klotz (2007)	Morrell et al. (2007)
...	SN2008A	Iax	0.01643	Theureau et al. (1998)	Nakano et al. (2008)	Blondin & Berlind (2008)
...	SN2008Q	N	0.00802	Cappellari et al. (2011)	Villi et al. (2008)	Stanishev & Pursimo (2008)
...	SN2009dc	SC	0.02139	Falco et al. (1999)	Puckett et al. (2009)	Harutyunyan et al. (2009)
...	SN2009ig	N	0.00877	Meyer et al. (2004)	Kleiser et al. (2009)	Kleiser et al. (2009)
...	SN2009le	N	0.01779	Theureau et al. (1998)	Pignata et al. (2009)	Challis & Berlind (2009)
...	SN2010ev	N	0.00921	Meyer et al. (2004)	Pignata et al. (2010)	Stritzinger (2010)
...	SN2010gp	N	0.02450	Downes et al. (1993)	Maza et al. (2010)	Folatelli et al. (2010b)
...	SN2010hg	N	0.00822	Meyer et al. (2004)	Monard & Africa (2010)	Prieto et al. (2010)
...	SN2010lp	91bg-like	0.01015	Huchra et al. (1999)	Cox et al. (2010)	Prieto & Morrell (2011)
...	SN2011K	N	0.01450	Monard et al. (2011)	Drake et al. (2011a)	Drake et al. (2011a)

**Table B2 – continued** All SNe Ia studied in this work.

Disc. Name	IAU Name	Pec?	z	Redshift Ref.	Discovery	Classification
SNhunt37	SN2011ae	N	0.00605	Meyer et al. (2004)	Howerton et al. (2011)	Howerton et al. (2011)
...	SN2011at	N	0.00676	Theureau et al. (1998)	Cox et al. (2011)	Cox et al. (2011)
...	SN2011by	N	0.00284	Verheijen & Sancisi (2001)	Drake et al. (2011b)	Zhang et al. (2011)
...	SN2011ek	N	0.00503	Rhee & van Albada (1996)	Nakano et al. (2011)	Nakano et al. (2011)
PTF11kly	SN2011fe	N	0.00080	Maguire et al. (2014)	Nugent et al. (2011b)	Cenko et al. (2011)
...	SN2011im	N	0.01623	Catinella et al. (2005)	Brimacombe et al. (2011)	Brimacombe et al. (2011)
...	SN2011iv	N	0.00649	Graham et al. (1998)	Noguchi et al. (2011a)	Noguchi et al. (2011a)
...	SN2011iy	N	0.00427	Corsini et al. (2003)	Noguchi et al. (2011b)	Noguchi et al. (2011b)
...	SN2012Z	Iax	0.00712	Koribalski et al. (2004)	Cenko et al. (2012)	Cenko et al. (2012)
...	SN2012cg	N	0.00146	Kent et al. (2008)	Kandrashoff et al. (2012)	Kandrashoff et al. (2012)
SNhunt136	SN2012cu	N	0.00347	de Vaucouleurs et al. (1991)	Marion et al. (2012)	Marion et al. (2012)
...	SN2012ei	N	0.00672	Galbany et al. (2014)	Nakano et al. (2012)	Nakano et al. (2012)
...	SN2012fr	N	0.00546	Bureau et al. (1996)	Klotz et al. (2012)	Klotz et al. (2012)
...	SN2012hr	N	0.00756	Tully et al. (2008)	Drescher et al. (2012)	Drescher et al. (2012)
...	SN2012ht	N	0.00356	Guthrie & Napier (1996)	Nishiyama et al. (2012)	Nishiyama et al. (2012)
...	SN2013aa	N	0.00400	Huchra et al. (1999)	Parker et al. (2013a)	Parker et al. (2013a)
SNhunt196	SN2013cs	N	0.00924	Pisano et al. (2011)	Howerton et al. (2013)	Howerton et al. (2013)
...	SN2013ct	N	0.00384	Smoker et al. (2000)	Parker et al. (2013b)	Parker et al. (2013b)
...	SN2013dy	N	0.00389	Pan et al. (2015)	Casper et al. (2013)	Casper et al. (2013)
...	SN2013gy	N	0.01402	Catinella et al. (2005)	Kim et al. (2013)	Kim et al. (2013)
...	SN2014J	N	0.00068	de Vaucouleurs et al. (1991)	Fossey et al. (2014)	Itagaki et al. (2014)
...	SN2014bv	N	0.00559	de Vaucouleurs et al. (1991)	Cortini et al. (2014)	Cortini et al. (2014)
...	SN2015F	N	0.00489	Meyer et al. (2004)	Monard et al. (2015)	Monard et al. (2015)
...	SN2015I	N	0.00759	Giovanelli et al. (1997)	Nakano et al. (2015)	Karamehmetoglu et al. (2015)
...	SN2016brx	91bg-like	0.01017	Jones et al. (2009)	Parker (2016)	Morrell & Shappee (2016)
...	SN2016bry	N	0.01602	Rhee & van Albada (1996)	Tinella (2016)	Ochner et al. (2016)
ASASSN-16eq	SN2016bsa	N	0.01431	Paturel et al. (2003)	Brimacombe et al. (2016)	Mattila et al. (2016)
Gaia16avm	SN2016ehy	N	0.04500	Halevi et al. (2016)	Delgado et al. (2016)	Halevi et al. (2016)
ATLAS16cpu	SN2016ffh	N	0.01820	Abazajian et al. (2005)	Tonry et al. (2016)	Terreran et al. (2016)
...	SN2016gxp	91T-like	0.01785	Huchra et al. (1999)	Gagliano et al. (2016)	Leadbeater (2016)
ASASSN-17cs	SN2017azw	N	0.02000	Nyholm et al. (2017)	Brimacombe et al. (2017)	Nyholm et al. (2017)
DLT17u	SN2017cbv	N	0.00399	Koribalski et al. (2004)	Tartaglia et al. (2017a)	Hosseinzadeh et al. (2017)
ATLAS17dfo	SN2017ckq	N	0.00989	Mathewson et al. (1992)	Tonry et al. (2017c)	Pan et al. (2017)
DLT17ar	SN2017cyy	N	0.00978	Meyer et al. (2004)	Tartaglia et al. (2017b)	Jha et al. (2017)
DLT17bk	SN2017ejb	91bg-like	0.00987	de Vaucouleurs et al. (1991)	Tartaglia et al. (2017c)	Valenti et al. (2017)
ASASSN-18hz	SN2017evn	N	0.01716	Adelman-McCarthy et al. (2008)	Wiethoff et al. (2017)	Everson et al. (2017)
...	SN2017ezd	N	0.01808	Jones et al. (2009)	Parker (2017)	Uddin et al. (2017)
DLT17bx	SN2017fgc	N	0.00772	Cappellari et al. (2011)	Sand et al. (2017)	Sand et al. (2017)
DLT17cd	SN2017fzw	91bg-like	0.00540	de Vaucouleurs et al. (1991)	Tartaglia et al. (2017d)	Hosseinzadeh et al. (2017)
ATLAS17jiv	SN2017gah	N	0.00891	Lauberts & Valentijn (1989)	Tonry et al. (2017d)	Hosseinzadeh et al. (2017)
...	SN2017glq	N	0.01176	Woods et al. (2006)	Gagliano et al. (2017)	Prentice & Ashall (2017)
ATLAS17nmh	SN2017isq	N	0.00939	Benetti et al. (2017)	Tonry et al. (2017a)	Benetti et al. (2017)
ATLAS17nse	SN2017iyb	N	0.01011	Meyer et al. (2004)	Tonry et al. (2017b)	Jones et al. (2017)
ASASSN-18hb	SN2018aqi	N	0.01251	Theureau et al. (1998)	Malesani et al. (2018)	Brimacombe et al. (2018)
ASASSN-18bt	SN2018oh	N	0.01098	Schneider et al. (1990)	Brown et al. (2018)	Leadbeater (2018)
ASASSN-18da	SN2018vw	91T-like	0.02000	Dong et al. (2018b)	Stanek (2018)	Stone et al. (2018)
DLT18h	SN2018xx	N	0.00999	Smith et al. (2000)	Sand et al. (2018b)	Sand et al. (2018c)
DLT18i	SN2018yu	N	0.00811	de Vaucouleurs et al. (1991)	Sand et al. (2018d)	Zhang et al. (2018)
...	SNF-012 <sup>b</sup>	SC	0.07454	Taubenberger et al. (2013a)	...	...

<sup>a</sup>PSN J1149 = PSN J11492548-0507138<sup>b</sup>SNF-012 = SNF20080723-012

**Table B3.** Spectra observations.

SN	Obs. Date (MJD)	Phase <sup>a</sup> (days)	Telescope <sup>b</sup>	Instrument <sup>b</sup>	Range <sup>c</sup> (Å)	Expt. (s)	$v_{exp}$ [km s <sup>-1</sup> ]	Qual.	Ref.
SN1972E	41651.00	205.1	P200	DBSP	4000 – 10000	...	5100 ± 800	Med	Kirshner & Oke (1975)
	41682.00	236.1	P200	DBSP	3300 – 10300	...	5900 ± 400	Med	Kirshner & Oke (1975)
	41795.00	349.1	P200	DBSP	3400 – 10200	...	6300 ± 100	Med	Kirshner & Oke (1975)
	41864.00	418.1	P200	DBSP	3400 – 9200	...	6600 ± 200	Med	Kirshner & Oke (1975)
SN1981B	44940.00	267.3	...	...	3400 – 7100	...	6200 ± 300	Med	Branch et al. (1993)
SN1986G	46816.50	255.5	ESO2.2m	BC	4500 – 6800	...	5500 ± 100	Med	Cristiani et al. (1992)
	46817.50	256.5	ESO3.6m	EFOSC	3700 – 9500	...	4900 ± 100	High	Cristiani et al. (1992)
	46818.50	257.5	ESO3.6m	EFOSC	4000 – 9300	...	5000 ± 200	High	Cristiani et al. (1992)
	46885.50	324.5	ESO3.6m	EFOSC	3800 – 7000	...	5100 ± 400	Med	Cristiani et al. (1992)
SN1990N	48268.50	186.0	WHT	FOS	3400 – 9700	1880	5000 ± 700	High	Gomez et al. (1996)
	48309.50	227.0	WHT	FOS	3500 – 9700	1800	5800 ± 600	High	Gomez et al. (1996)
	48337.50	255.0	WHT	FOS	3500 – 9700	1800	5800 ± 800	Med	Gomez et al. (1996)
	48362.50	280.0	WHT	FOS	3500 – 9700	1800	5500 ± 500	Med	Gomez et al. (1996)
	48415.50	333.0	WHT	FOS	3600 – 9700	2000	6100 ± 400	Med	Gomez et al. (1996)
SN1991T	48632.50	258.0	WHT	ISIS	3200 – 8500	1800	7100 ± 400	High	Gomez et al. (1996)
	48658.50	284.0	INT	FOS1	3800 – 8800	3600	6500 ± 100	Med	Gomez et al. (1996)
	48690.50	316.0	INT	FOS1	3800 – 9900	1800	6200 ± 1000	Med	Gomez et al. (1996)
	48694.93	320.4	Shane3m	KAST	3300 – 10100	3600	6500 ± 700	Med	BSNIP
	48723.86	349.3	Shane3m	KAST	3300 – 10400	3600	6600 ± 200	Med	BSNIP
SN1991bg	48802.50	198.4	WHT	FOS2	4900 – 9700	2000	(3 000)	Low	Gomez et al. (1996)
	48806.50	202.4	ESO3.6m	EFOSC2	3800 – 6800	...	1100 ± 100	Med	Turatto et al. (1996)
SN1992A	48931.00	291.7	HST	FOS	1600 – 4800	2000	(3 000)	Low	Kirshner et al. (1993)
SN1993Z	49428.50	181.4	Shane3m	KAST	3100 – 10300	1800	6700 ± 400	Med	BSNIP
	49460.00	212.9	Shane3m	KAST	3100 – 10400	2700	6200 ± 800	Med	BSNIP
SN1994ae	49904.71	219.4	Shane3m	KAST	3600 – 10400	1800	5900 ± 500	Med	BSNIP
	50053.97	368.7	MMT	BCS	3200 – 8600	1200	6000 ± 200	Med	CfA
SN1995D	50045.00	277.6	MMT	BCS	3200 – 8200	1200	7000 ± 200	Med	CfA
	50053.00	285.6	MMT	BCS	3200 – 8800	1200	5800 ± 400	Med	CfA
SN1996X	50437.00	247.2	ESO1.5m	BC	3500 – 9200	...	4100 ± 100	Low	Salvo et al. (2001)
	50489.00	299.2	ESO3.6m	EFOSC2	3700 – 6900	...	6200 ± 200	High	Salvo et al. (2001)
SN1998aq	51141.00	210.2	Till	FAST	3700 – 7500	2100	5900 ± 300	Med	CfA
	51161.00	230.2	Till	FAST	3700 – 7500	2400	6100 ± 100	Med	CfA
	51171.00	240.2	Till	FAST	3700 – 7500	2400	6200 ± 300	Med	CfA
	51143.04	191.2	Till	FAST	3700 – 7500	2400	6000 ± 500	High	CfA
	51161.04	209.2	Till	FAST	3700 – 7500	2400	6200 ± 200	High	CfA
SN1998bu	51169.98	218.1	Till	FAST	3700 – 7500	2400	6100 ± 200	Med	CfA
	51188.88	237.0	Shane3m	KAST	3400 – 10200	1800	6300 ± 200	High	BSNIP
	51195.96	244.1	Till	FAST	3700 – 7500	2400	6100 ± 200	Med	CfA
	51201.96	250.1	D1.54m	DFOSC	3000 – 8500	...	6300 ± 1500	Med	Cappellaro et al. (2001)
	51204.96	253.1	NTT	SOFI	9400 – 25400	4800	3000 ± 700	Med	Spyromilio et al. (2004)
	51232.92	281.0	Shane3m	KAST	3400 – 10500	1800	6100 ± 100	High	BSNIP
	51281.50	329.6	ESO3.6m	EFOSC2	3400 – 7500	...	5900 ± 100	Med	Cappellaro et al. (2001)
	51292.78	340.9	Shane3m	KAST	3300 – 10500	1800	6400 ± 200	Med	BSNIP
	51491.00	258.5	KeckI	LRIS	4100 – 9500	600	5700 ± 1400	Med	BSNIP
SN1999by	51517.00	284.5	KeckI	LRIS	3900 – 9900	600	6500 ± 100	Med	BSNIP
	51494.14	185.2	KeckI	LRIS	4000 – 9700	100	2100 ± 900	High	BSNIP
SN2000cx	51935.00	182.2	MMT	BCS	3700 – 7100	2400	6300 ± 200	Med	CfA
	52204.00	451.2	KeckII	ESI	3900 – 10100	1800	11300 ± 1000	Low	BSNIP
SN2001el	52492.40	310.1	VLT	FORS1	6200 – 10000	1500	(3 000)	Med	PI-Sollerman
	52500.35	318.1	VLT	FORS1	6200 – 10000	2400	(3 000)	Med	PI-Sollerman
SN2002bo	52580.15	397.9	VLT	FORS1	3800 – 9300	3000	5300 ± 800	Med	Mattila et al. (2005)
	52584.00	227.2	KeckII	ESI	4000 – 10100	240	(3 000)	low	BSNIP
	52668.00	311.2	MMT	BCS	3200 – 8700	3600	5800 ± 400	Med	Blondin et al. (2012)
	52647.15	232.1	KeckI	LRIS	3200 – 9200	1800	(3 000)	Low	BSNIP
SN2002cx	52699.11	284.0	KeckI	LRIS	3100 – 9200	2200	(3 000)	Low	BSNIP
	52699.14	284.1	KeckI	LRIS	6100 – 7300	2200	(3 000)	Low	BSNIP
	52731.81	316.7	Clay	LDSS	3600 – 9300	3600	(3 000)	Low	CfA
SN2002dj	52671.00	219.7	NTT	EFOSC2	3400 – 7400	...	6400 ± 400	Med	Pignata et al. (2008)
	52724.00	272.7	VLT	FORS1	3600 – 8500	...	6500 ± 300	Med	Pignata et al. (2008)

**Table B3 – continued** Spectra observations.

SN	Obs. Date (MJD)	Phase <sup>a</sup> (days)	Telescope <sup>b</sup>	Instrument <sup>b</sup>	Range <sup>c</sup> (Å)	Expt. (s)	$v_{exp}$ [km s <sup>-1</sup> ]	Qual.	Ref.
SN2002er	52739.00	213.7	TNG	DOLORES	3500 – 8000	...	5800 ± 100	Med	Kotak et al. (2005)
SN2003cg	53114.00	384.8	VLT	FORS1	3900 – 8000	3800	6000 ± 500	Med	Elias-Rosa et al. (2006)
SN2003du	52961.00	194.4	WHT	ISIS	4400 – 7000	...	5800 ± 100	Med	Stanishev et al. (2007)
	52974.00	207.4	CA3.5m	MOSCA	3200 – 9200	...	5500 ± 200	Med	Stanishev et al. (2007)
	52986.00	219.4	CA2.2m	CAFOS	3200 – 8700	...	6300 ± 900	Med	Stanishev et al. (2007)
	53037.00	270.4	CA2.5m	MOSCA	3200 – 9200	...	6600 ± 100	Med	Stanishev et al. (2007)
	53063.00	296.4	Sub	CISCO	10200 – 18900	4000	6700 ± 1700	Low	Höflich et al. (2004)
	53142.00	375.4	TNG	DOLORES	3400 – 8000	...	6300 ± 800	High	Stanishev et al. (2007)
	53049.30	207.1	KeckII	ESI	3900 – 10100	...	3900 ± 500	High	BSNIP
SN2003hv	53211.00	319.5	VLT	FORS1	3400 – 9800	...	6100 ± 100	High	Leloudas et al. (2009)
	53285.00	393.5	Sub	CISCO	10200 – 18900	12000	4900 ± 100	Med	Motohara et al. (2006)
SN2003kf	53381.00	400.7	Clay	LDSS	4000 – 8400	2400	6900 ± 200	Med	CfA
SN2004S	53355.00	315.3	KeckII	DEIMOS	4700 – 7100	1800	(3000)	Low	BSNIP
SN2004eo	53506.00	227.3	VLT	FORS1	3600 – 8700	2280	5600 ± 300	High	Pastorello et al. (2007)
SN2005W	53626.04	213.4	Sub	CISCO	10300 – 18900	4000	3900 ± 300	Med	Motohara et al. (2006)
SN2005am	53735.00	300.0	KeckI	LRIS	5400 – 7100	7200	6800 ± 600	Med	Leonard (2007)
	53818.00	383.0	GS	GMOS	5100 – 6800	10410	5700 ± 800	Med	Leonard (2007)
	53800.00	265.7	GN	GMOS	5500 – 7500	10800	5400 ± 600	High	Leonard (2007)
SN2005cf	53852.00	317.7	KeckI	LRIS	3200 – 9200	1200	5800 ± 300	Med	BSNIP
	53887.00	352.7	KeckI	LRIS	5800 – 7400	11000	5600 ± 800	Med	Leonard (2007)
	53917.00	382.7	KeckI	LRIS	5800 – 7400	6600	5900 ± 400	Med	Leonard (2007)
SN2005hk	54062.73	377.9	KeckI	LRIS	3100 – 9100	1800	(3000)	Low	McCully et al. (2014)
	54092.72	407.9	KeckII	DEIMOS	4900 – 9900	1800	(3000)	Low	McCully et al. (2014)
SN2006X	54063.14	276.9	KeckI	LRIS	3100 – 9200	500	7000 ± 1200	Med	BSNIP
	54093.15	306.9	KeckII	DEIMOS	4600 – 7200	600	(3000)	Low	BSNIP
	54146.00	359.7	KeckI	LRIS	3200 – 9200	1800	5500 ± 1400	Low	BSNIP
SN2006dd	54106.30	187.7	NTT	EMMI	4000 – 10100	600	6300 ± 100	Med	Stritzinger et al. (2010)
	54113.30	194.7	duPont	DPBC	3900 – 10000	2700	6800 ± 800	Med	Stritzinger et al. (2010)
SN2006gz	54360.70	339.0	Sub	FOCAS	3700 – 9900	3600	(3000)	Low	Maeda et al. (2009)
SN2007af	54476.00	302.0	MMT	BCS	3200 – 8300	2700	5400 ± 300	Med	CfA
SN2007if	54733.20	392.9	VLT	FORS2	3500 – 9000	5700	(3000)	Low	Taubenberger et al. (2013a)
	54761.20	420.9	VLT	FORS2	3500 – 9000	8550	(3000)	Med	Taubenberger et al. (2013a)
SN2007le	54705.50	306.5	KeckI	LRIS	3300 – 9200	1200	6500 ± 200	Med	BSNIP
SN2007on	54705.35	285.6	Clay	LDSS	4500 – 7000	7200	5500 ± 600	High	CSP
	54773.50	353.7	GS	GMOS	3800 – 9900	1200	5700 ± 300	High	Gall et al. (2018)
SN2008A	54800.50	380.7	GS	GMOS	3900 – 7900	1500	5600 ± 200	Med	Gall et al. (2018)
	54681.63	203.6	KeckI	LRIS	3400 – 9000	600	(3000)	Med	McCully et al. (2014)
SNF-012	54706.51	228.5	KeckI	LRIS	3200 – 9100	1200	(3000)	Med	McCully et al. (2014)
	54766.28	288.3	KeckI	LRIS	3200 – 9100	1200	(3000)	Med	McCully et al. (2014)
	54706.00	200.4	KeckI	LRIS	3300 – 9200	1200	6700 ± 400	High	BSNIP
SN2009dc	54947.50	265.4	VLT	FORS2	3300 – 8900	...	7100 ± 100	Med	Taubenberger et al. (2013a)
	54973.50	291.4	VLT	FORS2	3600 – 8900	...	6800 ± 100	Med	Taubenberger et al. (2013a)
SN2009ig	55001.50	319.4	VLT	FORS2	3600 – 8600	...	7300 ± 400	Med	Taubenberger et al. (2013a)
	55233.60	287.2	KeckI	LRIS	3400 – 9900	600	(3000)	Med	Silverman et al. (2011)
SN2009le	55326.20	379.8	VLT	XSH	3300 – 13000	5400	(3000)	Med	Taubenberger et al. (2013a)
	55485.27	405.1	VLT	FORS2	3500 – 10100	2400	7300 ± 2200	High	Maguire et al. (2016)
SN2009le	55482.14	316.5	VLT	FORS2	3400 – 10800	2700	7000 ± 200	Med	PI-Taubenberger
	55655.01	270.2	VLT	FORS2	4000 – 8400	2400	6500 ± 600	Med	PI-Taubenberger
SN2010gp	55682.29	276.2	VLT	FORS2	3400 – 9700	2700	6100 ± 200	High	Maguire et al. (2016)
	55654.16	203.2	VLT	FORS2	3500 – 10100	900	5900 ± 600	High	PI-Taubenberger
SN2010hp	55832.00	264.0	VLT	FORS2	3600 – 10200	8100	(3000)	High	Taubenberger et al. (2013b)
	55922.10	344.2	VLT	FORS2	3400 – 6500	5400	5600 ± 300	Med	PI-Taubenberger
SNhunt37	55926.31	306.2	VLT	FORS2	3600 – 8200	1200	7100 ± 800	Med	PI-Taubenberger
SN2011at	55984.10	359.1	VLT	FORS2	3600 – 10200	2400	6700 ± 400	Med	PI-Taubenberger
SN2011by	55897.60	207.1	KeckI	LRIS	3300 – 10100	450	5600 ± 800	High	Silverman et al. (2013)
SN2011ek	56211.21	422.4	VLT	FORS2	3400 – 10000	2700	5800 ± 100	Med	Maguire et al. (2016)
PTF11kly	56019.00	203.9	Shane3m	KAST	3500 – 10000	...	5700 ± 500	High	Mazzali et al. (2015)
	56040.00	224.9	Shane3m	KAST	3500 – 10000	...	5700 ± 300	High	Mazzali et al. (2015)
	56044.00	228.9	LBT	MODS	3200 – 10000	...	5800 ± 300	High	Shappee et al. (2013a)

**Table B3 – continued** Spectra observations.

SN	Obs. Date (MJD)	Phase <sup>a</sup> (days)	Telescope <sup>b</sup>	Instrument <sup>b</sup>	Range <sup>c</sup> (Å)	Expt. (s)	$v_{exp}$ [km s <sup>-1</sup> ]	Qual.	Ref.
SN2011iy	56046.25	231.1	KeckI	LRIS	3100 – 7300	300	5900 ± 100	Med	PI-Filippenko
	56073.00	257.9	WHT	ISIS	3500 – 9500	...	5500 ± 100	High	Mazzali et al. (2015)
	56103.00	287.9	WHT	ISIS	3400 – 10000	...	5700 ± 200	High	Mazzali et al. (2015)
	56125.00	309.9	Shane3m	KAST	3500 – 10000	...	5800 ± 200	High	Mazzali et al. (2015)
	56128.00	312.9	GTC	OSIRIS	3600 – 10400	...	5800 ± 100	High	Taubenberger et al. (2015)
	56161.00	345.9	WHT	ISIS	3500 – 10000	...	5800 ± 300	High	Mazzali et al. (2015)
	56098.10	204.9	duPont	WFCCD	3600 – 9200	1500	6300 ± 100	High	This work
SN2011im	56215.60	313.3	VLT	FORS2	3800 – 6300	5400	5900 ± 300	Med	PI-Taubenberger
SN2011iv	56149.50	243.5	duPont	WFCCD	3600 – 9100	1000	5500 ± 400	Med	Gall et al. (2018)
	56166.30	260.3	NTT	EFOSC	3600 – 9200	1800	6400 ± 200	High	Gall et al. (2018)
	56181.30	275.3	duPont	WFCCD	3600 – 9100	1200	7200 ± 600	Med	Gall et al. (2018)
	56210.37	304.4	VLT	FORS2	3400 – 10200	900	6800 ± 200	Med	Maguire et al. (2016)
SN2012Z	56161.00	193.3	SALT	RSS	3500 – 9300	...	(3 000)	Low	Stritzinger et al. (2015)
	56182.00	214.3	duPont	WFCCD	3800 – 9100	...	(3 000)	Low	Stritzinger et al. (2015)
	56215.00	247.3	KeckII	DEIMOS	4600 – 9700	...	(3 000)	Low	Stritzinger et al. (2015)
	56222.00	254.3	Sub	FOCAS	4000 – 8000	...	(3 000)	Low	Yamanaka et al. (2015)
SN2012cg	56368.40	286.3	LBT	MODS	3400 – 10000	9600	6500 ± 200	High	Shappee et al. (2018)
	56420.20	338.1	VLT	XSH	3700 – 24800	4800	6300 ± 300	High	Maguire et al. (2016)
	56424.15	342.1	VLT	FORS2	3400 – 10600	600	5400 ± 1100	High	Maguire et al. (2016)
SNhunt136	56424.16	319.1	VLT	FORS2	3400 – 10600	1800	5600 ± 200	High	Maguire et al. (2016)
SN2012ei	56414.38	254.4	LBT	MODS	3400 – 8900	3600	5300 ± 200	Med	Vallely et al. (2019)
SN2012fr	56466.26	222.2	ANU	WiFeS	3500 – 9500	4800	6200 ± 900	Med	Childress et al. (2015)
	56505.19	261.1	ANU	WiFeS	3500 – 9200	7200	6200 ± 400	Med	Childress et al. (2015)
	56533.50	289.5	GS	GMOS	4000 – 9500	3000	6100 ± 600	High	Graham et al. (2017)
	56581.81	337.8	NTT	EFOSC2	3600 – 9200	5400	5000 ± 700	Low	Smartt et al. (2015b)
	56584.37	340.3	SALT	RSS	3500 – 9300	2700	5900 ± 100	Med	Childress et al. (2015)
	56600.30	356.3	VLT	XSH	3700 – 24700	6000	4600 ± 1200	High	Maguire et al. (2016)
	56610.99	366.9	ANU	WiFeS	3500 – 9200	10800	6500 ± 200	Med	Childress et al. (2015)
SN2012hr	56659.50	415.5	GS	GMOS	4000 – 9500	12600	6300 ± 800	Med	Graham et al. (2017)
	56571.50	284.5	GS	GMOS	4000 – 9500	8000	5400 ± 300	High	Childress et al. (2015)
	56656.50	369.5	ANU	WiFeS	3500 – 9200	12000	5800 ± 100	Med	Childress et al. (2015)
SN2012ht	56745.50	458.5	GS	GMOS	4000 – 5800	7200	(3 000)	Low	Graham et al. (2017)
	56718.15	422.2	VLT	XSH	3700 – 24700	12600	(3 000)	Low	Maguire et al. (2016)
SN2013aa	56532.25	189.0	SALT	RSS	3500 – 9000	1350	5700 ± 900	High	Childress et al. (2015)
	56548.88	205.7	ANU	WiFeS	3500 – 9200	4800	5900 ± 700	Med	Childress et al. (2015)
	56689.08	345.9	ANU	WiFeS	3500 – 9200	10800	5800 ± 300	Med	Childress et al. (2015)
	56696.40	353.2	VLT	XSH	3700 – 10700	3800	6100 ± 100	High	Maguire et al. (2016)
	56743.50	400.3	GS	GMOS	4000 – 9500	4500	6000 ± 200	Med	Graham et al. (2017)
SN2013ct	56769.20	426.0	VLT	XSH	3700 – 24700	7500	4400 ± 700	High	Maguire et al. (2018)
	56645.05	228.9	VLT	XSH	3700 – 24700	1900	5500 ± 700	High	Maguire et al. (2016)
SNhunt196	56700.00	262.8	GS	GMOS	4000 – 9500	2700	5000 ± 700	Med	Graham et al. (2017)
	56738.00	300.8	ANU	WiFeS	3500 – 9200	10800	6500 ± 200	Low	Childress et al. (2015)
	56741.00	303.8	VLT	XSH	3700 – 24600	11700	5800 ± 1100	High	Maguire et al. (2016)
SN2013dy	56834.58	333.6	KeckII	DEIMOS	4500 – 9600	2400	7100 ± 200	High	Pan et al. (2015)
	56920.00	419.0	KeckII	DEIMOS	4000 – 7600	2400	6800 ± 100	Med	Childress et al. (2015)
	56924.34	423.4	KeckI	LRIS	3200 – 10100	2000	6400 ± 100	Med	Pan et al. (2015)
	56981.32	480.4	KeckI	LRIS	3200 – 10100	2000	(3 000)	Low	Pan et al. (2015)
SN2013gy	56883.50	234.6	Baade	IMACS	3000 – 8300	...	6600 ± 800	Med	Holmbo et al. (2018)
	56920.00	271.1	KeckII	DEIMOS	3900 – 7500	...	5300 ± 400	Med	Childress et al. (2015)
	56924.00	275.1	KeckI	LRIS	3200 – 10000	2400	5500 ± 500	Med	Childress et al. (2015)
SN2014J	57073.00	424.1	KeckI	LRIS	3200 – 10000	2400	(3 000)	Low	Graham et al. (2017)
	56902.00	211.7	WHT	ACAM	4900 – 9400	180	5500 ± 600	Med	Galbany et al. (2016)
	56920.00	229.7	KeckII	DEIMOS	4000 – 7600	...	5900 ± 600	High	Childress et al. (2015)
	56958.00	267.7	HCT	HFOSC	3700 – 9100	...	5500 ± 300	Med	Srivastav et al. (2016)
	57040.00	349.7	HCT	HFOSC	3700 – 9100	...	5600 ± 500	Med	Srivastav et al. (2016)
SN2014bv	57134.23	293.9	LBT	MODS	3400 – 9900	10800	5100 ± 400	Med	Vallely et al. (2019)
ASASSN-14hr	57405.06	467.6	VLT	MUSE	4600 – 9000	2800	(3 000)	Low	This work
ASASSN-14jg	57182.27	222.5	Baade	IMACS	4000 – 8100	1800	6500 ± 300	High	This work
	57228.15	268.4	GS	GMOS	4000 – 9400	14400	5900 ± 1000	Med	Graham et al. (2017)

**Table B3 – continued** Spectra observations.

SN	Obs. Date (MJD)	Phase <sup>a</sup> (days)	Telescope <sup>b</sup>	Instrument <sup>b</sup>	Range <sup>c</sup> (Å)	Expt. (s)	$v_{exp}$ [km s <sup>-1</sup> ]	Qual.	Ref.
	57285.20	325.5	VLT	XSH	3600 – 10100	2900	6300 ± 1100	Med	<a href="#">Maguire et al. (2018)</a>
ASASSN-14jc	57350.26	390.0	VLT	MUSE	4700 – 9200	2465	(3000)	Low	This work
ASASSN-14jz	57182.56	203.5	Baade	IMACS	4000 – 8100	1800	6000 ± 900	High	This work
ASASSN-14kq	57404.02	412.9	VLT	MUSE	4600 – 9000	2450	(3000)	Low	This work
ASASSN-14lv	57393.04	398.0	VLT	MUSE	4500 – 8900	2460	(3000)	Low	This work
ASASSN-14lu	57477.30	476.6	VLT	MUSE	4600 – 9100	2475	(3000)	Low	This work
ASASSN-14lt	57400.05	388.9	VLT	MUSE	4600 – 9000	4960	(3000)	Low	This work
ASASSN-14me	57327.21	304.1	VLT	MUSE	4700 – 9200	2470	(3000)	Low	This work
	57385.11	362.0	VLT	MUSE	4700 – 9200	2460	(3000)	Low	This work
ASASSN-15be	57317.30	264.8	VLT	XSH	3600 – 10000	5800	6200 ± 200	Med	BSNIP
SN2015F	57299.24	192.5	NTT	EFOSC	5900 – 9900	2700	(3000)	Med	<a href="#">Smartt et al. (2015b)</a>
	57302.33	195.6	NTT	EFOSC	3300 – 7400	5400	5300 ± 400	Med	<a href="#">Smartt et al. (2015b)</a>
	57331.36	224.6	VLT	XSH	5800 – 10100	1200	(3000)	Med	PI-Cartier
	57345.24	238.5	VLT	XSH	5800 – 10100	3300	(3000)	Med	PI-Cartier
	57372.22	265.5	VLT	XSH	5800 – 10100	3700	(3000)	Med	PI-Cartier
	57386.00	279.3	GS	GMOS	4000 – 9500	6000	6000 ± 600	High	<a href="#">Graham et al. (2017)</a>
	57402.18	295.5	Baade	MagE	3500 – 8200	32400	5200 ± 700	High	
ASASSN-15hx	57402.31	250.1	Baade	MagE	3100 – 8200	22800	6200 ± 500	High	
	57566.08	413.9	VLT	XSH	3000 – 24600	3000	(3000)	Med	<a href="#">Maguire et al. (2018)</a>
	57597.00	444.8	VLT	XSH	3000 – 24600	3000	(3000)	Med	PI-Maguire
SN2015I	57426.00	268.6	LBT	MODS	3000 – 9900	10800	6400 ± 800	Med	<a href="#">Valley et al. (2019)</a>
PSN J1149	57421.30	204.7	VLT	XSH	3700 – 24700	2900	5400 ± 600	High	<a href="#">Maguire et al. (2018)</a>
SN2016brx	57681.00	184.0	Clay	LDSS	3700 – 9500	12600	3100 ± 700	High	<a href="#">Dong et al. (2018a)</a>
SN2016bry	57712.14	205.7	LBT	MODS	3000 – 5700	...	(3000)	Low	<a href="#">Valley et al. (2019)</a>
ASASSN-16eq	57709.19	202.1	LBT	MODS	3200 – 5400	...	6100 ± 300	Low	<a href="#">Valley et al. (2019)</a>
Gaia16avm	57814.00	229.2	LBT	MODS	3200 – 8100	3600	7500 ± 600	Low	<a href="#">Valley et al. (2019)</a>
ATLAS16cpu	57814.30	182.3	LBT	MODS	3000 – 10800	...	6100 ± 600	Med	<a href="#">Valley et al. (2019)</a>
SN2016gxp	57900.43	218.3	LBT	MODS	3000 – 9800	...	5300 ± 1200	Med	<a href="#">Valley et al. (2019)</a>
ASASSN-17cs	58037.00	219.8	VLT	FORS2	4200 – 9100	2600	6100 ± 600	Med	100IAs
DLT17u	58158.27	316.0	Clay	LDSS	3900 – 9200	1800	5500 ± 200	Med	This work
ATLAS17dfo	58138.29	288.0	VLT	FORS2	4200 – 9100	2600	5900 ± 300	Med	100IAs
DLT17tar	58098.28	227.6	VLT	FORS2	4200 – 9100	2600	5200 ± 800	Med	100IAs
DLT17bk	58195.36	284.3	VLT	FORS2	4100 – 9400	2600	4100 ± 300	Med	100IAs
ASASSN-18hz	58164.28	228.5	VLT	FORS2	4100 – 9400	2600	5500 ± 500	Med	100IAs
SN2017ezd	58196.36	255.1	VLT	FORS2	4100 – 9300	2600	5500 ± 900	Low	100IAs
DLT17bx	58339.27	379.3	VLT	FORS2	4200 – 9500	2600	5800 ± 1500	Med	100IAs
ATLAS17jiv	58280.27	294.9	VLT	FORS2	4100 – 9400	2600	4800 ± 600	Med	100IAs
DLT17cd	58218.04	228.5	VLT	FORS2	4200 – 9500	2600	5100 ± 300	High	100IAs
SN2017glq	58347.25	331.3	VLT	FORS2	4200 – 7500	2600	5700 ± 400	Med	100IAs
ATLAS17nmh	58253.17	194.8	VLT	FORS2	4200 – 9500	2600	6300 ± 300	High	100IAs
ATLAS17nse	58371.38	253.0	VLT	FORS2	4100 – 9100	2600	5300 ± 400	High	100IAs
	58425.21	306.8	VLT	FORS2	4100 – 9600	2600	5300 ± 200	High	100IAs
ASASSN-18bt	58399.45	236.2	KeckII	DEIMOS	4600 – 9700	3600	5700 ± 700	High	<a href="#">Dimitriadis et al. (2019)</a>
	58427.25	264.0	KeckI	LRIS	3800 – 10000	3600	6100 ± 100	High	<a href="#">Dimitriadis et al. (2019)</a>
	58430.60	267.3	KeckI	LRIS	3100 – 10300	4800	5700 ± 300	Med	<a href="#">Tucker et al. (2018)</a>
ASASSN-18da	58399.20	220.4	VLT	FORS2	4000 – 9300	2600	7100 ± 600	High	100IAs
DLT18h	58521.21	335.9	VLT	FORS2	4100 – 9500	2600	7600 ± 200	Med	100IAs
DLT18i	58432.31	237.2	VLT	FORS2	4100 – 9600	2600	5300 ± 700	High	100IAs
ASASSN-18hb	58460.30	237.4	VLT	FORS2	4100 – 9100	2600	6200 ± 500	High	100IAs

<sup>a</sup> Relative to  $t_{\max}$ <sup>b</sup> See §2 for definitions and references.<sup>c</sup> In the observer rest-frame.

**Table B4.** Flux limits for each line in Table 2 and the corresponding H/He mass limit.

SN	H-rich Model				He-rich Model			
	Phase <sup>a</sup> (days)	Line <sup>b</sup>	Flux Limit (erg/s/cm <sup>2</sup> )	Mass Limit ( $M_{\odot}$ )	Phase <sup>a</sup> (days)	Line <sup>b</sup>	Flux Limit (erg/s/cm <sup>2</sup> )	Mass Limit ( $M_{\odot}$ )
SN1972E	418.1	H $\alpha$	$2.52 \times 10^{-16}$	$4.95 \times 10^{-5}$	349.1	HeI-a	$3.07 \times 10^{-17}$	$9.84 \times 10^{-5}$
SN1981B	267.3	H $\alpha$	$5.54 \times 10^{-16}$	$1.49 \times 10^{-3}$	267.3	HeI-a	$5.86 \times 10^{-16}$	$2.25 \times 10^{-3}$
SN1986G	324.5	H $\alpha$	$1.68 \times 10^{-15}$	$2.84 \times 10^{-4}$	256.5	HeI-b	$6.57 \times 10^{-16}$	$5.29 \times 10^{-4}$
SN1990N	280.0	H $\alpha$	$9.52 \times 10^{-17}$	$5.68 \times 10^{-4}$	280.0	HeI-a	$2.35 \times 10^{-16}$	$1.53 \times 10^{-3}$
SN1991T	258.0	H $\alpha$	$1.99 \times 10^{-14}$	$4.78 \times 10^{-2}$	349.3	HeI-a	$4.84 \times 10^{-14}$	$> 2.0$
SN1991bg	202.4	H $\alpha$	$1.81 \times 10^{-16}$	$1.26 \times 10^{-3}$	202.4	HeI-b	$1.35 \times 10^{-16}$	$2.39 \times 10^{-3}$
SN1992A	291.7	H $\gamma$	$1.87 \times 10^{-15}$	$2.91 \times 10^{-1}$	...	...	...	...
SN1993Z	212.9	H $\alpha$	$8.16 \times 10^{-16}$	$2.68 \times 10^{-2}$	212.9	HeI-b	$5.07 \times 10^{-16}$	$1.20 \times 10^{-1}$
SN1994ae	368.7	H $\alpha$	$5.58 \times 10^{-17}$	$2.84 \times 10^{-4}$	368.7	HeI-a	$6.44 \times 10^{-17}$	$4.20 \times 10^{-4}$
SN1995D	285.6	H $\beta$	$1.50 \times 10^{-16}$	$2.30 \times 10^{-3}$	285.6	HeI-a	$2.57 \times 10^{-16}$	$3.69 \times 10^{-3}$
SN1996X	247.2	H $\alpha$	$5.55 \times 10^{-17}$	$8.24 \times 10^{-4}$	247.2	HeI-a	$6.36 \times 10^{-17}$	$1.28 \times 10^{-3}$
SN1998aq	240.2	H $\alpha$	$7.75 \times 10^{-16}$	$4.84 \times 10^{-3}$	230.2	HeI-a	$8.05 \times 10^{-16}$	$1.40 \times 10^{-2}$
SN1998bu	329.6	H $\alpha$	$2.18 \times 10^{-16}$	$2.86 \times 10^{-4}$	281.0	HeI-b	$1.41 \times 10^{-16}$	$6.45 \times 10^{-4}$
SN1999aa	258.5	H $\alpha$	$5.41 \times 10^{-17}$	$2.82 \times 10^{-3}$	258.5	HeI-a	$4.89 \times 10^{-17}$	$3.85 \times 10^{-3}$
SN1999by	185.2	H $\alpha$	$3.05 \times 10^{-16}$	$1.74 \times 10^{-3}$	185.2	HeI-b	$2.04 \times 10^{-16}$	$3.11 \times 10^{-3}$
SN2000cx	451.2	H $\alpha$	$7.44 \times 10^{-16}$	$8.94 \times 10^{-4}$	451.2	HeI-a	$6.91 \times 10^{-16}$	$> 2.0$
SN2001el	318.1	H $\alpha$	$6.84 \times 10^{-17}$	$3.00 \times 10^{-4}$	310.1	HeI-b	$2.25 \times 10^{-17}$	$4.82 \times 10^{-4}$
SN2002bo	311.2	H $\alpha$	$3.35 \times 10^{-17}$	$3.03 \times 10^{-4}$	227.2	HeI-a	$3.41 \times 10^{-17}$	$6.66 \times 10^{-4}$
SN2002cx	284.0	H $\beta$	$1.47 \times 10^{-17}$	$2.55 \times 10^{-3}$	232.1	HeI-a	$2.30 \times 10^{-17}$	$2.19 \times 10^{-2}$
SN2002dj	272.7	H $\alpha$	$9.53 \times 10^{-17}$	$1.91 \times 10^{-3}$	272.7	HeI-a	$8.24 \times 10^{-17}$	$2.47 \times 10^{-3}$
SN2002er	213.7	H $\alpha$	$7.59 \times 10^{-15}$	$> 2.0$	213.7	HeI-a	$7.23 \times 10^{-15}$	$> 2.0$
SN2003cg	384.8	H $\alpha$	$2.35 \times 10^{-14}$	$3.52 \times 10^{-2}$	384.8	HeI-a	$2.12 \times 10^{-14}$	$> 2.0$
SN2003du	296.4	Pa $\beta$	$2.28 \times 10^{-15}$	$1.00 \times 10^{-2}$	219.4	HeI-b	$9.18 \times 10^{-16}$	$1.16 \times 10^{-1}$
SN2003gs	207.1	H $\alpha$	$5.65 \times 10^{-17}$	$1.05 \times 10^{-3}$	207.1	HeI-b	$3.77 \times 10^{-17}$	$1.80 \times 10^{-3}$
SN2003hv	319.5	H $\alpha$	$2.58 \times 10^{-17}$	$1.82 \times 10^{-4}$	319.5	HeI-a	$6.89 \times 10^{-17}$	$4.54 \times 10^{-4}$
SN2003kf	400.7	H $\beta$	$2.29 \times 10^{-17}$	$2.54 \times 10^{-4}$	400.7	HeI-a	$1.47 \times 10^{-17}$	$1.96 \times 10^{-4}$
SN2004AS	315.3	H $\alpha$	$9.10 \times 10^{-17}$	$1.43 \times 10^{-3}$	315.3	HeI-a	$1.26 \times 10^{-16}$	$2.69 \times 10^{-3}$
SN2004eo	227.3	H $\alpha$	$2.24 \times 10^{-15}$	$7.38 \times 10^{-1}$	227.3	HeI-a	$2.78 \times 10^{-15}$	$> 2.0$
SN2005W	213.4	Pa $\beta$	$5.28 \times 10^{-16}$	$6.59 \times 10^{-3}$	...	...	...	...
SN2005am	383.0	H $\alpha$	$2.17 \times 10^{-17}$	$2.00 \times 10^{-4}$	300.0	HeI-a	$3.50 \times 10^{-17}$	$1.05 \times 10^{-3}$
SN2005cf	352.7	H $\alpha$	$2.27 \times 10^{-17}$	$2.76 \times 10^{-4}$	265.7	HeI-a	$4.62 \times 10^{-17}$	$8.51 \times 10^{-4}$
SN2005hk	407.9	H $\alpha$	$1.48 \times 10^{-17}$	$2.69 \times 10^{-4}$	407.9	HeI-a	$1.44 \times 10^{-17}$	$3.56 \times 10^{-4}$
SN2006X	359.7	H $\alpha$	$4.13 \times 10^{-18}$	$3.43 \times 10^{-5}$	359.7	HeI-a	$3.51 \times 10^{-18}$	$4.01 \times 10^{-5}$
SN2006dd	194.7	H $\alpha$	$1.64 \times 10^{-14}$	$9.86 \times 10^{-1}$	187.7	HeI-a	$2.63 \times 10^{-14}$	$> 2.0$
SN2006gz	339.0	H $\alpha$	$3.22 \times 10^{-17}$	$1.89 \times 10^{-3}$	339.0	HeI-a	$8.49 \times 10^{-18}$	$9.77 \times 10^{-4}$
SN2007af	302.0	H $\alpha$	$2.49 \times 10^{-16}$	$1.11 \times 10^{-3}$	302.0	HeI-a	$1.24 \times 10^{-16}$	$9.36 \times 10^{-4}$
SN2007if	420.9	H $\beta$	$1.95 \times 10^{-18}$	$7.88 \times 10^{-4}$	420.9	HeI-a	$3.48 \times 10^{-18}$	$1.23 \times 10^{-3}$
SN2007le	306.5	H $\beta$	$4.99 \times 10^{-16}$	$4.34 \times 10^{-3}$	306.5	HeI-a	$3.72 \times 10^{-16}$	$3.42 \times 10^{-3}$
SN2007on	380.7	H $\alpha$	$2.79 \times 10^{-18}$	$3.33 \times 10^{-5}$	285.6	HeI-a	$3.33 \times 10^{-18}$	$3.64 \times 10^{-4}$
SN2008A	288.3	H $\alpha$	$2.96 \times 10^{-17}$	$1.40 \times 10^{-3}$	288.3	HeI-a	$3.32 \times 10^{-17}$	$2.20 \times 10^{-3}$
SN2008Q	200.4	H $\alpha$	$1.13 \times 10^{-16}$	$2.82 \times 10^{-3}$	200.4	HeI-b	$1.18 \times 10^{-16}$	$8.04 \times 10^{-3}$
SNF-012	319.4	H $\alpha$	$8.08 \times 10^{-18}$	$4.72 \times 10^{-3}$	265.4	HeI-a	$9.07 \times 10^{-18}$	$1.58 \times 10^{-2}$
SN2009dc	379.8	Pa $\beta$	$8.00 \times 10^{-18}$	$2.72 \times 10^{-4}$	287.2	HeI-a	$1.32 \times 10^{-17}$	$2.91 \times 10^{-3}$
SN2009ig	405.1	H $\alpha$	$7.76 \times 10^{-18}$	$8.72 \times 10^{-5}$	405.1	HeI-a	$1.34 \times 10^{-17}$	$1.56 \times 10^{-4}$
SN2009le	316.5	H $\alpha$	$6.89 \times 10^{-17}$	$2.45 \times 10^{-3}$	316.5	HeI-a	$1.29 \times 10^{-16}$	$6.42 \times 10^{-3}$
SN2010ev	270.2	H $\beta$	$6.34 \times 10^{-17}$	$2.39 \times 10^{-3}$	270.2	HeI-b	$1.70 \times 10^{-17}$	$1.44 \times 10^{-3}$
SN2010gp	276.2	H $\alpha$	$6.51 \times 10^{-18}$	$6.47 \times 10^{-4}$	276.2	HeI-a	$1.14 \times 10^{-17}$	$1.36 \times 10^{-3}$
SN2010hg	203.2	H $\alpha$	$3.55 \times 10^{-16}$	$8.95 \times 10^{-3}$	203.2	HeI-b	$7.22 \times 10^{-17}$	$5.61 \times 10^{-3}$
SN2010lp	264.0	H $\beta$	$2.00 \times 10^{-16}$	$4.88 \times 10^{-3}$	264.0	HeI-a	$1.87 \times 10^{-16}$	$4.70 \times 10^{-3}$
SN2011K	344.2	H $\beta$	$6.35 \times 10^{-17}$	$1.73 \times 10^{-3}$	344.2	HeI-a	$1.11 \times 10^{-16}$	$2.77 \times 10^{-3}$
SNhunt37	306.2	H $\beta$	$1.01 \times 10^{-16}$	$9.84 \times 10^{-4}$	306.2	HeI-a	$1.05 \times 10^{-16}$	$1.03 \times 10^{-3}$
SN2011at	359.1	H $\beta$	$1.54 \times 10^{-16}$	$1.17 \times 10^{-3}$	359.1	HeI-a	$2.87 \times 10^{-16}$	$1.93 \times 10^{-3}$
SN2011by	207.1	H $\alpha$	$2.60 \times 10^{-16}$	$2.33 \times 10^{-3}$	207.1	HeI-b	$1.75 \times 10^{-16}$	$4.28 \times 10^{-3}$
SN2011ek	422.4	H $\alpha$	$4.24 \times 10^{-17}$	$2.06 \times 10^{-4}$	422.4	HeI-a	$8.19 \times 10^{-17}$	$4.19 \times 10^{-4}$
PTF11kly	228.9	H $\alpha$	$3.70 \times 10^{-15}$	$2.63 \times 10^{-3}$	228.9	HeI-a	$8.68 \times 10^{-15}$	$8.74 \times 10^{-3}$
SN2011iy	204.9	H $\alpha$	$8.11 \times 10^{-16}$	$5.19 \times 10^{-3}$	204.9	HeI-b	$7.12 \times 10^{-16}$	$1.38 \times 10^{-2}$
SN2011im	313.3	H $\beta$	$5.13 \times 10^{-17}$	$3.79 \times 10^{-3}$	313.3	HeI-a	$8.73 \times 10^{-17}$	$6.30 \times 10^{-3}$
SN2011iv	304.4	H $\alpha$	$1.16 \times 10^{-16}$	$5.36 \times 10^{-4}$	304.4	HeI-a	$1.25 \times 10^{-16}$	$7.79 \times 10^{-4}$

**Table B4 – continued** Flux limits for each line in Table 2 and the corresponding H/He mass limit if computed. Flux limits are given in [erg/s/cm<sup>2</sup>] and stripped mass limits are given in [ $M_{\odot}$ ].

SN	H-rich Model				He-rich Model			
	Phase <sup>a</sup> (days)	Line <sup>b</sup>	Flux Limit (erg/s/cm <sup>2</sup> )	Mass Limit ( $M_{\odot}$ )	Phase <sup>a</sup> (days)	Line <sup>b</sup>	Flux Limit (erg/s/cm <sup>2</sup> )	Mass Limit ( $M_{\odot}$ )
SN2012Z	254.3	H $\beta$	$6.99 \times 10^{-16}$	$1.25 \times 10^{-2}$	247.3	HeI-a	$5.71 \times 10^{-16}$	$1.19 \times 10^{-2}$
SN2012cg	338.1	Pa $\alpha$	$1.33 \times 10^{-16}$	$2.08 \times 10^{-4}$	286.3	HeI-a	$2.30 \times 10^{-16}$	$1.13 \times 10^{-3}$
SNhunt136	319.1	H $\alpha$	$3.21 \times 10^{-16}$	$7.37 \times 10^{-4}$	319.1	HeI-a	$3.48 \times 10^{-16}$	$1.09 \times 10^{-3}$
SN2012ei	254.4	H $\alpha$	$1.71 \times 10^{-17}$	$2.99 \times 10^{-4}$	254.4	HeI-a	$2.43 \times 10^{-17}$	$5.08 \times 10^{-4}$
SN2012fr	356.3	Pa $\alpha$	$3.08 \times 10^{-16}$	$3.64 \times 10^{-4}$	289.5	HeI-a	$7.73 \times 10^{-17}$	$5.47 \times 10^{-4}$
SN2012hr	458.5	H $\beta$	$3.42 \times 10^{-17}$	$4.81 \times 10^{-4}$	284.5	HeI-a	$5.01 \times 10^{-17}$	$1.45 \times 10^{-3}$
SN2012ht	422.2	Pa $\alpha$	$1.27 \times 10^{-16}$	$1.84 \times 10^{-4}$	422.2	HeI-a	$1.73 \times 10^{-16}$	$4.88 \times 10^{-4}$
SN2013aa	426.0	Pa $\alpha$	$6.72 \times 10^{-17}$	$6.29 \times 10^{-5}$	345.9	HeI-b	$4.06 \times 10^{-17}$	$9.53 \times 10^{-4}$
SN2013ct	228.9	Pa $\alpha$	$2.23 \times 10^{-16}$	$4.10 \times 10^{-4}$	228.9	HeI-c	$3.17 \times 10^{-16}$	$6.49 \times 10^{-4}$
SNhunt196	303.8	Pa $\alpha$	$8.05 \times 10^{-17}$	$5.48 \times 10^{-4}$	262.8	HeI-a	$8.54 \times 10^{-17}$	$2.17 \times 10^{-3}$
SN2013dy	419.0	H $\alpha$	$4.30 \times 10^{-17}$	$1.25 \times 10^{-4}$	333.6	HeI-a	$3.53 \times 10^{-17}$	$4.85 \times 10^{-4}$
SN2013gy	424.1	H $\alpha$	$8.27 \times 10^{-18}$	$1.50 \times 10^{-4}$	271.1	HeI-a	$5.91 \times 10^{-18}$	$2.72 \times 10^{-3}$
SN2014J	267.7	H $\beta$	$2.60 \times 10^{-15}$	$7.47 \times 10^{-4}$	267.7	HeI-a	$5.19 \times 10^{-15}$	$1.26 \times 10^{-3}$
SN2014bv	293.9	H $\alpha$	$1.18 \times 10^{-16}$	$6.42 \times 10^{-4}$	293.9	HeI-a	$1.93 \times 10^{-16}$	$1.28 \times 10^{-3}$
ASASSN-14hr	467.6	H $\alpha$	$2.05 \times 10^{-16}$	$3.70 \times 10^{-3}$	467.6	HeI-a	$1.29 \times 10^{-16}$	$> 2.0$
ASASSN-14jg	325.5	H $\alpha$	$8.65 \times 10^{-17}$	$1.91 \times 10^{-3}$	222.5	HeI-a	$7.37 \times 10^{-17}$	$7.05 \times 10^{-3}$
ASASSN-14jc	390.0	H $\alpha$	$2.19 \times 10^{-16}$	$1.48 \times 10^{-3}$	390.0	HeI-a	$1.11 \times 10^{-16}$	$1.26 \times 10^{-3}$
ASASSN-14jz	203.5	H $\alpha$	$2.79 \times 10^{-16}$	$1.31 \times 10^{-2}$	203.5	HeI-b	$8.51 \times 10^{-17}$	$1.21 \times 10^{-2}$
ASASSN-14kq	412.9	H $\alpha$	$5.26 \times 10^{-16}$	$1.74 \times 10^{-2}$	412.9	HeI-a	$1.73 \times 10^{-16}$	$> 2.0$
ASASSN-14lv	398.0	H $\alpha$	$2.38 \times 10^{-16}$	$2.18 \times 10^{-2}$	398.0	HeI-a	$1.10 \times 10^{-16}$	$> 2.0$
ASASSN-14lu	476.6	H $\alpha$	$5.57 \times 10^{-16}$	$2.99 \times 10^{-3}$	476.6	HeI-a	$4.44 \times 10^{-16}$	$> 2.0$
ASASSN-14lt	388.9	H $\alpha$	$8.22 \times 10^{-17}$	$3.86 \times 10^{-3}$	388.9	HeI-a	$1.03 \times 10^{-16}$	$> 2.0$
ASASSN-14me	362.0	H $\alpha$	$1.22 \times 10^{-16}$	$2.47 \times 10^{-3}$	304.1	HeI-a	$1.36 \times 10^{-16}$	$1.32 \times 10^{-2}$
ASASSN-15be	264.8	H $\beta$	$2.90 \times 10^{-17}$	$4.20 \times 10^{-3}$	264.8	HeI-a	$9.48 \times 10^{-17}$	$1.38 \times 10^{-2}$
SN2015F	295.5	H $\alpha$	$1.63 \times 10^{-17}$	$1.64 \times 10^{-4}$	295.5	HeI-a	$1.10 \times 10^{-17}$	$1.70 \times 10^{-4}$
ASASSN-15hx	444.8	H $\alpha$	$1.08 \times 10^{-17}$	$8.98 \times 10^{-5}$	250.1	HeI-a	$3.25 \times 10^{-17}$	$2.51 \times 10^{-3}$
SN2015I	268.6	H $\alpha$	$2.53 \times 10^{-16}$	$4.21 \times 10^{-3}$	268.6	HeI-a	$1.91 \times 10^{-16}$	$4.97 \times 10^{-3}$
PSN J1149	204.7	Pa $\alpha$	$9.61 \times 10^{-17}$	$9.65 \times 10^{-4}$	204.7	HeI-c	$1.74 \times 10^{-16}$	$1.94 \times 10^{-3}$
SN2016brx	184.0	H $\alpha$	$3.83 \times 10^{-17}$	$1.77 \times 10^{-3}$	184.0	HeI-b	$3.59 \times 10^{-17}$	$4.24 \times 10^{-3}$
SN2016bry	205.7	H $\beta$	$1.33 \times 10^{-16}$	$8.25 \times 10^{-3}$	...	...	...	...
ASASSN-16eq	202.1	H $\beta$	$3.03 \times 10^{-16}$	$1.03 \times 10^{-2}$	...	...	...	...
Gaia16avm	229.2	H $\alpha$	$2.49 \times 10^{-17}$	$2.23 \times 10^{-2}$	229.2	HeI-a	$2.16 \times 10^{-17}$	$3.34 \times 10^{-2}$
ATLAS16cpu	182.3	H $\alpha$	$1.42 \times 10^{-16}$	$2.37 \times 10^{-2}$	182.3	HeI-b	$1.76 \times 10^{-16}$	$1.87 \times 10^{-1}$
SN2016gxp	218.3	H $\alpha$	$1.56 \times 10^{-16}$	$1.02 \times 10^{-2}$	218.3	HeI-a	$1.42 \times 10^{-16}$	$1.51 \times 10^{-2}$
ASASSN-17cs	219.8	H $\alpha$	$1.25 \times 10^{-16}$	$9.13 \times 10^{-3}$	219.8	HeI-a	$5.11 \times 10^{-17}$	$6.02 \times 10^{-3}$
DLT17u	316.0	H $\alpha$	$1.03 \times 10^{-16}$	$2.43 \times 10^{-4}$	316.0	HeI-a	$1.51 \times 10^{-16}$	$4.17 \times 10^{-4}$
ATLAS17dfo	288.0	H $\alpha$	$2.14 \times 10^{-17}$	$8.99 \times 10^{-4}$	288.0	HeI-a	$3.21 \times 10^{-17}$	$1.73 \times 10^{-3}$
DLT17ar	227.6	H $\alpha$	$4.06 \times 10^{-17}$	$1.70 \times 10^{-3}$	227.6	HeI-a	$2.82 \times 10^{-17}$	$1.84 \times 10^{-3}$
DLT17bk	284.3	H $\alpha$	$1.63 \times 10^{-16}$	$5.13 \times 10^{-3}$	284.3	HeI-a	$2.60 \times 10^{-16}$	$1.30 \times 10^{-2}$
ASASSN-18hz	228.5	H $\alpha$	$1.77 \times 10^{-16}$	$1.49 \times 10^{-2}$	228.5	HeI-a	$7.81 \times 10^{-17}$	$1.02 \times 10^{-2}$
SN2017ezd	255.1	H $\alpha$	$1.55 \times 10^{-17}$	$1.70 \times 10^{-3}$	255.1	HeI-a	$3.64 \times 10^{-17}$	$5.18 \times 10^{-3}$
DLT17bx	379.3	H $\alpha$	$1.14 \times 10^{-17}$	$1.27 \times 10^{-4}$	379.3	HeI-a	$1.69 \times 10^{-17}$	$2.11 \times 10^{-4}$
ATLAS17jiv	294.9	H $\alpha$	$7.74 \times 10^{-17}$	$1.14 \times 10^{-3}$	294.9	HeI-a	$1.74 \times 10^{-16}$	$3.14 \times 10^{-3}$
DLT17cd	228.5	H $\alpha$	$1.90 \times 10^{-16}$	$3.00 \times 10^{-3}$	228.5	HeI-b	$1.82 \times 10^{-16}$	$7.95 \times 10^{-3}$
SN2017glq	331.3	H $\alpha$	$2.04 \times 10^{-17}$	$4.02 \times 10^{-4}$	331.3	HeI-a	$1.64 \times 10^{-17}$	$4.73 \times 10^{-4}$
ATLAS17nmh	194.8	H $\alpha$	$5.42 \times 10^{-17}$	$2.31 \times 10^{-3}$	194.8	HeI-b	$5.35 \times 10^{-17}$	$6.05 \times 10^{-3}$
ATLAS17nse	306.8	H $\alpha$	$2.31 \times 10^{-17}$	$5.95 \times 10^{-4}$	253.0	HeI-a	$2.01 \times 10^{-17}$	$1.69 \times 10^{-3}$
ASASSN-18bt	236.2	H $\alpha$	$4.48 \times 10^{-17}$	$1.94 \times 10^{-3}$	267.3	HeI-a	$5.52 \times 10^{-17}$	$5.54 \times 10^{-3}$
ASASSN-18da	220.4	H $\alpha$	$8.98 \times 10^{-17}$	$9.96 \times 10^{-3}$	220.4	HeI-a	$6.54 \times 10^{-17}$	$1.16 \times 10^{-2}$
DLT18h	335.9	H $\alpha$	$1.55 \times 10^{-17}$	$3.38 \times 10^{-4}$	335.9	HeI-a	$1.69 \times 10^{-17}$	$4.87 \times 10^{-4}$
DLT18i	237.2	H $\alpha$	$2.26 \times 10^{-17}$	$6.84 \times 10^{-4}$	237.2	HeI-a	$1.18 \times 10^{-17}$	$6.00 \times 10^{-4}$
ASASSN-18hb	237.4	H $\alpha$	$3.28 \times 10^{-17}$	$2.68 \times 10^{-3}$	237.4	HeI-a	$5.08 \times 10^{-17}$	$5.96 \times 10^{-3}$

<sup>a</sup> Relative to  $t_{\max}$ .

<sup>b</sup> Corresponds to the lines listed in Table 2.

**Table B5.** New photometry presented in this study. Some data stem from archival images processed by this study for flux calibration purposes.

SN	MJD	Filter	AB Mag
ASASSN-14jg	57183.78	V	20.49 ± 0.08
ASASSN-15hx	57396.33	V	21.33 ± 0.04
SN2001el	52492.37	I	19.82 ± 0.07
SN2001el	52549.24	I	20.24 ± 0.07
SN2001el	52552.37	I	20.23 ± 0.08
SN2001el	52618.04	I	22.08 ± 0.15
SN2001el	52492.36	R	20.68 ± 0.10
SN2001el	52549.23	R	21.47 ± 0.08
SN2001el	52552.35	R	21.34 ± 0.08
SN2001el	52612.04	R	22.31 ± 0.10
SN2001el	52617.10	R	22.16 ± 0.10
SN2001el	52492.35	V	19.93 ± 0.09
SN2001el	52549.22	V	20.76 ± 0.09
SN2001el	52552.34	V	20.55 ± 0.08
SN2001el	52612.10	V	21.02 ± 0.15
SN2007on	54800.23	r	24.70 ± 0.35
SN2007on	54772.70	r	24.15 ± 0.14
SN2009ig	55484.29	I	22.39 ± 0.07
SN2009ig	55484.28	R	22.53 ± 0.08
SN2009ig	55484.28	V	22.09 ± 0.06
SN2009le	55484.30	V	21.88 ± 0.18
SN2009le	55484.31	I	21.79 ± 0.45
SN2009le	55484.31	R	21.47 ± 0.35
SN2010ev	55655.00	V	20.41 ± 0.07
SN2010ev	55655.00	R	20.58 ± 0.08
SN2010ev	55655.00	I	20.65 ± 0.07
SN2010ev	55655.00	B	20.22 ± 0.05
SN2010gp	55682.27	V	23.19 ± 0.06
SN2010gp	55682.27	R	23.09 ± 0.11
SN2010gp	55682.28	I	22.76 ± 0.11
SN2010gp	55682.26	B	22.16 ± 0.22
SN2010hg	55654.15	B	19.15 ± 0.11
SN2010hg	55654.15	V	19.35 ± 0.07
SN2010hg	55654.15	R	20.05 ± 0.06
SN2010hg	55654.15	I	20.06 ± 0.08
SN2010lp	55834.24	V	20.66 ± 0.16
SN2010lp	55834.26	I	19.50 ± 0.09
SN2010lp	55834.25	R	20.09 ± 0.07
SN2011K	55831.38	I	21.69 ± 0.06
SN2011K	55831.37	R	21.59 ± 0.05
SN2011K	55831.36	V	22.41 ± 0.09
SNhunt37	55932.34	V	20.98 ± 0.11
SNhunt37	55932.34	R	20.25 ± 0.15
SNhunt37	55932.34	I	19.89 ± 0.12
SN2011at	55943.18	I	20.13 ± 0.06
SN2011at	55943.18	R	20.17 ± 0.05
SN2011at	55943.18	V	21.02 ± 0.06
SN2011ek	56210.20	V	23.07 ± 0.17
SN2011ek	56210.20	R	21.95 ± 0.12
SN2011ek	56210.21	I	21.62 ± 0.12
SN2011im	56213.03	I	21.05 ± 0.07
SN2011im	56213.02	R	21.37 ± 0.08
SN2011im	56206.08	R	20.77 ± 0.08
SN2011im	56213.01	V	22.84 ± 0.11
SN2011im	56206.08	V	22.11 ± 0.09
SN2011iv	56207.29	I	17.55 ± 0.13
SN2011iv	56207.29	R	18.08 ± 0.11
SN2011iv	56207.29	V	17.49 ± 0.11
SN2012cg	56444.99	I	19.49 ± 0.11
SN2012cg	56444.99	R	18.40 ± 0.09
SN2012cg	56444.99	V	20.76 ± 0.10
SNhunt136	56423.19	I	21.50 ± 0.13
SNhunt136	56423.19	R	21.67 ± 0.12
SNhunt136	56423.18	V	22.06 ± 0.12
SN2012ei	56414.88	r	20.54 ± 0.11
SN2013gy	56883.41	R	23.50 ± 0.27
SN2014bv	57134.16	g	20.91 ± 0.06
SN2015F	57273.30	V	18.90 ± 0.02
SN2015F	57306.35	V	19.31 ± 0.02
SN2015F	57334.29	V	19.66 ± 0.02
SN2015F	57403.20	V	20.87 ± 0.07
SN2015F	57424.11	V	20.99 ± 0.03
SN2015F	57443.15	V	21.33 ± 0.07
SN2015F	57494.06	V	22.28 ± 0.08

**Table B5 – continued** New photometry presented in this study.

SN	MJD	Filter	AB Mag
SN2015F	57273.30	g	18.74 ± 0.02
SN2015F	57306.35	g	19.10 ± 0.02
SN2015F	57334.30	g	19.65 ± 0.02
SN2015F	57403.24	g	20.48 ± 0.05
SN2015F	57424.12	g	20.82 ± 0.03
SN2015F	57443.16	g	20.89 ± 0.05
SN2015F	57494.04	g	22.07 ± 0.05
SN2015F	57273.30	r	19.08 ± 0.03
SN2015F	57306.35	r	19.64 ± 0.03
SN2015F	57334.31	r	20.17 ± 0.06
SN2015F	57403.26	r	21.03 ± 0.08
SN2015F	57424.13	r	21.18 ± 0.04
SN2015F	57443.17	r	21.28 ± 0.07
SN2015F	57494.09	r	21.72 ± 0.08
SN2015F	57273.30	i	19.07 ± 0.04
SN2015F	57306.36	i	19.44 ± 0.04
SN2015F	57334.32	i	19.81 ± 0.05
SN2015F	57403.28	i	20.31 ± 0.05
SN2015F	57424.14	i	20.74 ± 0.04
SN2015F	57443.17	i	19.99 ± 0.04
SN2015F	57494.11	i	21.12 ± 0.05
SN2015F	57395.26	B	20.37 ± 0.07
SN2015F	57395.26	V	20.33 ± 0.09
SN2015I	57426.17	r	20.29 ± 0.04
SN2015I	57396.93	V	20.29 ± 0.02
SN2015I	57396.93	I	19.95 ± 0.04
SN2016bry	57712.14	r	20.71 ± 0.09
ASASSN-16eq	57709.19	r	21.00 ± 0.06
Gaia16avm	57814.42	r	22.55 ± 0.05
ATLAS16cpu	57814.30	r	22.29 ± 0.08
SN2016gxp	57900.43	r	20.82 ± 0.14
ASASSN-17cs	58037.23	V	19.08 ± 0.11
DLT17u	58158.27	r	20.05 ± 0.04
ATLAS17dfo	58138.29	V	20.18 ± 0.08
DLT17ar	58098.28	V	20.81 ± 0.03
DLT17bk	58195.34	V	23.34 ± 0.08
ASASSN-18hz	58164.27	V	20.09 ± 0.07
SN2017ezd	58196.35	V	23.24 ± 0.22
DLT17bx	58339.26	V	21.04 ± 0.08
DLT17cd	58218.03	V	20.08 ± 0.04
ATLAS17jiv	58280.26	V	20.71 ± 0.11
SN2017glq	58347.25	V	22.87 ± 0.06
ATLAS17nmh	58253.17	V	19.47 ± 0.08
ATLAS17nse	58371.38	V	21.24 ± 0.08
ATLAS17nse	58381.36	V	21.47 ± 0.08
ATLAS17nse	58425.20	V	22.21 ± 0.09
ASASSN-18hb	58460.28	V	21.65 ± 0.08
SN2018ctv	58458.15	V	22.51 ± 0.18
SN2018dda	58462.05	V	19.63 ± 0.17
SN2018ghb	58541.13	V	19.95 ± 0.05
SN2018imd	58543.16	V	18.81 ± 0.09
ASASSN-18da	58399.20	V	20.20 ± 0.15
DLT18h	58521.21	V	22.57 ± 0.06
DLT18i	58432.31	V	21.45 ± 0.11

**Table B6.** Photometry data for each SN Ia studied in this work.  $N_{tot}$  refers to the total number of photometric points for a given SN. Phases are given relative to maximum light. Objects denoted with a  $\star$  are used in deriving the NPPR (Appendix A).

SN	$N_{tot}$	Phases	Filters	Refs.
ASASSN-14jg $\star$	113	5 – 268	B, V, g, r, i	ASAS-SN; Graham et al. (2017); This work
ASASSN-15hx	202	-16 – 325	V, g, SwiftU, SwiftB, SwiftV	ASAS-SN; This work
PSN J1149	16	-12 – 141	B, V, I	ASAS-SN
SN1972E $\star$	468	-23 – 359	U, B, V, R, I	Przybylski (1972); Cousins (1972); Barbbon et al. (1972); Ardeberg & de Groot (1973); van Genderen (1975); Osmer et al. (1972); Lee et al. (1972); Frye et al. (1972); Przybylski (1972)
SN1980N $\star$	238	-11 – 368	U, B, V, R, I, H	Hamuy et al. (1991); Blanco et al. (1980); Blanco et al. (1980); Olszewski (1982); Elias & Frogel (1983)
SN1981B	281	-9 – 136	U, B, V, R, J, H, K	Busko et al. (1981); Tsvetkov (1982); Buta & Turner (1983); Tsvetkov (1982); Barbon et al. (1982); Vettolani et al. (1981); Elias & Frogel (1983)
SN1981D $\star$	30	-14 – 274	B, V, J, H	Cragg et al. (1981); Hamuy et al. (1991); Elias & Frogel (1983)
SN1983W $\star$	57	-7 – 161	U, B, V	
SN1986G	93	-7 – 403	U, B, V, R, I	Munch et al. (1986); Phillips et al. (1987); Bues et al. (1986); Blanco et al. (1986); Turatto et al. (1990); Schaefer (1987)
SN1989B $\star$	350	-5 – 263	U, B, V, R, I, J, H, K	Barbon et al. (1990); Suntzeff et al. (1989); Lavery (1989); Tsvetkov et al. (1990); Wells et al. (1994); Pollas et al. (1989); Volkov (1991); Gaskell et al. (1989)
SN1990N $\star$	289	-12 – 376	U, B, V, R, I	Lira et al. (1998)
SN1990O $\star$	41	2 – 309	B, V, R, I	Hamuy et al. (1996)
SN1991T $\star$	669	-13 – 454	U, B, V, R, I, J, H, K	Tsvetkov (1986); Altavilla et al. (2004); Waagen et al. (1991); Lira et al. (1998); Menzies et al. (1991); Krisciunas et al. (2004); Holberg et al. (1991); Ford et al. (1993); Gilmore (1991); Schmidt et al. (1994)
SN1991bg	171	10 – 528	B, V, R, I, J, H, K	Leibundgut et al. (1993); Turatto et al. (1996); Krisciunas et al. (2004)
SN1992A $\star$	62	7 – 526	B, V	Tillier & Pinto (1992)

**Table B6 – continued** Continuation of Table B6.

SN	$N_{tot}$	Phases	Filters	Refs.
SN1994D $\star$	371	-14 – 432	U, B, V, R, I, J, H, K	Treffers et al. (1994); Richmond et al. (1995); Cumming et al. (1994); Heradeau et al. (1994); Argyle et al. (1994); Mikuz (1994); Altavilla et al. (2004)
SN1994ae $\star$	301	-15 – 530	U, B, V, R, I	Vanmunster et al. (1994); Riess et al. (2005); Riess et al. (1999); Vanmunster et al. (1994); Ho et al. (2001); Tsvetkov & Pavlyuk (1997); Altavilla et al. (2004)
SN1995D $\star$	225	-8 – 424	B, V, R, I	Mikuz (1995); Riess et al. (1999); Altavilla et al. (2004); Ho et al. (2001)
SN1995ac $\star$	100	-5 – 250	B, V, R, I	Riess et al. (1999); Altavilla et al. (2004)
SN1995al $\star$	115	-13 – 182	U, B, V, R, I	Riess et al. (1999)
SN1996X $\star$	241	-4 – 502	U, B, V, R, I, J, H, K	Strohmayer et al. (1996); Salvo et al. (2001); Riess et al. (1999)
SN1997bp $\star$	101	0 – 416	U, B, V, R, I	CfA; Altavilla et al. (2004)
SN1997br $\star$	223	-9 – 402	U, B, V, R, I	Li et al. (1999); CfA; Altavilla et al. (2004)
SN1997cw $\star$	75	13 – 181	U, B, V, R, I	CfA
SN1998V $\star$	60	2 – 187	U, B, V, R, I	CfA
SN1998aq $\star$	257	-10 – 344	U, B, V, R, I	Riess et al. (2005)
SN1998bu	914	-7 – 56	U, B, V, R, I, J, H, K	Jha et al. (1999); Hernandez et al. (2000); Suntzeff et al. (1999)
SN1998ec $\star$	59	5 – 186	U, B, V, R, I	BSNIP; CfA
SN1999aa	289	-11 – 79	U, B, V, R, I, J, K	Kowalski et al. (2008); BSNIP; CfA; Krisciunas et al. (2000); Altavilla et al. (2004)
SN1999ac $\star$	356	-13 – 183	U, B, V, R, I, H, Ks	Phillips et al. (2006); BSNIP; CfA
SN1999by $\star$	377	-12 – 212	U, B, V, R, I, J, H, K	Garnavich et al. (2004); BSNIP; Toth & Szabó (2000)
SN1999dq $\star$	247	-11 – 154	U, B, V, R, I	BSNIP; CfA
SN1999gd $\star$	35	-3 – 150	U, B, V, R, I	CfA
SN2000E $\star$	287	-16 – 484	U, B, V, R, I, J	Valentini et al. (2003); Lair et al. (2006)

**Table B6 – continued** Continuation of Table B6.

SN	$N_{tot}$	Phases	Filters	Refs.
SN2001V*	370	-14 - 351	U, B, V, R, I	Hicken et al. (2009); Vinkó et al. (2003); Lair et al. (2006); BSNIP
SN2001bg*	91	-2 - 358	B, V, R, I	BSNIP; Lair et al. (2006)
SN2001el*	566	-13 - 435	U, B, V, R, I, J, H, K	Krisciunas et al. (2003); This work
SN2002bo	656	-14 - 100	U, B, V, R, I, J, H, K	BSNIP; Benetti et al. (2004); Hicken et al. (2009); Szabó et al. (2003); Krisciunas et al. (2004)
SN2002cx	110	-8 - 50	B, V, R, I	BSNIP
SN2002dj	166	-14 - 65	U, B, V, R, I, J, H, K	Pignata et al. (2008); BSNIP; Hicken et al. (2009)
SN2002dp*	190	-6 - 183	U, B, V, R, I	BSNIP; Hicken et al. (2009)
SN2002er*	339	-16 - 323	U, B, V, R, I	Pignata et al. (2004); BSNIP; Christensen et al. (2003)
SN2002ha*	162	-12 - 237	U, B, V, R, I	BSNIP; Hicken et al. (2009)
SN2003K*	38	1 - 169	U, B, V, R, I	Hicken et al. (2009)
SN2003cg	439	-18 - 413	U, B, V, R, I, J, H, K	Elias-Rosa et al. (2006); Ganeshalingam et al. (2010); Hicken et al. (2009)
SN2003du	628	-12 - 465	U, B, V, R, I, J, H, K	Anupama et al. (2005); Stanishev et al. (2007); Hicken et al. (2009); BSNIP
SN2003gs*	188	8 - 378	B, V, R, I, J, H, K	Krisciunas et al. (2009); BSNIP
SN2003hv	217	0 - 538	B, V, R, I, J, H, K	Leloudas et al. (2009); BSNIP
SN2003kf	180	-3 - 104	U, B, V, R, I	BSNIP; Hicken et al. (2009)
SN2004S	215	1 - 375	B, V, R, I, J, H, K	BSNIP; Krisciunas et al. (2007); Misra et al. (2005)
SN2004eo	768	-12 - 345	U, B, V, R, I, J, H, K, u, g, r, i	CSP; Pastorello et al. (2007); BSNIP
SN2005W	115	-8 - 16	B, V, u, g, r, i	CSP
SN2005am	388	-2 - 76	U, B, V, R, I, J, H, K, u, g, r, i	CSP; BSNIP; Hicken et al. (2009)

**Table B6 – continued** Continuation of Table B6.

SN	$N_{tot}$	Phases	Filters	Refs.
SN2005ki*	344	-12 - 155	U, B, V, J, H, u, g, r, i	Hicken et al. (2009); CSP
SN2006X*	638	-11 - 151	U, B, V, R, I, J, H, K, Ks, u, g, r, i	Brown et al. (2014); BSNIP; CSP; Hicken et al. (2009); Friedman et al. (2015)
SN2006dd*	284	-11 - 228	B, V, R, I, J, H, K, u, g, r, i	Stritzinger et al. (2010)
SN2006gz	107	-14 - 49	U, B, V, r, i	Hicken et al. (2007)
SN2007af*	807	-12 - 274	U, B, V, R, I, J, H, K, u, g, r, i	Brown et al. (2014); Hicken et al. (2009); CSP; BSNIP
SN2007bd*	120	-10 - 214	B, V, J, H, u, g, r, i	Hicken et al. (2009); CSP
SN2007if	224	14 - 358	B, V, R, I, J, H, Ks, u, g, r, i	CSP; Hicken et al. (2012); Friedman et al. (2015); Taubenberger et al. (2013a)
SN2007is*	24	2 - 163	B, V, r, i	Hicken et al. (2012)
SN2007le	484	-11 - 84	B, V, R, I, J, H, Ks, u, g, r, i	CSP; Friedman et al. (2015); BSNIP; Hicken et al. (2012)
SN2007on	665	-9 - 405	U, B, V, Y, J, H, K, u, g, r, i	CSP; Brown et al. (2014); This work; Gall et al. (2018)
SN2007sr*	347	5 - 196	U, B, V, R, I, J, H, Ks	Hicken et al. (2009); BSNIP; Brown et al. (2014); Friedman et al. (2015)
SN2007sw*	101	-2 - 154	B, V, r, i	Hicken et al. (2012)
SN2008A	201	-7 - 208	U, B, V, R, I, J, H, Ks, r, i	Hicken et al. (2012); Brown et al. (2014); Friedman et al. (2015); BSNIP
SN2008Q	84	-9 - 208	U, B, V, R, I, r, i	Brown et al. (2014); Hicken et al. (2012); BSNIP
SN2009dc	672	-20 - 286	U, B, V, R, I, J, H, Ks, u, g, r, i	Silverman et al. (2011); Friedman et al. (2015); Hicken et al. (2012); CSP; Brown et al. (2014) MNRAS <b>000</b> , 1–21 (2019)
SN2009ig	258	-15 - 404	U, B, V, R, I, J, H, Ks, u, g, r, i	Brown et al. (2014); Brown et al. (2012); Hicken et al. (2012); Friedman et al. (2015)

**Table B6 – continued** Continuation of Table B6.

SN	$N_{tot}$	Phases	Filters	Refs.
SN2009kq*	128	-4 - 177	B, V, J, H, Ks, u, r, i	Hicken et al. (2012); Friedman et al. (2015)
SN2009le	57	-12 - 318	B, V, R, I, J, H, Ks, u, r, i	Hicken et al. (2012); Friedman et al. (2015); This work
SN2009nr*	147	-13 - 175	U, B, V, R, I	Khan et al. (2011)
SN2010ag*	102	-3 - 179	B, V, J, H, Ks, u, r, i	Friedman et al. (2015); Hicken et al. (2012)
SN2010dd*	96	-23 - 523	R	Maguire et al. (2014)
SN2010ev*	67	-7 - 270	U, B, V, R, I, u, g, r, i, z	Gutiérrez et al. (2016); Brown et al. (2014); This work
SN2010gp	59	-4 - 276	U, B, V, R, I	Brown et al. (2014); This work
SN2011K	40	-1 - 253	V, R, I, J, H, Ks	Friedman et al. (2015); This work
SNhunt37	90	1 - 312	V, R, I, J, H, Ks	Friedman et al. (2015); This work
SN2011at	57	7 - 463	U, B, V, R, I, J, H, Ks	Brown et al. (2014); Friedman et al. (2015); This work
SN2011by	158	-11 - 44	U, B, V, J, H, Ks	Brown et al. (2014); Friedman et al. (2015)
SN2011ek	68	-6 - 421	U, B, V, R, I	Maguire et al. (2014); Brown et al. (2014); This work
PTF11kly	1956	-19 - 571	U, B, V, R, I, J, H, K, g, r	Firth et al. (2015); Nugent et al. (2011a); Brown et al. (2014); Guillochon et al. (2017); Tsvetkov et al. (2013); Munari et al. (2013); Rich- mond & Smith (2012); Weyant et al. (2018)
SN2011im	63	-13 - 310	U, B, V, R, I	Firth et al. (2015); Maguire et al. (2014); Brown et al. (2014); This work
SN2011iv	235	-6 - 301	B, V, R, I, Y, J, H, u, g, r, i	This work; Gall et al. (2018)
SN2011iy	2	127 - 127	J, H	Weyant et al. (2018)
SN2012Z	306	-8 - 265	U, B, V, J, H, u, g, r, i	Stritzinger et al. (2015); Brown et al. (2014); Foley et al. (2013)
SN2012cg	176	-16 - 598	U, B, V, R, I	Brown et al. (2014); Munari et al. (2013); This work

**Table B6 – continued** Continuation of Table B6.

SN	$N_{tot}$	Phases	Filters	Refs.
SNhunt196	233	-20 - 261	U, B, V, R, I, J, H, u, g, r, i	Graham et al. (2017); Walker et al. (2015); Brown et al. (2014); Weyant et al. (2018)
SN2013ct	7	80 - 228	g, r, z	Inserra et al. (2013)
SN2013dy	1210	-16 - 337	U, B, V, R, I, J, H, g, r, i	Graham et al. (2017); Pan et al. (2015); Brown et al. (2014); Zhai et al. (2016)
SN2013gy	155	-17 - 234	U, B, V, R, g, r, i	Zheng et al. (2013); Graham et al. (2017); Brown et al. (2014); This work
SN2014J	706	-12 - 76	U, B, V, R, I, g, r, i, z	Goobar et al. (2014); Foley et al. (2014); Brown et al. (2014); Zhang et al. (2014); Tsvetkov et al. (2014)
SN2014bv	45	0 - 293	U, B, V, g	Brown et al. (2014); This work
SN2015F*	477	-14 - 594	U, B, V, I, g, r, i, SwiftB, SwiftV	ASAS-SN; Graham et al. (2017); Brown et al. (2014); Nucita et al. (2017); Wyrzykowski et al. (2015); This work
SN2015I	70	-10 - 322	U, B, V, I, g, r, i, z, SwiftU, SwiftB, SwiftV	ASAS-SN; Foley et al. (2018); Brown et al. (2014); Karamehmetoglu et al. (2015); This work
SN2016brx	11	10 - 185	V, R, g, r	ASAS-SN
SN2016bry	61	5 - 205	B, V, R, I, g, r	ASAS-SN; This work
ASASSN-16eq	55	-14 - 202	B, V, R, I, g, r	ASAS-SN; This work
SN2016ccz*	198	-15 - 185	B, V, R, I, g, r, i, z, SwiftU, SwiftB, SwiftV	ASAS-SN; Foley et al. (2018); Petrushevska et al. (2016)
SN2016coa*	98	-32 - 189	B, V, R, I, g, r, i	ASAS-SN
Gaia16avm	5	-11 - 325	V, r	ASAS-SN; This work
SN2016ei*	82	-78 - 195	B, V, r, i, SwiftU, SwiftB, SwiftV	ASAS-SN
ATLAS16cpu	81	-6 - 182	V, g, r, i, z, SwiftU, SwiftB, SwiftV	ASAS-SN; Foley et al. (2018); This work

**Table B6 – continued** Continuation of Table B6.

SN	$N_{tot}$	Phases	Filters	Refs.
SN2016ghu*	65	-11 - 154	B, V, r, i	ASAS-SN; <a href="#">Inserra et al. (2013)</a>
SN2016gxp*	331	-9 - 267	B, V, r, i, SwiftU, SwiftB, SwiftV	ASAS-SN; This work
SN2016hht*	169	-7 - 174	B, V, r, i, SwiftU, SwiftB, SwiftV	ASAS-SN; <a href="#">Brown et al. (2016)</a>
SN2016hsc*	90	-13 - 178	B, V, r, i	ASAS-SN
ASASSN-17cs	180	-11 - 219	B, V, r, i, SwiftU, SwiftB, SwiftV	ASAS-SN; This work
DLT17u	622	-33 - 315	U, B, V, r, i, SwiftU, SwiftB, SwiftV	ASAS-SN; <a href="#">Brown et al. (2014)</a> ; This work
ATLAS17dfo	166	-17 - 288	B, V, r, i, SwiftU, SwiftB, SwiftV	ASAS-SN; This work
DLT17ar	184	-14 - 227	B, V, r, i, SwiftU, SwiftB, SwiftV	ASAS-SN; This work
DLT17bk	212	-8 - 284	B, V, r, i, SwiftU, SwiftB, SwiftV	ASAS-SN; This work
ASASSN-18hz	88	-10 - 228	B, V, r, i, SwiftU, SwiftB, SwiftV	ASAS-SN; This work
SN2017ezd	139	-7 - 255	B, V, g, r, i, SwiftU, SwiftV	ASAS-SN; This work
DLT17bx	781	-13 - 379	B, V, g, r, i, SwiftU, SwiftB, SwiftV	ASAS-SN; This work
DLT17cd	427	-13 - 228	B, V, g, r, i, SwiftU, SwiftB, SwiftV	ASAS-SN; This work
ATLAS17jiv	269	-7 - 294	B, V, r, i, SwiftU, SwiftB, SwiftV	ASAS-SN; This work

**Table B6 – continued** Continuation of Table B6.

SN	$N_{tot}$	Phases	Filters	Refs.
SN2017glq	828	-17 - 331	B, V, g, r, i, SwiftU, SwiftB, SwiftV	ASAS-SN; This work
ATLAS17nmh	301	35 - 194	B, V, g, r, i	ASAS-SN; This work
ATLAS17nse	10	-4 - 306	V, i	<a href="#">Inserra et al. (2013)</a> ; This work
SN2017yv*	129	-14 - 196	B, V, r, i, SwiftB, SwiftV	ASAS-SN
ASASSN-18hb	108	-7 - 237	B, V, g, r, i	ASAS-SN; This work
ASASSN-18bt	576	-9 - 265	B, V, g, r, i, SwiftU, SwiftB, SwiftV	ASAS-SN; <a href="#">Tucker et al. (2018)</a> ; <a href="#">Dimitriadis et al. (2019)</a>
ASASSN-18da	31	-10 - 220	B, V, r, i, SwiftU, SwiftB, SwiftV	ASAS-SN; This work
DLT18h	200	-24 - 335	B, V, g, r, i, SwiftU, SwiftB, SwiftV	ASAS-SN; This work
DLT18i	340	-18 - 237	B, V, g, r, i, SwiftU, SwiftB, SwiftV	ASAS-SN; This work
SNF-012	4	55 - 272	B, V, R, I	<a href="#">Taubenberger et al. (2013a)</a>